Institut für Nutzpflanzenwissenschaften und Ressourcenschutz
– Pflanzenernährung –

Assessing the Impacts of Hygroscopic Leaf Surface Material on Plant Water Relations: Stomatal Responses and Nocturnal Transpiration

Dissertation

zur Erlangung des Grades
Doktor der Agrarwissenschaften (Dr. agr.)
der Landwirtschaftlichen Fakultät
der Rheinischen Friedrich-Wilhelms-Universität Bonn

von

Chia-Ju Ellen Chi

aus

Taipei, Taiwan

Bonn, 2024

Referent:	PD Dr. Juergen Burkhardt
Korreferent:	Prof. Dr. Mathias Becker
	Prof. Dr. Otto Klemm
Fachnahes Mitglied:	Prof. Dr. Claudia Knief
Vorsitzende:	Prof. Dr. Heiner Goldbach
Tag der mündlichen Prüfung:	27.03.2024

Printed and published with the support of the German Academic Exchange Service.

Angefertigt mit Genehmigung der Landwirtschaftlichen Fakultät der
Rheinischen Friedrich-Wilhelms-Universität Bonn.

Acknowledgements

As I reach the end of my doctoral journey, I reflect with immense gratitude on the incredible support and guidance that has enabled me to complete my dissertation with health and happiness. The years spent on this remarkable path have flown by, but they have been enriched by the kindness and assistance of many individuals.

First and foremost, I extend my gratitude to my supervisor, Jürgen. Our journey together began during the fieldwork in Taiwan, even before I officially joined the doctoral program. Through the challenges of the pandemic and beyond, your guidance has been unwavering, not only in academics but also in providing diverse support and invaluable care. I am always grateful for your patience, understanding, and encouragement. You have been a mentor in the truest sense, and have made a profound impact on me.

I am also thankful to Prof. Goldbach, your referral introduced Jürgen to me and facilitated my journey to Germany. I am grateful to our group members, especially Daniel and Gerry, you provided invaluable assistance and became my first two friends in this foreign country; and to Irmgard and Shyam, for your close collaboration and exchange of ideas. My sincere appreciation extends to the friendly colleagues in our office – Deborah, Kai, Felix, Katy, Marion, Menino. Sharing an office with all of you has been a stroke of luck, adding a touch of camaraderie to our sometimes monotonous academic routine. I am also grateful for the warmth and support of my wonderful friends in the greenhouse area, particularly Christian and Tomas, and the rest of the HGoTech team, Jan, Waltraud. Your assistance and post-work gatherings have always been heartwarming. I would like to express my gratitude to the professors in INRES, Gabriel and Mathias, as well as the dedicated technicians – Angelika G., Angelika V., Nur, Ira, Yaron, and the other fellow doctoral students. Your presence has made our department a close-knit family, also made me feel fully integrated and adapted to life in Germany.

My heartfelt thanks go out to my Taiwanese friends in Germany – Scully, Zoe, Tsung-Hao, Molly, Wingki; to the Marburg girls – Abby, Karla, Khatia, Anna; to the friends in Bonn and those back home with whom I have remained in contact, your friendship has been a source of joy, and the driving force that keeps me moving forward when the homesick hits. Lastly, I would like to express my most profound appreciation to my family and Billy, for their unwavering support throughout my educational journey and especially during the challenging final stages.

To those not mentioned by name, your contributions have been integral in shaping my journey, and I am sincerely grateful for your assistance in reaching where I stand today.

With heartfelt gratitude,

Ellen

Abstract

The rise in anthropogenic industrial and agricultural activities has increased the deposition of atmospheric aerosols on plant leaf surfaces, potentially impacting plant physiology due to their hygroscopic nature. While earlier studies concentrated on the indirect effects of these aerosols, examining their influence on the radiation balance and, consequently, on photosynthesis, recent research has shifted towards investigating the direct effects of hygroscopic actions on plant foliage. This study addresses hygroscopic leaf surface material which originates mostly from aerosol deposition or agricultural sprays, e.g., foliar fertilizers. Hygroscopic compounds on leaf surfaces can deliquesce within the leaf boundary layer by atmospheric moisture and stomatal transpiration, forming highly concentrated solutions which enter stomata as thin films and merge with liquid water coming from the roots (“hydraulic activation of stomata” - HAS). The thin films represent an extension of the plants hydraulic system to the leaf surface, potentially facilitating bidirectional stomatal transport of liquid water and dissolved substances. The deliquescent compounds therefore play a key role in reducing water potential, affecting the saturation vapor pressure close to leaf surfaces and influencing the local vapor pressure deficit (VPD). The transport along these pathways depends on the prevalent gradients of water potential, gradients of nutrient concentrations, and other factors, operating independently of stomatal aperture.

Based on the HAS theory, this doctoral research investigates the comprehensive impacts of hygroscopic leaf surface material on plant physiology and plant water relations at the leaf-level scale, with a particular emphasis on the examination of stomatal responses and nocturnal transpiration. Experiments were carried out in greenhouse and field environments with different aerosol levels: Poplar clones (*Populus maximowiczii x nigra, Populus trichocarpa x maximowiczii*) and camphor seedlings (*Cinnamomum camphora*) were cultivated in greenhouses under conditions of ambient air and filtered air. Additionally, investigations on camphor trees were conducted at forest sites in Taiwan characterized by high and low aerosol concentrations.

This research reveals that the deliquescent hygroscopic material, when deposited on leaf surfaces, forms amorphous crusts on the cuticle and covers the tubular wax fibrils. Due to its direct contact with the atmosphere and the hydraulic connection into the leaf, the hygroscopic material may lead to an additional desiccant effect. These symptoms of enhanced long-term plant water deficit are reflected to varying degrees in the researched species (poplar clones and camphor seedlings), with higher minimum leaf conductance (g_{min}), lower leaf water potential at turgor loss, lower leaf water potential at noon, and altered water use efficiency; as well as secondary effects like reduced stomatal density, in the poplar clones.

However, the effects of hygroscopic material on stomatal responses varied between poplar plants with different water use strategies. Anisohydric plants demonstrated greater stomatal responses and lowered water potential in the presence of hygroscopic material, with higher variations among individuals. In contrast, isohydric plants significantly regulated stomatal responses due to changes in atmospheric VPD, and were less influenced by hygroscopic leaf surface material. However, isohydric plants are likely more affected by increasing g_{min} and the subsequent decrease in osmotic potential. The differences between isohydric and anisohydric plants help explain the inconsistencies in experimental indicators from previous studies. Furthermore, with the utilization of diverse tree species, as well as the comparative analysis between greenhouse experiments and field investigations, this research also highlights the species-specific and environment-specific nature of the HAS effect.

The bidirectionality of the HAS pathway became evident by an experiment addressing nocturnal transpiration with nutrient deficient, hydroponic poplars: *exclusively* if the deficient nutrient was present on the leaf surface *did poplars open the* stomata during nighttime. Plants can mobilize hygroscopic leaf surface material and stomata can take it up by diffusional movement of ions, implying a specific sensing and regulation mechanism of stomata and demonstrating a trade-off between water loss and nutrient uptake through the leaf.

Overall, the results in this doctoral study support the HAS theory and its influence on water and nutrient relations of plants.

Zusammenfassung

Auf den Blattoberflächen von Pflanzen kommt es aufgrund industrieller und landwirtschaftlicher Aktivitäten verstärkt zur Ablagerung atmosphärischer Aerosole, die sich aufgrund ihrer hygroskopischen Eigenschaften potenziell auf die Pflanzenphysiologie auswirken können. Während sich frühere Studien auf die indirekten Auswirkungen von Aerosolen konzentrierten und deren Einfluss auf die Strahlungsbilanz und damit auf die Photosynthese untersuchten, hat sich die Forschung in jüngster Zeit verlagert, hin zur Untersuchung der direkten Wirkungen auf Pflanzenblätter aufgrund der Hygroskopizität. Diese Studie befasst sich mit hygroskopischem Material auf der Blattoberfläche, welches neben Aerosolablagerungen zumeist aus landwirtschaftlichen Spritzmitteln, z. B. Blattdünger, stammt. Hygroskopische Verbindungen auf der Blattoberfläche können sich in der Blattgrenzschicht durch atmosphärische Feuchtigkeit und stomatäre Transpiration verflüssigen (Deliqueszenz) und hochkonzentrierte Lösungen bilden, die als dünne Filme in die Spaltöffnungen eindringen und sich mit dem von den Wurzeln aufgenommenen flüssigen Wasser verbinden ("hydraulische Aktivierung der Stomata " - HAS). Die dünnen Filme stellen eine Erweiterung des hydraulischen Systems der Pflanzen auf die Blattoberfläche dar und erleichtern potenziell den bidirektionalen stomatären Transport von flüssigem Wasser und gelösten Substanzen. Die deliqueszenten, hoch konzentrierten Substanzen spielen daher eine Schlüsselrolle bei der Verringerung des Wasserpotenzials, sie reduzieren den Sättigungsdampfdruck in der Nähe der Blattoberfläche und beeinflussen das lokale Dampfdruckdefizit (VPD). Der Transport entlang dieser Pfade hängt von den vorherrschenden Gradienten des Wasserpotenzials, den Gradienten der Nährstoffkonzentrationen und anderen, unabhängig von der stomatären Öffnung wirkenden Faktoren ab.

Auf der Grundlage der HAS-Theorie werden in dieser Doktorarbeit die Auswirkungen von hygroskopischem Blattoberflächenmaterial auf die Pflanzenphysiologie und den Wasserhaushalt der Pflanzen auf Blattebene eingehend untersucht, wobei ein besonderer Schwerpunkt auf der Untersuchung der stomatären Reaktionen und der nächtlichen Transpiration liegt. Die Experimente wurden im Gewächshaus und im Freiland bei unterschiedlichen

Aerosolkonzentrationen durchgeführt: Pappelklone (*Populus maximowiczii x nigra, Populus trichocarpa x maximowiczii*) und Kampferkeimlinge (*Cinnamomum camphora*) wurden in Gewächshäusern unter Umgebungs- und gefilterten Luftbedingungen kultiviert. Zusätzlich wurden Untersuchungen an Kampferbäumen an Waldstandorten in Taiwan mit stark unterschiedlichen Aerosolkonzentrationen durchgeführt.

Die Studie zeigt, dass aus zerfließendem hygroskopischen Material auf der Kutikula amorphe Krusten entstehen, welche die röhrenförmigen Wachsfibrillen bedecken. Aufgrund des direkten Kontakts mit der Atmosphäre und der hydraulischen Verbindung in das Blatt kann das hygroskopische Material zu einem zusätzlichen Austrocknungseffekt führen. Diese Symptome eines verstärkten langfristigen Wasserdefizits der Pflanzen spiegeln sich in unterschiedlichem Ausmaß in den untersuchten Arten (Pappelklone und Kampfer-Sämlinge) wider, wobei höhere minimale Blattleitfähigkeit (g_{min}), niedrigeres Blattwasserpotenzial bei Turgorverlust, niedrigeres Blattwasserpotenzial zur Mittagszeit und veränderte Wassernutzungseffizienz auftraten sowie sekundäre Effekte wie die geringere Stomatadichte bei den Pappelklonen.

Die Auswirkungen des hygroskopischen Materials auf die stomatären Reaktionen variierten jedoch zwischen Pappelpflanzen mit unterschiedlichen Wassernutzungsstrategien. Anisohydrische Pflanzen zeigten in Gegenwart von hygroskopischem Material stärkere stomatäre Reaktionen und ein niedrigeres Wasserpotenzial, wobei die Unterschiede zwischen den Individuen bei anisohydrischen Pflanzen größer waren als bei isohydrischen Pflanzen. Bei Letzteren reagierten die Stomata sehr stark auf Veränderungen des atmosphärischen Sättigungsdefizits (VPD), sie wurden aber kaum durch hygroskopisches Blattmaterial beeinflusst. Isohydrische Pflanzen sind jedoch wahrscheinlich stärker von steigender minimalen Blattleitfähigkeit (g_{min}) und dem dadurch verursachten Rückgang des osmotischen Potenzials betroffen. Die Unterschiede zwischen isohydrischen und anisohydrischen Pflanzen machen einige Unstimmigkeiten früherer experimenteller Studien erklärlich. Durch die Verwendung verschiedener Baumarten und die vergleichende Analyse von

Gewächshausexperimenten und Felduntersuchungen belegt diese Studie die arten- und umweltspezifische Natur des HAS-Effekts.

Die Bidirektionalität der durch HAS entstandenen Verbindung wurde durch ein Experiment zur nächtlichen Transpiration von hydroponischen Pappeln deutlich, bei denen ein bestimmter Nährstoff im Mangel war: Nur dann, wenn der fehlende Nährstoff auf der Blattoberfläche vorhanden war, öffneten die Pappeln die Spaltöffnungen in der Nacht. Pflanzen können durch Öffnen der Stomata hygroskopisches Material auf der Blattoberfläche mobilisieren, und die Spaltöffnungen können die sich über Diffusion fortbewegenden Ionen aufnehmen, was auf einen spezifischen Wahrnehmungs- und Regulierungsmechanismus der Spaltöffnungen hindeutet und einen Kompromiss zwischen Wasserverlust und Nährstoffaufnahme durch das Blatt aufzeigt.

Insgesamt unterstützen die Ergebnisse dieser Doktorarbeit die HAS-Theorie und ihren Einfluss auf die Wasser- und Nährstoffverhältnisse von Pflanzen.

Table of Contents

List of Abbreviations

HAS	Hydraulic activation of stomata
A	Assimilation rate
C_i	Intercellular CO_2
E	Transpiration rate
VPD / VPD_{leaf}	Vapor pressure deficit at leaf temperature
CO_2_r	Reference cell CO_2 concentration
CO_2_s	Sample cell CO_2 concentration
H_2O_r	Reference cell H_2O concentration
H_2O_s	Sample cell H_2O concentration
T / T_{leaf}	Temperature
Q_{in} / PPFD	Photosynthetic photon flux density incident on the leaf
RH / R.H.	Relative humidity
DRH	Deliquescence relative humidity
ERH	Efflorescence relative humidity
AA	Greenhouse ventilated with ambient air
FA	Greenhouse ventilated with filtered air
SEM	Scanning electron microscopy
A_{sat}	Light saturated photosynthetic rate
V_{cmax}	Maximum carboxylation rate of Rubisco
J / J_{max}	Maximum rate of electron transport for the given light intensity
TPU	Maximum rate of triose phosphate use
R_d	Daytime respiration
g_m	Mesophyll conductance to CO_2 transfer
WUE	Intrinsic water use efficiency (A/g_{sw})
WUE_{photo}	Photosynthetic/instantaneous water use efficiency (A/E)
$\delta^{13}C$	Carbon isotope discrimination
Ψ	Total leaf water potential
ψ_{noon}	Total leaf water potential at noon
π_{tlp}	Leaf water potential at the turgor loss point
π_o	Osmotic potential
g_{sw}	Stomatal conductance to water vapor
g_{min}	Minimum leaf conductance
g_1	Slope of Ball-Berry model
g_0	Intercept of Ball-Berry model
A_n	Assimilation rate in Ball-Berry model
H_s	R.H. at the leaf surface in Ball-Berry model
C_s	CO_2 concentration at the leaf surface in Ball-Berry model
ISO	Isohydric poplar clone
ANI	Anisohydric poplar clone

List of Figures

List of Tables

Chapter 1

This chapter presents the general introduction and motivation for the research.

1 General Introduction

1.1 Impacts of atmospheric aerosols on plant physiology

Atmospheric aerosols are liquid, solid, or mixed suspensions with a heterogeneous chemical composition, spanning a size range from a few nanometers to nearly 100 μm in diameter (Burkhardt & Grantz, 2017). Natural atmospheric aerosols such as sea salt, dust, and volcanic ash, can be beneficial for plants as they carry nutrients (Chadwick *et al.*, 1999). However, in many regions aerosol concentrations are dominated by emissions from anthropogenic sources, including combustion and construction, potentially exerting negative effects on both environments and organisms (Chappelka & Neufeld, 2018; Pariyar & Noga, 2018). Over recent decades, these aerosols have increased substantially due to anthropogenic emissions from industrialization, deforestation, and the increasing agricultural production (Hamilton, 2015; Lu & Tian, 2017).

Extensive studies have been dedicated to investigate the relationship between atmospheric aerosols and plant physiological responses. On both global and regional scales, previous research has primarily focused on the indirect impacts of atmospheric aerosols on plants, including effects on the water cycle, alterations in radiation balance, and nutrient transport (Mahowald *et al.*, 2017). Theoretical and eddy covariance studies suggest a positive contribution of aerosols to canopy photosynthesis efficiency, although empirical evidence linking aerosols to tree growth remains limited (Wang *et al.*, 2018). Positive correlations have been observed between aerosol levels and stem growth rates, with variations from the fraction of diffuse radiation and vapor pressure deficit (VPD) (Wang, Xin; *et al.*, 2021). Additionally, aerosol effects on the micro-environment near the ground have implications for plant dry matter accumulation and water utilization (Liu *et al.*, 2016).

1.2 From indirect aerosol effects to direct hygroscopic actions on foliage

Due to the hygroscopic nature of the majority of aerosols, recent research has shifted its focus towards understanding the direct impact of aerosols on plants, particularly the hygroscopic action of accumulated aerosols deposited on foliage. Hygroscopic particulate salts on leaf surfaces facilitate the formation of microscopic leaf wetness, potentially leading to “wax degradation” symptoms and influencing the trace gas exchange in plants (Burkhardt & Pariyar, 2014; Coopman *et al.*, 2021; Katata & Held, 2021).

In particular, these hygroscopic aerosols deposited close to transpiring stomata become mobile through deliquescence, leading to the formation of highly concentrated solutions capable of entering the stomata and connecting with the liquid water that presents the end of the hydraulic system. This process has been characterized as hydraulic activation of the stomata (i.e., HAS) and results in additional loss of liquid water through the stomata. It reduces stomatal control over plant water loss, independently of the stomatal regulations influenced by VPD changes, and without the concurrent occurrence of larger stomatal apertures and compensating CO_2 influx. Therefore, it is considered unproductive transpiration with a negative impact on water use efficiency, and thereby reducing the tolerance of plants to meteorological drought (Burkhardt, 2010; Song *et al.*, 2015; Burkhardt & Grantz, 2017; Burkhardt *et al.*, 2018; Grantz *et al.*, 2018).

1.3 Characteristics of hygroscopic leaf surface material

These hygroscopic materials on leaf surfaces exhibit varying degrees of chaotropicity in accordance with the Hofmeister series. The ion-specific physicochemical properties defined in the Hofmeister series (Hofmeister, 1888), known as chaotropicity/kosmotropicity, also contribute significantly to the establishment of the HAS effect. Specifically, chaotropic compounds reduce the surface tension of water, thus the thin film formed by hygroscopic particles penetrates more easily along the perimeter of the stomatal pore, and extends

towards the apoplastic surfaces within the leaf (Dutcher *et al.*, 2010; Burkhardt *et al.*, 2012; Chappelka & Neufeld, 2018).

1.4 Stomatal responses to plant water use

Considering the key indicators used in investigating plant water relations from the leaf-level scale, the hypothesis derived from HAS theory suggests that physiological responses to hygroscopic leaf surface material may encompass higher g_{min} values, higher $\delta^{13}C$ values (i.e., less negative), lower π_{tlp}, lower g_1, and higher proline concentration (Bartlett *et al.*, 2012a; Pariyar *et al.*, 2013; Marechaux *et al.*, 2015; Burkhardt *et al.*, 2018). Previous research has indicated that the hygroscopic foliar depositions had caused higher g_{min} for *Quercus petraea*, *Abies alba*, *Pinus sylvestris* (Burkhardt & Pariyar, 2014; Burkhardt *et al.*, 2018), and *Vicia faba (L.)* (Grantz *et al.*, 2018), and less negative $\delta^{13}C$ for second year *Abies alba* needles (Burkhardt et al., 2018), while *Helianthus annuus*, *Pinus sylvestris*, and *Fagus sylvatica* were found to have more negative $\delta^{13}C$ values (Burkhardt & Pariyar, 2016). That is to say, the impact of this HAS establishment from hygroscopic leaf surface material has not been consistently confirmed by experiments.

On the other hand, the stomatal responses to plant water use are also a significant focus in gas exchange research. Given that the current understanding of the physiological mechanisms governing stomatal responses remains incomplete, most models for stomatal conductance (g_{sw}) are empirical or semi-empirical (Buckley & Mott, 2013). However, the water use models developed in the past did not account for the HAS effect, which operates independently of stomatal water vapor loss. Consequently, there may be a need to introduce additional parameters to refine these models. Both instantaneous WUE_{photo} (A/E) and intrinsic WUE (A/g_{sw}) obtained from $\delta^{13}C$ or other models (e.g., Ball-Berry model) exhibit sensitivity to variations in VPD. Specifically, WUE_{photo} tends to decrease as VPD rises, whereas WUE increases with increasing VPD. Nevertheless, the influence of foliar hygroscopic actions and the HAS establishment on these parameters cannot be neglected in this context.

1.5 Research objectives

Numerous aspects surrounding the HAS pathway remain poorly understood, including its potential species-specific nature, the magnitude of effect under different environmental conditions, the comprehensive functions of the formed thin film, the influence of various hygroscopic compounds, its full integration with gas exchange measurements, the extent of its overall impact on plant water status and water use efficiency since each stomatal pore develops an independent film, and whether it presents challenges to the accuracy of existing models pertaining to plant water relations.

This research work aims to investigate three main objectives, providing a more comprehensive understanding of the HAS effect.

- ***Objective 1****: Evaluating the comprehensive impact of HAS on plant water relations and its suitability in greenhouse and field environments.*

- ***Objective 2****: Evaluating differential effects of HAS on plants with varying isohydricity and associated stomatal responses.*

- ***Objective 3****: Exploring additional functions of the thin film in HAS theory beyond uncontrollable water loss.*

1.6 Structure of the dissertation

- **Chapter 1**:

  General Introduction presents the general background information of the research, its development up to the present, existing research gaps, and the extension of this motivation to the formulation of the three primary research questions addressed in this dissertation.

- **Chapter 2**:

  Study 1 comprehensively investigates the influence of hygroscopic leaf surface materials on the stomatal control over plant water use (*Cinnamomum camphora*). It is also aimed to establish an empirical program for gas exchange measurements and to bridge the applicability of greenhouse studies with field experiments.

- **Chapter 3**:

  Study 2 extends the investigation of the impact of hygroscopic leaf surface material on stomatal regulation, delving into the differential stomatal responses related to plant isohydricity (*Populus maximowiczii x nigra, Populus trichocarpa x maximowiczii*).

- **Chapter 4**:

  Study 3 explores the impact of various hygroscopic leaf surface material on the regulation of stomatal conductance in plants (*Populus maximowiczii x nigra*) while incorporating the concepts of nutrient deficiency and nocturnal transpiration.

- **Chapter 5**:

  General Discussion and Conclusion summarize the findings and progresses obtained in this research, and suggest potential directions for future studies.

Chapter 2

The content of this chapter is published in Frontiers in Plant Science, 2022.

Chi, C. J. E., Zinsmeister, D., Lai, I., Chang, S. C., Kuo, Y. L., & Burkhardt, J. (2022). Aerosol Impacts on Water Relations of Camphor (*Cinnamomum camphora*). *Frontiers in Plant Science*, *13*, 892096. https://doi.org/10.3389/fpls.2022.892096.

2 Aerosol Impacts on the Stomatal Part of Plant Water Relations

Abstract

Major parts of anthropogenic and natural aerosols are hygroscopic and deliquesce at high humidity, particularly when depositing to leaf surfaces close to transpiring stomata. Deliquescence and subsequent salt creep may establish thin, extraordinary pathways into the stomata, which foster stomatal uptake of nutrients and water but may also cause stomatal liquid water loss by wicking. Such additional water loss is not accompanied by a wider stomatal aperture with a larger CO_2 influx and hypothetically reduces water use efficiency (WUE). Here, the possible direct impacts of aerosols on physical and physiological parameters of camphor (*Cinnamomum camphora*) were studied (i) in a greenhouse experiment using aerosol exclusion and (ii) in a field study in Taiwan, comparing trees at two sites with different aerosol regimes. Scanning electron microscopy (SEM) images showed that leaves grown under aerosol exclusion in filtered air (FA) were lacking the amorphous, flat areas that were abundant on leaves grown in ambient air (AA), suggesting salt crusts formed from deliquescent aerosols. Increasing vapor pressure deficit (VPD) resulted in half the Ball-Berry slope and double WUE for AA compared to FA leaves. This apparent contradiction to the wicking hypothesis may be due to the independent, overcompensating effect of stomatal closure in response to VPD, which affects AA more than FA stomata. Compared to leaves in a more polluted region in the Taiwanese Southwest, NaCl aerosols dominated the leaf surface conditions on mature camphor trees in Eastern Taiwan, while the considerably lower contact angles and the 2.5 times higher minimum epidermal conductances might have come from organic surfactants. Interpretations of SEM images from leaf surface microstructures should consider amorphous areas as possible indicators of aerosol deposition and other hygroscopic material. The amount and type of the material determine the resulting impacts on plant water relations, together with the surrounding atmosphere and ecophysiological traits.

2.1 Introduction

Atmospheric aerosols are liquid, solid, or mixed suspensions of heterogeneous chemical composition, ranging from a few nanometers to almost 100 μm in diameter (Burkhardt & Grantz, 2017). Natural atmospheric aerosols can be beneficial for plants as they carry nutrients (Chadwick *et al.*, 1999), but in many regions aerosol concentrations are dominated by emissions from anthropogenic sources and may negatively influence both environments and organisms (Pariyar & Noga, 2018). On both global and regional scales, previous studies have long focused on the indirect impacts that atmospheric aerosols bring to plants such as the impact on water cycle, changes in radiation balance, and nutrient transport (Mahowald *et al.*, 2017); it has been shown that the scattering of radiation caused by aerosols contributes to the photosynthesis efficiency of canopy and stem growth, and that the micro-environment near the ground also affects plant dry matter accumulation and water utilization (Liu *et al.*, 2016; Wang *et al.*, 2018). On the other hand, recent research has started paying more attention to the direct impact of aerosols on plants, mostly centering on the hygroscopic action of accumulated deposited aerosols on foliage. Hygroscopic particulate salts on leaf surfaces facilitate the formation of microscopic leaf wetness, may cause “wax degradation” symptoms, and affect the trace gas exchange in plants (Burkhardt & Pariyar, 2014; Coopman *et al.*, 2021; Katata & Held, 2021); moreover, the aerosols deposited close to transpiring stomata become mobile by deliquescence and form highly concentrated solutions that may enter the stomata and connect with the liquid water that forms the end of the hydraulic system. This process (i.e., hydraulic activation of stomata, HAS) leads to liquid stomatal water loss; it is not accompanied by larger stomatal aperture and compensating CO_2 influx, so it can be considered unproductive transpiration with a negative impact on water use efficiency (Burkhardt, 2010; Song *et al.*, 2015; Burkhardt & Grantz, 2017). However, such an impact has not been consistently confirmed by experiment (Pariyar *et al.*, 2013; Burkhardt & Pariyar, 2016).

Since the hygroscopic action is proposed as a primary factor of aerosol impact on plants (Burkhardt *et al.*, 2018), and the stomata play a key role in the adaptation to changing environmental conditions (Berry *et al.*, 2010; Bauerle &

Bowden, 2011; Miner & Bauerle, 2017), this study focused on the stomatal response to the impact of aerosols, as well as its consequences for plant water relations and CO_2 assimilation. Leaf-level physiological differences between *Cinnamomum camphora* (camphor) seedlings, grown under the exposure of aerosols and the elimination of aerosols, were compared, and similarly, the situation of mature camphor trees was studied at two Taiwanese field sites with different aerosol concentrations.

The camphor tree is a well-known versatile tree species growing in eastern Asia. The leaves are rich in bioactive compounds, and the extracted compounds are extensively used in medical treatments. With antifungal activities, the timbers of camphor are often used as building materials and furniture. Based on these characteristics and additional historical influences, camphor has become one of the most important evergreen species in Taiwan, as well as in many other tropical and subtropical areas close by (Hsieh, 1981; Zhou & Yan, 2016; Li *et al.*, 2020). On the other hand, the regional aerosol distribution pattern in Taiwan is strongly related to industry, geography, and season. The high density of the population and the subsequent industrial development causes higher anthropogenic aerosol emissions in western Taiwan (Tsai & Kuo, 2005; Kishcha *et al.*, 2018). Due to the natural barrier formed by the Central Mountain Range, eastern Taiwan has relatively small air pollution. The seasonal difference in aerosol concentrations is most likely caused by the meteorological phenomena that dominate the dispersion of aerosols, and particularly the NaCl concentration varies with distance to the sea (Tsai & Chen, 2006; Chou *et al.*, 2010; Fang & Chang, 2010). Based on the information above, the research species was chosen and the field sites in Taiwan were defined.

In this study, the aerosol loading of camphor leaves was accessed by scanning electron microscopy (SEM) and quantification of water soluble and insoluble particulate matter from leaf washing. The light saturated photosynthetic rate (A_{sat}) and AC_i response curves were measured in order to ensure the comparable photosynthetic performance of plants from different environments. The physiological responses to aerosols were determined by foliar carbon isotope discrimination ($\delta^{13}C$) as a long term measure of WUE (Condon *et al.*,

1992; Cabrera-Bosquet *et al.*, 2007); the minimum leaf conductance (g_{min}) as an indicator of uncontrollable water loss and, together with the leaf water potential at turgor loss (π_{tlp}), as indicators of drought tolerance (Marechaux *et al.*, 2015; Duursma *et al.*, 2019); and the proline accumulation as an additional indicator of osmotic adjustment to water deficit (Bates *et al.*, 1973; Dolatabadian *et al.*, 2008). The results of the gas exchange measurements were then introduced into the semi-empirical Ball-Berry model, which in the original form uses the relative humidity on the leaf surface and is coupled to a photosynthesis model (Farquhar *et al.*, 1980; Ball *et al.*, 1987). This model has been found to reflect differences in drought stress conditions between plants, and the slope factor g_1 is inversely related to both WUE and carbon isotope composition during carbon assimilation (Knauer *et al.*, 2017; Miner & Bauerle, 2017; Miner *et al.*, 2017). The attraction of aerosols to water vapor might affect modeling outputs, mainly because the HAS mechanism creates a parallel transpiration pathway of liquid water, while the model relies on equivalent pathways of water vapor and CO_2 (Aphalo & Jarvis, 1993; Monteith, 1995; Burkhardt, 2010). The original objective of this first study on aerosol- and HAS-caused effects under field conditions was the identification of physiological responses to aerosols on *C. camphora* in two field sites with different aerosol regimes, and their confirmation and explanation under greenhouse conditions with seedlings of the same species in filtered versus unfiltered air. Although the results did not follow the initial expectations, the study still found differential support for aerosol caused physiological responses under both field and greenhouse conditions.

2.2 Materials and methods

2.2.1 Materials preparation and sampling design

2.2.1.1 Plant material

Eight seedlings of camphor were prepared with an initial height of circa 60 cm. All the present leaves were marked nondestructively before the seedlings were assigned randomly and equally into one of two greenhouses for research. After the placement, all seedlings were irrigated regularly, pruned properly due to

the spatial restriction, and fertilized every other week with a complete nutrient solution including micro-nutrients (Ferty 3; Planta Duengemittel GmbH, Hohenstauf, Germany). All measurements were obtained at 12-24 months after the seedlings were placed respectively into the greenhouses, with the plant height circa 150 cm, and only using leaves that developed inside the greenhouses.

2.2.1.2 Greenhouse growing environment

The main research of this study was held in the greenhouses at the Institute of Crop Science and Resource Conservation of the University of Bonn, Germany. The two adjacent greenhouses were located on the margin of an urban area, near a multi-lane highway. One greenhouse was ventilated with ambient air (hereinafter called AA), and the other one was ventilated with filtered air (hereinafter called FA), with only about 1% of ambient aerosols remaining, representing the particles-removed environment (Grantz *et al.*, 2018). The total aerosol concentrations were monitored by a cloud chamber condensation nuclei counter (TSI 3783; TSI, Shoreview, MN, USA). The relative humidity and temperature of the greenhouses were recorded every minute by a Tinytag data logger (TGP 4017, 1-Kanal Temperatur Datenlogger, Sensor NTC; Gemini, RS Components GmbH, Germany), showing that the environmental parameters and conditions besides the concentration of aerosols were very similar in both greenhouses (AA: 14.35 ± 6.66°C, 58.81 ± 16.58% R.H., VPD: circa 0.86 kPa; FA: 13.48 ± 7.10°C, 51.79 ± 16.45% R.H., VPD: circa 0.95 kPa).

2.2.1.3 Field sites in Taiwan

In addition to the greenhouse study, two sites with camphor tree plantations were chosen to verify and compare the results with. According to previous long-term monitoring results (between 2008 and 2016), the southwestern region is likely to have a higher $PM_{2.5}$ concentration (49.14 ± 15.95 μg/m^3) than the eastern region (15.62 ± 8.73 μg/m^3), especially during winter time (Chen *et al.*, 2018; Chen *et al.*, 2020; Ho *et al.*, 2020; Wang, YS *et al.*, 2021). Therefore, the two plantations which are located in Pingtung county (southwestern Taiwan) and Hualien county (eastern Taiwan) were chosen for the field research. Both sites are afforestation after the abandonment of a long history of sugarcane plantation

and are composed of circa 15 endemic broad-leaf tree species. The 675 ha Pingtung site was planted since 2006, while the 1,250 ha Hualien site was planted since 2002. On both sites the plantations are managed and owned by the Taiwan Sugar Corporation. In order to understand the growth status of plants and their contribution to carbon sequestration, flux towers were built and research instruments were installed for monitoring (Wu *et al.*, 2015; Maneke-Fiegenbaum *et al.*, 2018). The canopies of camphor trees were accessed by the existing scaffoldings. In Pingtung site 3 camphor trees were accessible (7 December to 13 December 2019), and in Hualien site 4 camphor trees were accessible (28 November to 4 December 2019).

2.2.1.4 Sampling design and data analysis

An overview of measured parameters is given in *Table 2.1*. The investigations tackled physical and physiological processes, which affected statistical procedures. Measurements of physical parameters (aerosol loading, contact angle, SEM) were evaluated as single leaf data in each treatment; while measurements of physiological parameters (A_{sat} , AC_i fitting data, $\delta^{13}C$, g_{min}, π_{tlp}, water potential, proline concentration, g_{sw} to VPD, Ball-Berry model) were evaluated with the mean value of each individual tree, then further compared between treatments. Statistical analysis was performed using R Studio (R version 4.0.3). Shapiro-Wilk test was used as a normality test for distributed data, and F-test was performed for comparing two variances. For normally distributed data, the significance of differences between different groups was estimated by using the Student's t-test. For data with non-normal distribution, statistical analysis was performed with the non-parametric method using Wilcoxon-Mann-Whitney U-test to find out the differences between groups. In all statistical analyses, the differences were considered significant if the $p < 0.05$.

Table 2.1. An overview of *Cinnamomum camphora* measurements in the greenhouses and the fields.

Measurement	Greenhouse		Field	
	AA	**FA**	**Pingtung**	**Hualien**
A_{sat}	v	v	v	v
AC_i fitting parameters	v	v	v	v
SEM	v	v		
Particulate matter	v	v		
Dissolvable aerosols	v	v	v	v
g_{min}	v	v	v	v
$\delta^{13}C$	v	v	v	v
π_{tlp}	v	v		
Water potential (predawn, noon)			v	v
g_{sw} to VPD curves	v	v		
Contact angle	v	v	v	v
Proline	v	v		

The measurements include light saturated net photosynthetic rate (A_{sat}), photosynthetic parameters fitted from AC_i response curve (the response of net CO_2 assimilation to the CO_2 concentration in the intercellular airspaces of the leaf), scanning electron microscopy images (SEM), aerosol loading evaluation (the concentration of not dissolvable particulate matter and dissolvable aerosols), minimum leaf conductance (g_{min}), carbon isotope composition ($\delta^{13}C$), water potential at predawn, noon, turgor loss (π_{tlp}), the response curve of stomatal conductance (g_{sw}) to vapor pressure deficit at leaf temperature (VPD), contact angle, and proline content.

2.2.2 Methodologies and experimental design

2.2.2.1 Scanning electron microscopy

The amount and behavior of deposited aerosols on leaf surfaces were visualized by scanning electron microscopy (SEM, Leo 1450 VP, Zeiss, Jena, Germany), in the Nees Institute for Biodiversity of Plants of the University of Bonn, Germany. Fresh leaves were obtained from camphor seedlings grown in AA and FA greenhouses and transferred immediately into the laboratory. All samples were taken from fully expanded and dark-green leaves from the 120 cm height of the plants. Due to the requirement of a conductive coating on the surface of samples, the samples of both adaxial and abaxial sides were covered by a commonly-used palladium coating for high-vacuum SEM imaging (Achneck *et al.*, 2010). While interpreting the SEM images, the edges of the pictures were avoided due to the possible instabilities caused by the limitation and disturbance from the instrument.

2.2.2.2 Aerosol loading

The concentration of deposited aerosols on leaf surfaces was determined by foliar rinsing. Each leaf sample was taken pictures before placing into falcon tubes with 40 ml of Millipore water. Without the petiole steeped in the deionized water, falcon tubes were brought to ultrasonic baths (SONOREX, BANDELIN electronic GmbH & Co. KG, Berlin, Germany) for 5 min at 30°C. After taking out the washed leaves, the solution in each falcon tube was filtered with a pore size 0.45 μm and outer diameter 33 mm syringe filter (Carl Roth GmbH & Co. KG, Karlsruhe, Germany) in order to remove the not dissolvable particulate matter (Dzierzanowski *et al.*, 2011; Chen *et al.*, 2022). The filter was weighed before and after filtering to measure the amount of not dissolvable particulate matter deposited on leaf surfaces. The ion concentrations of the solution in falcon tubes were then measured using ion chromatography (Cl^-, NO_3^-, SO_4^{2-}), atomic absorption spectrometer (Mg^{2+}), flame photometer (Na^+, K^+, Ca^{2+}), and a continuous flow analyzer with photometric detection (NH_4^+) (Burkhardt & Pariyar, 2016). For calculating the ion concentration based on the unit of certain leaf area (including both adaxial and abaxial sides of leaf surface), ImageJ was used to

analyze the leaf area of samples (Schneider *et al.*, 2012; Grantz *et al.*, 2018). The measurements of the greenhouse study were conducted in March 2021 (AA: n = 12, FA: n = 9); field research was in November to December 2019 (Pingtung: n = 17, Hualien: n = 12).

2.2.2.3 Contact angle

In the greenhouse study, contact angles of 1-μl droplets of water on the cuticles were measured by a goniometer (DSA 30E; Kruess GmbH, Hamburg, Germany). Fully expanded fresh leaves were harvested from a 120 cm height of camphor seedlings in both greenhouse AA and FA (AA: n = 12, FA: n = 9; conducted in February 2021). The surface tension of the solution was determined by the pendant drop method and shown as angles (Burkhardt *et al.*, 2012). In the field research in December 2018 (Pingtung: n = 8, Hualien: n = 16), the droplets of water were manually applied on the leaf surfaces and the images were captured by a portable microscope (DigiMicro Profi, dnt Innovation GmbH, Germany). The contact angles were then calculated with ImageJ (Schneider *et al.*, 2012).

2.2.2.4 Photosynthetic parameters

Photosynthetic light response curve and AC_i response curve [the response of net CO_2 assimilation (A) to the CO_2 concentration in the intercellular airspaces of the leaf (C_i)] were measured by LI-6400 and LI-6800 Portable Photosynthesis System (LICOR Biosciences, Lincoln, NE, USA) on fully expanded leaves at 120 cm height. For the light response curve, measurements began with the saturating irradiance (1,400 μmol m^{-2} s^{-1}) followed by the reductions of 1,400, 550, 200, 100, 50, 20 μmol m^{-2} s^{-1}, until the irradiance was 0 μmol m^{-2} s^{-1}. The other environmental settings remained as leaf temperature close to environment temperature, leaf vapor pressure deficit (VPD_{leaf}) circa 1.5-2 kPa, and chamber CO_2 concentration 400 μmol mol^{-1}. Light saturated net photosynthetic rate (A_{sat}) was then defined as the net CO_2 assimilation (A) at irradiance 1,400 μmol m^{-2} s^{-1} (Herrick & Thomas, 1999; Oliveira & Penuelas, 2004; Sazeides *et al.*, 2021). On the other hand, before measuring the AC_i response curve, leaves were acclimated to saturating irradiance (1,400 μmol m^{-2} s^{-1}) for 30 min with leaf

temperature 20°C, VPD_{leaf} 1.5 kPa, and flow rate 300 μmol s^{-1}. Without changing the above environmental settings, net CO_2 assimilation rate (A) was measured at a sequence of chamber CO_2 concentrations: 400, 300, 200, 100, 50, 400, 400, 400, 600, 800, 1,000, 1,200, 1,600, 2,000 μmol mol^{-1} (Feng & Dietze, 2013). Afterward, maximum carboxylation rate of Rubisco (V_{cmax}), maximum rate of electron transport for the given light intensity (J), maximum rate of triose phosphate use (TPU), daytime respiration (R_d), and mesophyll conductance to CO_2 transfer (g_m) were fitted with an Excel spreadsheet tool published in previous research (Sharkey *et al.*, 2007). The measurements of the greenhouse study were conducted in May 2021 (n = 4); field research was in November to December 2019 (Pingtung: n = 3, Hualien: n = 4).

2.2.2.5 Carbon dioxide discrimination

The carbon isotope composition was measured with an isotope ratio mass spectrometer (IRMS, C-N-S Analyzer, and MS-2020; SerCon Ltd., Crewe, UK). Three leaves from 120 cm height of camphor seedlings were taken for each sample. The harvested leaves were dried in a laboratorial oven at 60°C for 1 week to reach the absolute dry weight and were ground to a fine powder. 1 ± 0.1 mg of ground samples were weighed with an electronic micro-balance (M2P, Sartorius Lab Instruments GmbH & Co. KG, Goettingen, Germany) and loaded into tin capsules. During operation in the C-N-S Analyzer, the tin capsule reached 1,800°C and fell into the combustion furnace as CO_2 was injected. Soon after oxidation, the sample went through a purification process (Cr_2O_3, CuO, Ag-wool layer) with He carrier gas, in order to assure the complete oxidation and removal of unnecessary S in the sample. The sample then passed through the reduction furnace containing Cu at 600°C, where the excess CO_2 and H_2O were removed. The resulting gas stream was carried to a gas chromatography column and then the separated CO_2 was brought to the mass spectrometer. During operation in the mass spectrometer, the inlet gas stream was ionized as an ion beam and was separated by a permanent magnet while passing through the passage, and then reached the final isotope detector. From the ratio of signals which were collected at the detector, the ^{13}C value was calculated. The carbon isotope composition ($\delta^{13}C$) was then calculated by comparison to a standard (Condon *et al.*, 2002;

Burkhardt & Pariyar, 2016). The measurements of the greenhouse study were conducted in March 2021 (n = 3); field research was in November to December 2019 (Pingtung: n = 3, Hualien: n = 4).

2.2.2.6 Minimum leaf conductance

The samples of camphor were taken from fresh leaves and then immediately brought to the lab (n = 4; conducted in March 2021). After sealing the basis of the petiole to prevent the water loss from the petiole, the samples were labeled and the pictures of leaf surfaces were taken for calculating the leaf area with a known scale by ImageJ (Schneider *et al.*, 2012). During dehydration, the samples were hung on a framework with proper spaces separating the leaves in a ventilated fume hood. The samples were weighed on a digital semi-micro balance (EX125M, EXPLORER® SEMIMICRO, Ohaus Corporation, Parsippany, NJ, USA) once an hour, meanwhile both the temperature and humidity of the drying environment were continuously recorded by a Tinytag data logger. This process was repeated for about 72 h, with 6-8 measurements in the linear part of the regression line. The modified Arden Buck equation (Buck, 1981) was used to calculate the saturated vapor pressure (VP_{sat} , kPa). Together with the leaf drying weight, relative humidity, temperature, and leaf area, g_{min} values were finally calculated by the spreadsheet tool (Sack & Scoffoni, 2011). The mean g_{min} value of each sample was calculated by the 6-8 measurements from the linear part of the regression line in the graph, which was supposed to be close to the g_{min} value calculated by the slope in the graph. In order to compare the differences between different groups, the g_{min} values were then statistically analyzed.

2.2.2.7 Leaf water potential

The leaf water potential at turgor loss (π_{tlp}) is strongly related to plant drought tolerance (Marechaux *et al.*, 2015). Instead of the standard pressure-volume (p-v) curve approach, using an osmometer is one of the most rapid and reliable methods to predict π_{tlp} (Bartlett *et al.*, 2012a). In the greenhouse study (AA: n = 4, FA: n = 3; conducted in March 2021), branches from a certain height of the plants were cut and quickly placed into water, and then cut again

underwater at least 2 cm distal to the original cut. This standard pre-treatment of rehydration was covered by a black plastic bag and performed overnight (from sunset to shortly after sunrise) 1 day before measuring. The next morning, the branches were wrapped slightly in a wet paper towel and placed in zipper bags while transferring to the lab. The bags were then stored in the fridge, with only one leaf sample taken out each time for measurements. One leaf disc was taken from one mature and fully expanded leaf per branch. The discs were taken in the middle between the midrib and margin and between the leaf tip and base, using a 6 mm diameter cork borer and avoiding secondary veins. The leaf disc was then immediately folded inside the foil square (3×3 cm^2) and frozen in liquid nitrogen for 2 min in order to fracture the cell walls. Afterward, the leaf disc was punctured using tweezers 10-12 times and then rapidly sealed in the vapor pressure osmometer (VAPRO 5600, Wescor, Inc, Logan, UT, USA). The osmolality (mmol kg^{-1}) was measured after the values reached equilibrium (8-12 min waiting time). The osmotic potential (π_o) was then calculated by using osmolality obtained from the vapor pressure osmometer of freeze-thawed leaf discs, following Van't Hoff Equation (2-1) which relates solute concentration to vapor pressure:

$$\pi_o = -C_o \times R \times T \quad (2\text{-}1)$$

where C_o is the molar solute concentration (mmol kg^{-1}), R is the universal gas constant 8.3144598E-0.6 (m^3 MPa K^{-1} mol^{-1}), T is the temperature (K) (Khare, 2015). Due to the strong correlation between π_o and π_{tlp} (Bartlett *et al.*, 2012a), π_{tlp} was then calculated from π_o by using the adapted regression Equation (2-2) from previous research (Bartlett *et al.*, 2012b; Sjoman *et al.*, 2015; Banks & Hirons, 2019):

$$\pi_{tlp} = -0.2554 + 1.1243 \times \pi_o \quad (2\text{-}2)$$

where the R^2 of this π_{tlp} prediction from π_o is proposed as 0.91.

In the field study, the leaf water potential was measured at predawn and noon time in the Pingtung site and Hualien site (n = 3 and 4, respectively). A small twig with leaves was cut off from individual camphor trees with aluminum foil slightly wrapped in order to prevent water loss; the twig was then immediately transferred into Scholander Pressure Chamber (Model 3005, Soil Moisture Equipment Corp., Santa Barbara, CA, USA) for measuring (Pariyar *et al.*, 2013; Kuo *et al.*, 2017).

2.2.2.8 Proline concentration

Fully expanded fresh leaves were harvested from a 120 cm height of camphor seedlings in both greenhouse AA and FA (AA: n = 4, FA: n = 3; conducted in April 2021). Five samples were taken from each seedling, and each sample contained 1-2 leaves depending on the leaf size. Samples were placed separately in zipper bags at −20°C for deep-freezing. Afterward, samples were freeze-dried for 2 days under vacuum without thawing (ALPHA 1-4 LDplus/ALPHA 2-4 LDplus, Martin Christ Gefriertrocknungsanlagen GmbH, Osterode am Harz, Germany). The samples were then ground into a fine powder (Mixer Mill MM 301, Retsch GmbH, Haan, Germany) and weighed 100 mg per sample with an analytical balance (BP 210 S, Sartorius Lab Instruments GmbH & Co. KG, Goettingen, Germany). For the extraction, 3 ml of 3% sulfosalicylic acid was added to each sample. The samples were then shaken for 20 s and centrifuged at room temperature for 20 min at 4,200 rpm. For each sample, 2 ml of supernatant solution, 2 ml of glacial acetic acid (100%), and 2 ml of ninhydrin acid solution (ninhydrin mixed with glacial acetic acid and orthophosphoric acid) were mixed in a clean test tube. After being shaken homogeneously, the samples were placed in a hot-bath (100°C) for 1 h to boost the chemical reaction and then brought into an ice-bath to stop the chemical reaction until they reached room temperature. Four milliliters of toluene was added to each test tube, and the test tube was closed tightly with a rubber plug before mixed on a vortex mixer for 30 s. In order to get stratification, the test tube was left standing for 15 min until the toluene and aqueous phases were separated distinctly. The toluene phase (red-colored, upper part) was then carefully transferred into a half microacryl cuvette, and the absorbance of the solution was measured with a spectrophotometer at

wavelength 520 nm (Lambda 35 UV/Vis Spectrophotometer, Perkin Elmer LAS GmbH, Solingen, Germany). The concentration of proline was calculated from a proline standard curve following Equation (2-3) and was expressed as μeq g^{-1} dry matter (Dolatabadian *et al.*, 2008; Pariyar & Noga, 2018)

$$Proline\ (\mu mol\ g^{-1}\ dry\ matter) = \frac{(A_{520nm} - b)/a \times V \times DF}{M_{proline} \times Wt_{sample}} \quad (2\text{-}3)$$

In Equation (2-3), A_{520nm} is the absorbance of the solution at wavelength 520 nm, a and b are the coefficients of slope and intercept from the linear equation ($y = ax + b$) of the standard proline concentrations gradient curve, V is the volume of sulfosalicylic acid (3 ml), DF is the dilution factor (1.5), the ratio of sulfosalicylic acid and supernatant solution, $M_{proline}$ is the molecular weight of proline (115.5 g mol^{-1}), and Wt is the weight of the initial sample (0.1 g).

2.2.2.9 Stomatal conductance to water vapor measurements

The gas exchange measurements were conducted in the greenhouses during cloudy days in winter (February 2021) in order to reduce the influence of circadian changes (Grantz *et al.*, 2018). The response curve of stomatal conductance (g_{sw}) to vapor pressure deficit at leaf temperature (VPD) was determined using a steady-state gas exchange system (LI-6800). The photosynthetic photon flux density (PPFD) incident on the leaf (i.e., Q_{in}) was set as 500 μmol m^{-2} s^{-1} to avoid over saturation. Sample cell CO_2 concentration was set as 400 μmol mol^{-1}, flow rate to the chamber as 300 μmol s^{-1}, chamber fan rotation rate as 14,500 rpm, and leaf temperature as 15°C (evaluated by the ambient environment and temperature restriction). Considering the sensibility of g_{sw} to changing VPD and the instrument limitation of CO_2 supply, the sample was measured at a stepwise sequence of VPD: 0.50, 0.75, 1.00, 1.25, 1.50 kPa. Before switching to the next VPD set point, the gas analyzers of the sample and reference were matched to assure accuracy and stability. With each VPD, measurements were recorded every minute until the photosynthetic parameters reached equilibrium, resulting in a 40-min to 2-h acclimation. For data collection, the mean of the last 10 measurements of each VPD was taken for further

statistical analysis. Not only the response curve of stomatal conductance to increasing vapor pressure deficit was displayed, but also the parameter g_{sw} was performed according to the Ball-Berry model, Equation (2-4). This model presents g_{sw} as a function of assimilation (A_n), relative humidity (H_s), and CO_2 concentration at the leaf surface (C_s).

$$g_{sw} = g_1 \times A_n \times \frac{H_s}{C_s} + g_0 \quad (2\text{-}4)$$

The g_{sw} results from the linear approach, where the slope constant (g_1) is the slope of the relationship between g_{sw} and $A_n{}^* H_s/C_s$ (i.e., Ball Index), and g_0 comes from the intercept when A_n is zero. The slope represents a compromise between the costs and benefits of g_{sw} relative to the photosynthetic activity of the leaf (Ball *et al.*, 1987; Medlyn *et al.*, 2017; Miner & Bauerle, 2017).

2.3 Results

2.3.1 SEM images

Scanning electron microscopy images in *Figure 2.1* show the cuticular and stomatal patterns on abaxial surfaces of *C. camphora* leaves, with clear differences in the microstructures of AA leaves (*Figure 2.1A,C*) compared to FA leaves (*Figure 2.1B,D*). On the surfaces of AA leaves, there are more particles deposited visibly, which are shown as non-transparent, brighter, and randomly distributed granules in the SEM images, compared to FA. Flat, amorphous areas are only observed on AA leaf surfaces (*Figure 2.1A,C*), and may indicate salt crusts resulting from hygroscopic aerosols after deliquescence. Around these flat areas, the wax crystals are faintly covered; additionally, the original wax structures of stomata and epidermal cells are changed in AA leaves. In *Figure 2.1C,* it is visible that the arrangement of wax on the stomata and surrounding cells is less neatly distributed than in *Figure 2.1D*. Their appearance supports the hypothesis of the hygroscopic layer formed by deliquescent aerosols, which resulted in the overall impression of more disturbed surfaces, less defined stomatal structures, and a less visible stomata distribution for AA compared to FA leaves.

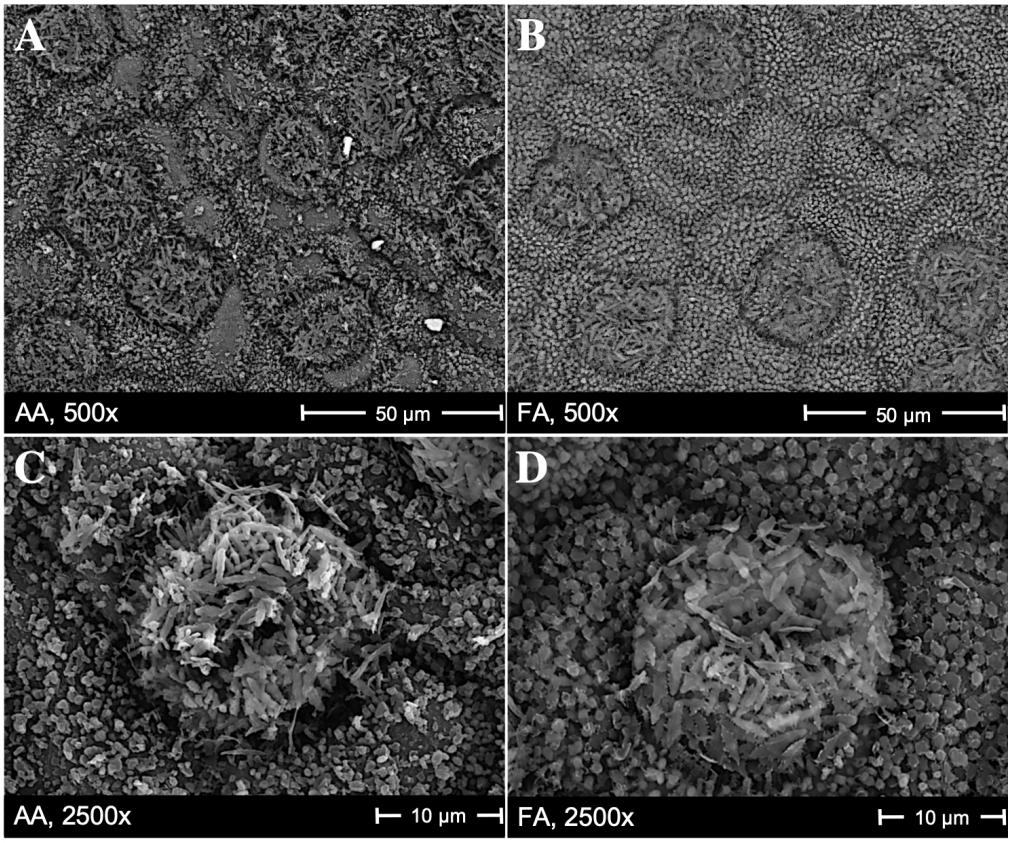

Figure 2.1. Scanning electron microscopy images of stomata patterns on the abaxial surface of *Cinnamomum camphora*.

With magnification 500x and 2,500x. (A,C) are from AA leaves (the greenhouse with ambient air) and (B,D) are from FA leaves (the greenhouse with filtered air). Flat, amorphous areas in (A,C) are probably caused by deliquescent, hygroscopic aerosols. Such an area is, e.g., in (A) above the left part of the 50 µm scale.

2.3.2 Deposited aerosol concentration on leaf surfaces

Table 2.2 shows the concentration of not dissolvable particulate matter and the overall amount of dissolvable aerosols deposited on leaf surfaces in greenhouse AA and FA, each number referring to the total adaxial and abaxial leaf area. The weight of not dissolvable particulate matter deposited on AA leaves was higher than on FA leaves, with the comparable median value of 3.59 µg/cm^2 (n = 12) and 1.40 µg/cm^2 (n = 9), respectively. The total amount of dissolvable

aerosols in AA was more than 9 times higher than in FA. The ratio of not dissolvable particulate matter to total deposited aerosol amount within a square centimeter in AA is 74%, and in FA is 93%. *Figure 2.2A* details the ionic composition of the dissolvable aerosols, respectively. Nitrate, sulfate, and chloride are the dominant compounds of aerosol deposition in AA, while Na, K, Mg, and ammonium are the subordinate ones. In FA, the concentration of chloride, sulfate, and K is relatively higher than the other ions. *Figure 2.2B* shows the concentration of dissolvable aerosols deposited on leaf surfaces from field sites in Taiwan. The dominant compounds in Pingtung are K and Cl, which are much higher than the concentration of nitrate, sulfate, and ammonium. Mg and Na show a value close to zero of the concentration in Pingtung. A different distribution pattern is found in Hualien, with Cl having the highest concentration, followed by Na, sulfate, K, Mg, nitrate, and ammonium. Although there are differences between compound species in Pingtung and Hualien, the total concentration of dissolvable deposited aerosols in Pingtung (1.54 ± 0.142 μg/cm^2, n = 17) is not significantly higher than in Hualien (1.26 ± 0.132 μg/cm^2, n = 12).

2.3.3 Contact angle

Table 2.2 shows the difference in contact angles on adaxial and abaxial leaves from greenhouse AA and FA, as well as of leaves from the fields. There is no significant difference in adaxial contact angles between AA (124.56 ± 2.62 °, n = 12) and FA (127.00 ± 2.47 °, n = 9) leaves, neither between Pingtung (65.96 ± 7.59 °, n = 14) and Hualien (53.16 ± 1.87 °, n = 16). With abaxial contact angles, AA leaves (140.13 ± 1.37 °, n = 12) and FA leaves (143.14 ± 1.18 °, n = 9) do not differ either. However, Pingtung leaves (119.33 ± 9.47 °, n = 8) have higher values than Hualien leaves (75.68 ± 5.13 °, n = 16).

2.3.4 Photosynthetic parameters

In *Table 2.2*, the key photosynthetic parameters of leaves from AA and FA are presented (n = 4). There are no significant differences in A_{sat} , V_{cmax}, J, TPU, R_d, and g_m between the leaves from two greenhouses, nor between the two field sites.

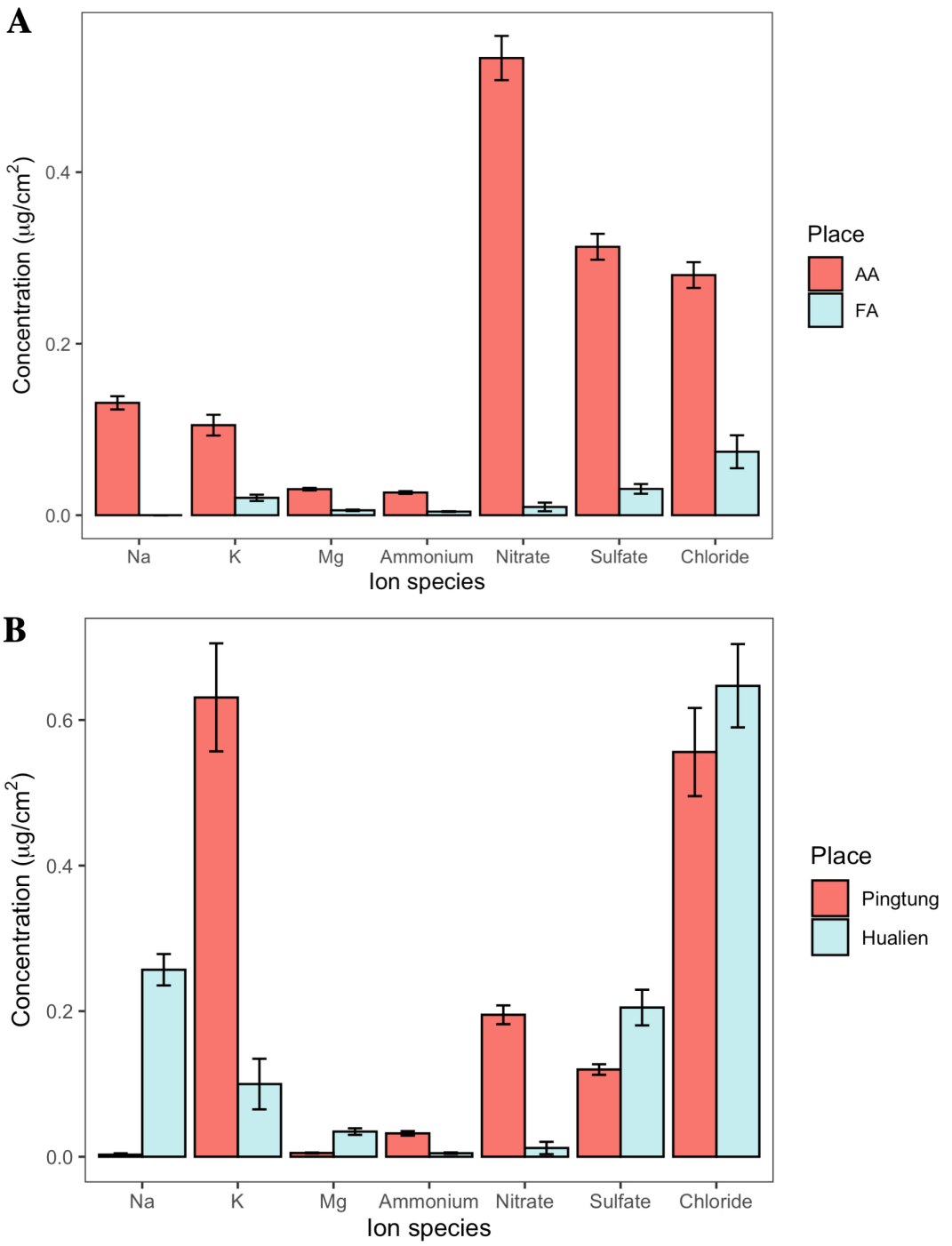

Figure 2.2. The concentration of dissolvable aerosols deposited on leaf surfaces from greenhouses and fields, determined by foliar rinsing.

(A) Ion concentration on camphor leaves from the AA (unfiltered, ambient air) and FA (filtered air) greenhouses. (B) Ion concentration on camphor leaves at Pingtung and Hualien field site.

Table 2.2. Measurements of *Cinnamomum camphora* leaves from different growing environments.

Measurement		Greenhouse			Field		
		AA	FA	Significance	Pingtung	Hualien	Significance
A_{sat}	(μmol m^{-2} s^{-1})	6.70 ± 0.90	7.29 ± 1.37	$p = 0.731$	12.30 ± 3.27	15.30 ± 1.12	$p = 0.367$
V_{camx}	(μmol m^{-2} s^{-1})	102.11 ± 9.05	111.21 ± 8.02	$p = 0.480$	102.42 ± 17.97	74.53 ± 9.02	$p = 0.191$
J	(μmol m^{-2} s^{-1})	135.89 ± 7.08	138.83 ± 8.06	$p = 0.793$	113.06 ± 12.28	99.52 ± 7.45	$p = 0.363$
TPU	(μmol m^{-2} s^{-1})	10.69 ± 0.41	10.73 ± 0.59	$p = 0.961$	8.32 ± 0.82	7.82 ± 0.71	$p = 0.667$
R_d	(μmol m^{-2} s^{-1})	8.73 ± 1.16	8.00 ± 1.82	$p = 0.747$	0.93 ± 0.15	0.85 ± 0.07	$p = 0.583$
g_m	(μmol m^{-2} s^{-1} Pa^{-1})	14.24 ± 4.19	5.03 ± 2.23	$p = 0.100$	19.73 ± 9.44	22.00 ± 5.31	$p = 0.831$
Particulate matter	(μg/cm^2)	3.59a	1.40b	$p < 0.01$			
Dissolvable aerosols	(μg/cm^2)	1.42 ± 0.06a	0.15 ± 0.03b	$p < 0.001$	1.54 ± 0.14	1.26 ± 0.13	$p = 0.177$
g_{min}	(mmol m^{-2} s^{-1})	0.49 ± 0.03	0.48 ± 0.03	$p = 0.967$	0.99 ± 0.13a	2.46 ± 0.20b	$p < 0.01$
$\delta^{13}C$		-28.10 ± 0.20	-27.70 ± 0.55	$p = 0.510$	-31.58 ± 0.50	-32.99 ± 0.40	$p = 0.077$
π_{tlp}	(MPa)	-3.43 ± 0.09	-3.26 ± 0.08	$p = 0.210$			
Water potential, predawn	(MPa)				-0.09 ± 0.01	-0.10 ± 0.02	$p = 0.840$
Water potential, noon	(MPa)				-0.64 ± 0.10	-0.52 ± 0.03	$p = 0.210$
Contact angle, adaxial	°	124.56 ± 2.62	127.00 ± 2.47	$p = 0.520$	65.96 ± 7.59	53.16 ± 1.87	$p = 0.093$
Contact angle, abaxial	°	140.13 ± 1.37	143.14 ± 1.18	$p = 0.128$	119.33 ± 9.47a	75.68 ± 5.13b	$p < 0.001$
Proline content	(μmol g^{-1})	1.57 ± 0.57	1.22 ± 0.39	$p = 0.659$			

AA is the greenhouse with ambient air and FA is the greenhouse with filtered air; Pingtung is the expectedly more polluted field and Hualien is the expectedly less polluted field. The results show the key photosynthetic parameters (light saturated net photosynthetic rate (A_{sat}), maximum carboxylation rate of Rubisco (V_{cmax}), maximum rate of electron transport for the given light intensity (J), maximum rate of triose phosphate use (TPU), daytime respiration (R_d), and mesophyll conductance to CO_2 transfer (g_m), the concentration of not dissolvable particulate matter, total concentration of dissolvable deposited aerosols, minimum epidermal conductance (g_{min}), carbon isotope composition ($\delta^{13}C$) values, leaf water potential at turgor loss (π_{tlp}), predawn, noon, contact angles, and proline concentration. The values are presented as mean ± SE (statistically analyzed with Student's t-test), besides the values of particulate, which are presented as median (statistically analyzed with Wilcoxon-Mann-Whitney U-test). Sample size and research conducted time for each measurement are indicated in the text. Statistical significance is shown with the p-value.

2.3.5 Plant water relations and drought tolerance measurements

2.3.5.1 Carbon dioxide discrimination

In *Table 2.2*, $\delta^{13}C$ values are generally less negative in the greenhouses than in the fields, but the results between more polluted and less polluted environments are not consistent. It is noted that there is a tendency toward lower values at Hualien compared to Pingtung, although the comparison is not useful (refer to below). Between the different greenhouses, where the isotope ratio could possibly allow comparison of long-term stomatal aperture due to equal environmental conditions, there is no significant difference in $\delta^{13}C$ between AA (-28.10 ± 0.20) and FA (-27.70 ± 0.55), respectively (n = 3).

2.3.5.2 Minimum leaf conductance

There is no significant difference in g_{min} of *C. camphora* leaves between AA (n = 4) and FA (n = 4). The g_{min} value of leaves in AA shows 0.49 ± 0.03 mmol m^{-2} s^{-1}, very close to the g^{min} value of leaves in FA which is 0.48 ± 0.03 mmol m^{-2} s^{-1}. On the other hand, the g_{min} of leaves from Pingtung (n = 3) is found much lower than in Hualien (n = 4), with the value of 0.99 ± 0.13 mmol m^{-2} s^{-1} and 2.46 ± 0.20 mmol m^{-2} s^{-1}, respectively (*Table 2.2*).

2.3.5.3 Leaf water potential at predawn, noon, and turgor loss

There is no significant difference in leaf water potential at turgor loss (π_{tlp}) in the greenhouses. Predawn and noon leaf water potential at the field sites are not significantly different (*Table 2.2*), supporting comparable water status during the measurement campaign.

2.3.5.4 Proline concentration

There is no significant difference in proline concentration of *C. camphora* leaves between AA (n = 4) and FA (n = 3). The accumulated proline content of leaves in AA is 1.57 ± 0.57 μmol g^{-1}, and in FA it is 1.22 ± 0.39 μmol g^{-1} (*Table 2.2*).

2.3.6 Stomatal conductance to water vapor

Stomatal conductance (g_{sw}) shows a decreasing tendency as VPD increases, both in AA and FA (*Figure 2.3*; n = 3, respectively). In AA, the g_{sw} value decreases more moderately from 0.015 ± 0.001 mol m^{-2} s^{-1} (while VPD 0.50 kPa) to 0.009 ± 0.0005 mol m^{-2} s^{-1} (while VPD1.50 kPa), with small SEs. However, in FA, the g_{sw} value falls more rapidly from 0.042 ± 0.005 mol m^{-2} s^{-1} (while VPD 0.50 kPa) to 0.017 ± 0.001 mol m^{-2} s^{-1} (while VPD 1.50 kPa). With each VPD set point, leaves in AA show a lower g_{sw} value than in FA ($p < 0.01$), especially when VPD is low (i.e., 0.50 kPa). Additionally, it is shown that in both AA and FA, the g_{sw} of leaves maintain a similar value instead of decreasing while VPD changes from 1.25 to 1.50 kPa. Subsequently, differences are also found for the stomatal model parameters g_0 and g_1, calculated from the Ball Index on the basis of assimilation (A_n), relative humidity (H_s), and CO_2 concentration at the leaf surface (C_s), and then further performed with the Ball-Berry model (*Figure 2.4*). The values of An in AA are generally lower than FA, causing a lower range of the Ball Index.

The regression line of AA leaves is, therefore, extended to the full range of the x-axis by using the data points predicted with the linear model; and two regression lines are compared based on the actual data points. Both regression lines indicate a positive correlation between g_{sw} and Ball Index, representing the fitted data calculated from the leaf-scale measurements, where both of the R^2 values are higher than 0.90. The slope of the linear regression (g_1) for AA is about half the slope for FA (*Figure 2.4*), and the g_{sw} intercept (g_0) of the linear regression for AA is also smaller than g_0 for FA ($p < 0.005$).

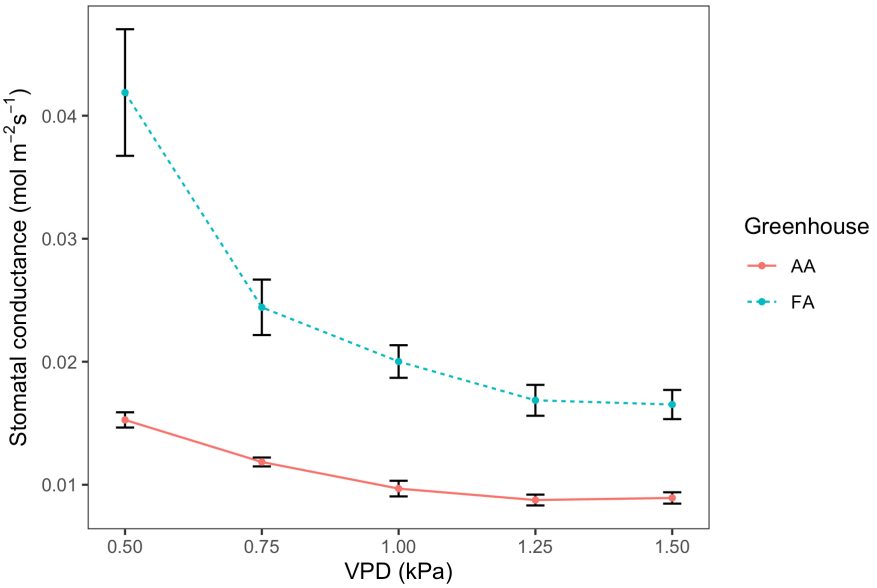

Figure 2.3. Stomatal conductance (g_{sw}) to vapor pressure deficit (VPD) response curve for camphor leaves in greenhouse AA and FA.

The points and error bars represent mean ± SE (n = 3). The solid line is AA and the dashed line is FA.

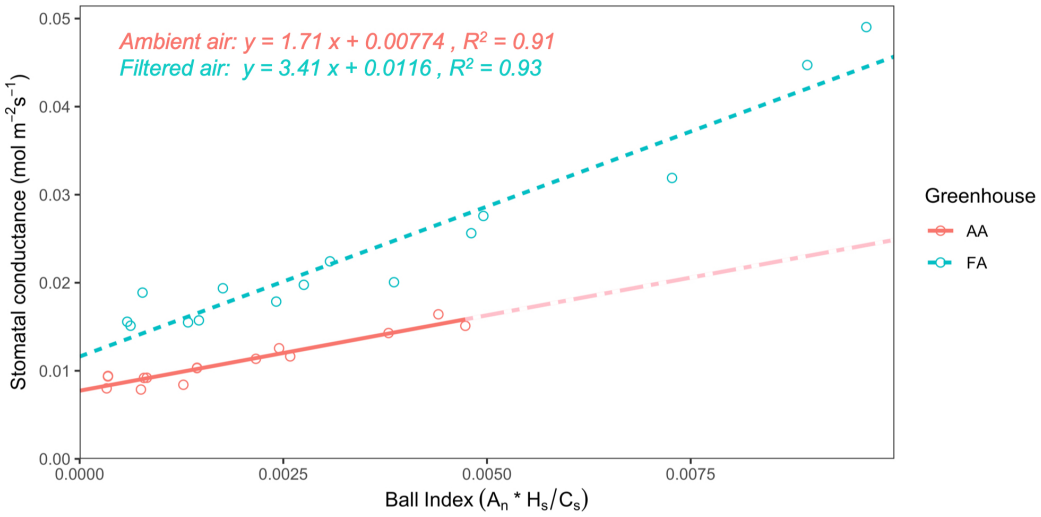

Figure 2.4. Relationship of stomatal conductance with the Ball Index for camphor leaves from greenhouse AA and FA.

The linear regressions of the Ball-Berry model represent the means of linear functions fitted to data from individual leaves at all measured vapor pressure deficit (VPD) levels; the Ball Index is calculated with assimilation (A_n), relative humidity (H_s), and CO_2 concentration at the leaf surface (C_s). The solid line is AA, with a partially dash-dotted line showing the extension to the full range of the x-axis, based on predicted data points from the linear regression; and the dashed line is FA. A statistical analysis of the slope and intercept indicates a significant difference in the Ball-Berry model between leaves from AA and FA ($p < 0.005$).

2.4 Discussion

2.4.1 Aerosol deposition on leaf surfaces

The SEM images of *C. camphora* bring out comparable results with previous research regarding the relation of deposited aerosols and leaf morphology, and the formation of amorphous regions similar to so-called “wax degradation” on the cuticle or close to stomata (Burkhardt, 2010; Burkhardt & Grantz, 2017; Chen *et al.*, 2017). The pattern of hypothetical aerosol layer and amorphous wax degradation have been as well found on the leaf surfaces of *Cryptomeria japonica* (Sase *et al.*, 1998), *Brassica oleracea* (*Gongylodes* Group) (Burkhardt *et al.*, 2001), *Platanus orientalis L.* (Pourkhabbaz *et al.*, 2010), *Pinus sylvestris L.* (Burkhardt & Pariyar, 2014), *Quercus variabilis* (Mo *et al.*, 2015), and *Vigna radiata (L.) R. Wilczek* (Shabnam *et al.*, 2021). Moreover, research has indicated that identified wax degradation might be actually a mixture of deliquescent aerosols and disturbed wax crystallization; the development of amorphous wax appearance can result from deliquescent salts covering tubular wax fibrils, following the process of:

(i) the attraction of water vapor by hygroscopicity;

(ii) the dissolution of hygroscopic aerosols;

(iii) the resulting mobility and distribution across the leaf surface,

leading to the coverage of tubular waxes by amorphous crusts and consequently showing the typical appearance of wax degradation (Burkhardt, 2010; Burkhardt & Pariyar, 2014; Burkhardt *et al.*, 2018). In this study, few larger deposited aerosols on AA leaf surfaces are observed as crystalline, but most of them appear to be amorphous crusts caused by the humidity cycle correlated with the deliquescence of salt and the transpiration of stomata. This phenomenon consists of the previous studies aforementioned.

As for the results of not dissolvable particulate matter and dissolvable aerosol concentration from leaves grown in the greenhouses, it is significant that AA leaves accumulated higher aerosol concentration than FA leaves, regardless of the total aerosol concentration and specific aerosol compounds. Compounds such as Na and Cl may come from sea salts, even though the greenhouses locate

a bit distant from the coast (Burkhardt & Eiden, 1990). In general, the dominant aerosol compounds in AA are similar to previous research which was done in the same greenhouse environment (Burkhardt & Pariyar, 2016). Although the epicuticular wax may partially also contain aerosols (Dzierzanowski *et al.*, 2011; Victório *et al.*, 2022), it is neglectable in this study since the focus is on researching the aerosol effects within one species, instead of the quantification and classification of deposited aerosols. The water dissolvable ions contributed about 30% to the overall aerosol mass found on AA leaves, which is in agreement with the reported range of European aerosol composition (Putaud *et al.*, 2010).

The ionic deposition load on leaves at Pingtung was 1.54 μg/cm^2, exceeding the amounts on Hualien leaves (1.26 μg/cm^2) by 22%. This difference was less than expected from long term monitoring data and literature (Lin *et al.*, 2008; Li *et al.*, 2016; Lee *et al.*, 2020). The ionic composition on Hualien leaves was dominated by sea salt (Na, Cl), reflecting the small distance to the sea (50 km in the main wind direction). Nitrate and sulfate are mainly composed of secondary ammonium sulfate and ammonium nitrate from industry (Yang *et al.*, 2017; Shen *et al.*, 2019; Shen *et al.*, 2020). Nitrate, ammonium, and potassium strongly contributed to the composition of particles on Pingtung leaves, whereas the sulfate and magnesium concentrations were higher on Hualien leaves (Figure 2B). The daily monitoring data were extracted from Taiwan Air Quality Monitoring Network, Environmental Protection Administration, Taiwan, in order to inspect the environmental aerosol concentration with an accurate time range (*Figure 2.5*). Continuous torrential rain probably caused the strong decrease of $PM_{2.5}$ concentrations shortly before the experiment at the Pingtung site, and also the removal of particles from leaves (Wang *et al.*, 2015), particularly from upper leaf surfaces. However, rainfall itself is also able to contribute to the ion concentrations besides washing off particles; consequently, rainfalls might affect aerosol retention and long term accumulation of ionic aerosols on leaf surfaces, and foliage traits are the more important factors related to these effects (Xu *et al.*, 2017; Pariyar & Noga, 2018; Zhang *et al.*, 2019; Zhou *et al.*, 2020). As an evergreen tree species, *C. camphora* is likely subject to a higher wash off rate of fine aerosols at high rainfall intensities, causing the indistinct aerosol distribution and concentration on leaf surfaces in the Pingtung site (Xu *et al.*, 2019; Zhou *et*

al., 2021). Therefore, this inconsistency is challenging the accuracy of the other field measurements.

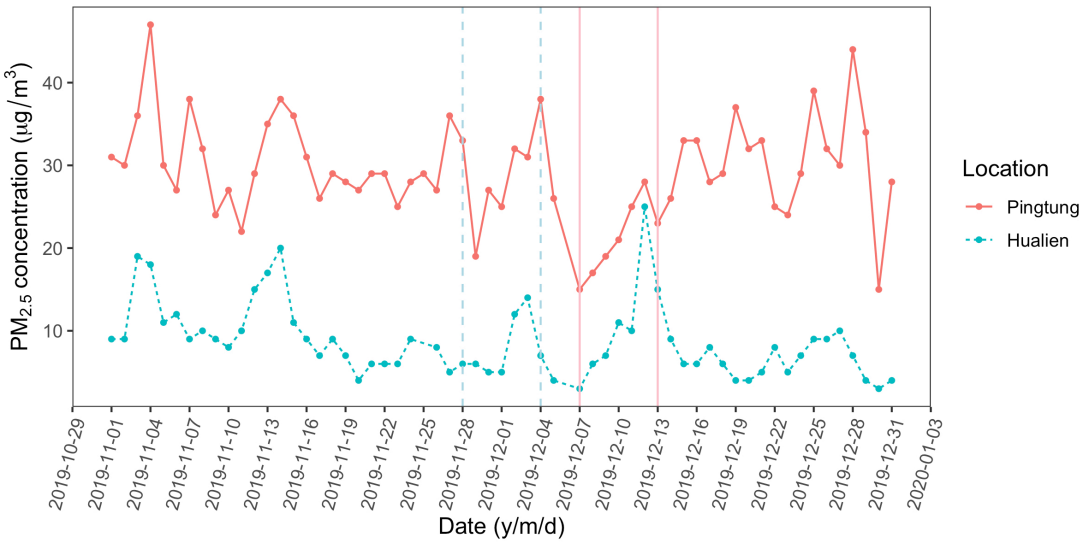

Figure 2.5. Daily monitoring data of PM2.5 in the fields while experiments were conducted.

The solid line is the Pingtung site (expectedly more polluted) and the dashed line is the Hualien site (expectedly less polluted). The vertical lines indicate the periods while experiments were conducted (Hualien site: 28 November to 4 December 2019; Pingtung site: 7 December to 13 December 2019) (Source: Taiwan Air Quality Monitoring Network, Environmental Protection Administration, Taiwan).

2.4.2 Aerosol impacts on plant water relations in the field

The high g_{min} values and the low abaxial contact angles of leaves at the Hualien site likely are connected effects of aerosol deposition. The g_{min} values were more than twice as high and the ratio between adaxial and abaxial contact angles differed compared to the Pingtung site. Although other, e.g., biotic factors cannot be excluded, both effects are likely linked to the relatively high, sea salt dominated deposition at the Hualien site. Normally, NaCl is a kosmotropic salt

that does not easily extend on hydrophobic cuticles, so coastal plants are usually not affected too much by sea salt. However, this may considerably change in the presence of detergents, as shown by a strong g_{min} increase in a previous experiment, where pine seedlings were sprayed with different salt solutions (Burkhardt & Pariyar, 2014). The detergent reduces the contact angle and promotes stomatal penetration by the salt, i.e., HAS establishment. Several cases of this process in the environment were reported in Italy and Australia, where detergents from close-by landfills caused the coating of sea-spray aerosols leading to the decline of coastal forests (Bussotti *et al.*, 1995). A similar process might actually have played a role at the Hualien site because a landfill in the major source region of NaCl aerosols had been eroded by the sea for several years (News, 2018). The occurrence of such detergents on the leaves was not measured and the distance of 50 km is considerable, but still, there is a realistic chance that the high g_{min} values and low contact angles were connected with this incidence.

Low contact angles particularly on the lower (abaxial) leaf sides of Hualien leaves point to enhanced deposition of fine, sub-micrometer aerosols, which are less affected by gravity but more by molecular mechanisms. The g_{min} parameter describes the uncontrollable water loss of leaves with closed stomata. A g_{min} increase is indicative of reduced drought tolerance and reflects the cuticular permeance, but also the contribution of “malfunctioning stomata,” which are linked to aerosols and HAS (Kerstiens, 1996; Burkhardt, 2010). The higher g_{min} values indicate that in the case of extended droughts, aerosol deposition might possibly become problematic for the trees at the Hualien site. It is not possible to deduct further impacts of aerosols on the trees from the field measurements. The $\delta^{13}C$ values between the two field sites cannot be meaningfully compared, as they are influenced by too many different environmental factors, particularly soil water availability, temperature, and VPD.

2.4.3 Aerosol impacts on plant water relations in the greenhouse

The greenhouse study with equal environmental conditions between AA and FA enables the comparison of single parameters like g_{min} or $\delta^{13}C$. Differences

between the groups can be attributed to the differences between AA and FA aerosol concentrations, as long as the AA and FA plants are physiologically comparable. This requirement was met in the present case, as seen by the comparison of A_{sat} and the AC_i curves, from which the photosynthetic parameters were extracted. These parameters were very similar between AA and FA. The higher daytime respiration R_d was consistent between AA and FA but was several times higher than at the field sites and in an earlier field study with camphor trees (Kosugi & Matsuo, 2006); possibly due to the effects of the incomparable temperature differences between the greenhouses and the fields, or the inaccuracy caused by different calculators while fitting AC_i curve data (Sharkey, 2016). It was hypothesized that physiological responses to aerosols would include higher g_{min}, less negative $\delta^{13}C$ value, lower leaf water potential at turgor loss (Bartlett *et al.*, 2012a; Marechaux *et al.*, 2015), and higher proline concentration in the AA compared to the FA greenhouse. With a similar experimental approach, aerosols had caused higher g_{min} for *Quercus petraea*, *Abies alba*, *Pinus sylvestris* (Burkhardt & Pariyar, 2014; Burkhardt *et al.*, 2018), and *Vicia faba (L.)* (Grantz *et al.*, 2018), as well as less negative $\delta^{13}C$ for second year *Abies alba* needles (Burkhardt et al., 2018), while *Helianthus annuus*, *Pinus sylvestris*, and *Fagus sylvatica* were found to have more negative $\delta^{13}C$ values (Burkhardt & Pariyar, 2016).

In this study, particularly the results of g_{min} and $\delta^{13}C$ did not confirm the hypothesis. The g_{min} results were almost identical between AA and FA greenhouses, which was about half the Pingtung values and only about one-fifth of the Hualien value. A major reason for missing significant differences probably was the small number of repetitions (n = 4). This is particularly relevant for the g_{min} parameter, where due to high variances and small effects often about 20 repetitions are required to reach significant results. The high variability probably comes from the situation that the water loss by incompletely closed, ‘leaky’ stomata is an individual process affecting single stomata, but often is the dominating pathway of water loss in the g_{min} measurement compared to water loss across the cuticle (Heinsoo & Koppel, 1998; Burkhardt, 2010; Duursma *et al.*, 2019). A study of *Hedera helix* indicated that 35% of water loss occurred

across the incompletely closed stomatal pores and 65% across the other part of the cuticle which is without stomata, and the cuticular transpiration of the stomatous leaf surface was about 11 times higher than the astomatous leaf surface (Santrucek *et al.*, 2004). Moreover, taking conifer species as research material, it is concluded that the percentage of water loss from stomatal pores of detached leaves might depend on species-specific strategies for conserving water during drought (Brodribb *et al.*, 2014). Because only few studies have found significant correlations between g_{min} and environmental factors, other procedures may be more useful under certain conditions (Brodribb *et al.*, 2014; Schuster *et al.*, 2017; Duursma *et al.*, 2019). Under less defined conditions, another possible reason for questioning the reliability of g_{min} is the acclimation of plants to the environment. In general, research has shown that plants change the chemical composition of the cuticle while facing water stress, leading to a decreased g_{min} value (Bengtson *et al.*, 1978; Premachandra *et al.*, 1992; Mackova *et al.*, 2013; Bi *et al.*, 2017). The observation that older leaves have higher g_{min} values (Jordan & Brodribb, 2007), might however be caused by the damage of cuticle on old leaves or the increasing contribution of HAS establishment and induced water loss across the stomatal pore (Burkhardt, 2010).

The discrimination value of carbon isotope composition ($\delta^{13}C$) provides information on the long term transpiration efficiency of plants, and a lower $\delta^{13}C$ value is often determined as lower WUE (Farquhar & Richards, 1984; Farquhar *et al.*, 1989; Hubick & Farquhar, 1989; Condon *et al.*, 1992; Cabrera-Bosquet *et al.*, 2007), but requires equal environmental conditions between the compared groups. However, recent studies have focused on more comprehensive and practical conditions instead of an ideal growing environment such as breeding fully fertilized plants in the greenhouse (Conte *et al.*, 2003; Cabrera-Bosquet *et al.*, 2007; Burkhardt, 2010; Berriel *et al.*, 2020; Vogado *et al.*, 2020). Thus, the correlation between $\delta^{13}C$ and WUE might be influenced by deposited aerosols and HAS, but also by soil water, the nutrient conditions, and the acclimation to stresses (Cabrera-Bosquet *et al.*, 2007; Berriel *et al.*, 2020; Tarin *et al.*, 2020), which is why the field values cannot be compared.

The hypothesis of lower leaf water potential at wilting (i.e., turgor loss point, π_{tlp}) by aerosols was also not confirmed. π_{tlp} is considered another important determinant of ecological and physiological drought tolerance, which is also strongly correlated with the cell solute potential at full hydration (i.e., osmotic potential, π_o) (Bartlett *et al.*, 2012a; Bartlett *et al.*, 2012b; Banks & Hirons, 2019). Previous research has focused on π_{tlp} of plant species such as woody species, crops, and herbaceous grassland species, concluding that this indicator of drought tolerance varied across species and environmental conditions; π_{tlp} is as well correlated slightly with several leaf functional traits such as leaf dry matter, leaf vulnerability to hydraulic failure, leaf toughness, and leaf thickness (Marechaux *et al.*, 2015; Griffin-Nolan *et al.*, 2019). Normally, a more negative π_{tlp} increases the functional range of foliar water potential, showing a greater leaf-level drought tolerance (Mart *et al.*, 2016; Banks & Hirons, 2019). Under defined conditions, a more negative π_{tlp} would thus mean that the plant had experienced drought stress by aerosols (Navarro *et al.*, 2007; Burkhardt, 2010). This should be further evaluated using experiments with higher numbers of biological repetitions, including the evaluation of an eventual accumulation of proline. Proline is an additional indicator of osmotic adjustment, responding to environmental stress such as water deficit, salinity, heat, and pollutants (Bates *et al.*, 1973; Dolatabadian *et al.*, 2008; Acosta-Motos *et al.*, 2017). In this study, the proline concentration of leaves did not differ with aerosol exposure, and concentrations in both AA and FA were relatively low.

2.4.4 Aerosols and water use efficiency

Aerosols did not decrease WUE, as it originally had been expected. Contrariwise, the VPD curve of the FA plants had higher g_{sw} values than AA, which was highly significant. The subsequently calculated Ball-Berry g_1 parameter for FA was twice the value compared to AA. Because g_{min} (which can be considered the g_0 factor of the Ball-Berry equation; Duursma *et al.*, 2019) was negligible compared to g_{sw} for both AA and FA, this means double WUE of AA compared to FA (Equation (2-4); Miner and Bauerle, 2017). The relationship between g_1 and WUE is originally linked to intrinsic WUE (A/g_s) but is also indicative of actual ("instantaneous") WUE_{photo} (A/E) (Franks *et al.*, 2017).

According to the original HAS hypothesis (Burkhardt, 2010), AA leaves should have lost more water than FA at the same degree of stomatal opening; and because this additional water loss is not accounted for by CO_2 uptake, AA leaves should have lower WUE than FA. But probably this is not the full picture and there may be several independent responses to aerosols. In an AA/FA experiment with *Vicia faba (L.)*, aerosol exposure (i.e., AA) had three effects (Grantz *et al.*, 2018):

(i) reduced stomatal apertures of *Vicia faba (L.)* at each level of VPD;
(ii) increased stomatal conductance at comparable levels of aperture;
(iii) lower heterogeneity between apertures of single pores, i.e., reduced patchiness.

In the present study with camphor, the HAS effect of additional water loss at the equal aperture (effect ii) was likely overcompensated by the aperture reduction of AA stomata (effect i). A reduction of stomatal aperture, however, is known to increase the WUE of seed plants, e.g., in response to drought stress (Franks *et al.*, 2015; Guerrieri *et al.*, 2019; Xu *et al.*, 2021; Yang *et al.*, 2021). The measured increase of WUE by aerosols thus indicates a reduction of stomatal aperture, in agreement with the results of the *Vicia faba (L.)* experiment (Grantz *et al.*, 2018; Grantz *et al.*, 2020). It is also in agreement with these earlier results that the error bars of the AA data points were smaller than for FA, indicating lower variation, higher coordination between stomatal apertures (effect iii), and less patchiness—a general susceptibility of the *C. camphora* to the stomatal patchiness phenomenon has earlier been reported (Takanashi *et al.*, 2006). The aperture reduction was not directly measured but would have been independently supported if lower $\delta^{13}C$ values of AA compared to FA leaves were observed. This was not the case, possibly because the results of the VPD curves and the $\delta^{13}C$ signals were determined by different micro-climatological conditions: The VPD curves were measured within ventilated cuvettes. The $\delta^{13}C$ values are a time integrated signal of gas exchange, produced under the calm greenhouse conditions with a thick leaf boundary layer surrounding the leaves most of the time; so stomatal responses are decoupled from the environmental VPD and its interaction with deposited aerosols.

Generally, the g_1 parameter represents a compromise between the costs and benefits of g_{sw} relative to the photosynthetic activity of the leaf (Ball *et al.*, 1987; Miner & Bauerle, 2017). The g_0 is normally defined as either (i) a fit parameter extrapolated as the intercept of the least squares regression between g_{sw} and the Ball Index (Ball *et al.*, 1987; Collatz *et al.*, 1991), or (ii) the residual conductance when $A_n \leq 0$ (Leuning, 1995). The g_1 values here were 1.71 (AA) and 3.41 (FA) and, thus, considerably lower than the value of 7.4 observed for *C. camphora* in a field study (Kosugi & Matsuo, 2006). Both g_0 and g_1 were at the lower end but still within the range of previously recorded values (Miner *et al.*, 2017; Wolz *et al.*, 2017). Drought affected plants, e.g., *Eucalyptus*, *Quercus*, *Zea mays*, and *Helianthus*, often have lower g_1 and g_0 values compared with well-watered plants of the same species (Cavender-Bares *et al.*, 2007; Heroult *et al.*, 2013; Zhou *et al.*, 2013; Miner & Bauerle, 2017; Miner *et al.*, 2017). The lower g_1 value of AA camphor leaves compared to FA can thus possibly be interpreted as aerosol induced drought stress. The reason for the involvement of Hs for plant transpiration in the original, semi-empirical Ball-Berry model has remained elusive and its relevance was questioned, compared to VPD which seems to be physiologically more meaningful (e.g., Monteith, 1995). The successful H_s use, however, might well be due to the direct interaction of hygroscopic, deposited aerosols with water vapor on the leaf surface. This kind of interaction is immediate and direct and the method to determine water absorption to specific salts has been used to determine the relative humidity in weather balloons (Wylie, 1955).

2.5 Conclusion

Fine hygroscopic aerosols are ubiquitous. Their presence on leaf surfaces often is not obvious, but the comparison of SEM images from AA and FA greenhouses is a useful method for identifying aerosol related surface structures. Greenhouse and field results behaved differently. The controlled conditions in the greenhouse aerosol exclusion study with camphor seedlings enabled a detailed perspective of aerosol interaction with the stomatal part of the water relations. Aerosols surprisingly caused higher WUE of camphor trees in the greenhouse study, which was the first detailed observation of this kind and may also have relevance on larger scales beyond the leaf-level. The sharply increased WUE of forests over the last century is a globally observed phenomenon and has mainly, but not sufficiently, been explained as a consequence of CO_2 increase (Keenan *et al.*, 2013; Knauer *et al.*, 2017; Kannenberg *et al.*, 2021). The atmospheric aerosol deposition could be a hidden, contributing factor, which should be investigated.

In the field experiment, the particular challenges came from the cumulative, long-term nature of aerosol effects and the uncontrolled environmental conditions. However, contact angles and g_{min} of leaves from the adult camphor trees were probably attributed to the amount and type of aerosols. These parameters seem to be suitable to determine aerosol effects on those parts of plant water relations which are not under stomatal control, i.e., cuticular loss and stomatal leakage by HAS. Marine aerosols, possibly polluted by organic material, might have decreased the drought tolerance of camphor trees at the Hualien site, but additional studies would be needed to confirm this.

Chapter 3

The revised version of this chapter is submitted to Plant, Cell & Environment, 2023, with the title “Plants Perceive Aerosols as an Intensification of Atmospheric Dryness and React According to their Isohydricity”.

3 Differential Stomatal Responses of Isohydric and Anisohydric Poplar Clones to Ambient Aerosols and VPD

Abstract

The atmospheric vapor pressure deficit (VPD) serves as a key driver of plant transpiration, with a pronounced influence on stomatal conductance, particularly in the case of plants with an isohydric water strategy. Hygroscopic aerosols deposited onto leaves act as localized water vapor sinks and can impact stomatal conductance through deliquescence, leading to the formation of hydraulic films within stomata. In this study, we explored the interactions between VPD, ambient aerosols, and plant water use strategies by investigating the responses of two hydroponically grown poplar clones in ventilated greenhouses, under conditions with and without ambient aerosols. This study conducted a comprehensive analysis of stomatal functions and structure.

Our findings reveal that increasing VPD resulted in a 70% reduction in stomatal conductance for the isohydric clone (ISO) and a 30% reduction for the more anisohydric clone (ANI). ISO, likely due to its sensitive VPD response and smaller stomata, exhibited higher intrinsic water use efficiency compared to ANI. Aerosols exerted distinct effects on isohydric and anisohydric poplar clones. For ANI, aerosols significantly reduced stomatal conductance, reduced stomatal aperture in long-term observation, increased water use efficiency at lower VPD, and decreased noon water potential. In the case of ISO, aerosols led to a reduction in water potential at the turgor loss point. Furthermore, aerosols were observed to reduce stomatal density by 20-25% for both clones. This study suggests the significance of considering aerosols as an independent factor contributing to atmospheric drought.

3.1 Introduction

Atmospheric aerosols are a natural part of the environment, ranging from few nanometers to about 100 µm. Deposition to vegetation is a function of aerodynamic diameter and canopy surface characteristics (Lindberg *et al.*, 1986). Particles across this size range are found on foliar surfaces. Aerosol comprises a dynamic mixture of solid and liquid particles, originating from natural sources such as sea salt, geologic dust, and volcanic ash; as well as anthropogenic sources including combustion, construction and agricultural production (Hamilton, 2015; Burkhardt & Grantz, 2017; Lu & Tian, 2017; Burkhardt *et al.*, 2018; Chappelka & Neufeld, 2018). Aerosol loading of the troposphere and deposition to terrestrial vegetation are increasing along with the hygroscopicity of ambient aerosol in the Anthropocene (Andreae, 2007), which has been shown to enhance crop canopy photosynthesis (Chameides *et al.*, 1999) and tree stem growth rates, associated with increased diffuse radiation, lower VPD, and reduced midday leaf temperatures (Steiner & Chameides, 2005; Wang *et al.*, 2018; Wang, X. *et al.*, 2021).

More than 30% of the European atmospheric aerosol mass consists of inorganic ions (mainly ammonium, sulfate, nitrate; Bressi *et al.*, 2021), often forming hygroscopic salts that deliquesce at relative humidity lower than 80%. Within the leaf boundary layer of transpiring leaves, this humidity level can easily be exceeded even during daytime (Burkhardt *et al.*, 2012). Repeated drying and rehydration of the saturated aqueous films formed lead to salt creep (Qazi *et al.*, 2019), and on the otherwise hydrophobic waxy cuticle this process is particularly effective for chaotropic ions that reduce the surface tension of water (Burkhardt & Pariyar, 2014). As a result the solutions spread across the leaf surface, as is visible in electron micrographs, eventually entering into the pores along the stomatal walls (Burkhardt & Pariyar, 2014; Grantz *et al.*, 2018). Through a process of hydraulic activation of stomata (HAS; Burkhardt, 2010), this provides a thin film pathway for liquid water flow from leaf interior towards the leaf surface, where it evaporates and is replenished from apoplastic water within the leaf. This linkage has been demonstrated repeatedly for foliar fertilization, herbicide uptake,

and nanoparticle infiltration (Eichert *et al.*, 1998; Eichert & Goldbach, 2008; Basi *et al.*, 2014).

The water flux by this pathway may be relatively small, but the resistance of the liquid pathway is not reduced by stomatal closure, which functions effectively to reduce diffusional conductance. In this way, and by increasing minimum leaf conductance (Burkhardt & Pariyar, 2016; Grantz *et al.*, 2018), aerosol deposition could reduce stomatal control over plant water loss. Under conditions of high temperature or VPD, both increasing with global change (Novick *et al.*, 2016), this uncontrolled liquid transpiration stream may reduce the tolerance of plants to increasing atmospheric and edaphic drought (Burkhardt, 2010; Burkhardt *et al.*, 2018; Grantz *et al.*, 2018).

Plants regulate diffusional loss of water vapor, the dominant component of transpiration (E) along a continuum of isohydricity, implying regulation that either favors prolonged stomatal opening, thus sustaining carbon acquisition and leaf cooling, or sensitive stomatal response to rising VPD or drying soil, thereby maintaining leaf water status (Mitchell *et al.*, 2013). Isohydric plants exhibit strict stomatal regulation with large declines in stomatal conductance (g_{sw}) and net photosynthesis (A) but minimal changes in leaf water potential (Ψ), during midday and drought. Anisohydric plants maintain g_{sw} and A across a wide range of Ψ at the risk of photosynthetic inhibition and enhanced vulnerability to hydraulic failure (Klein, 2014; Meinzer *et al.*, 2016; Meinzer *et al.*, 2017).

The interaction of the HAS enhancement of water loss and the complexity of isohydricity has received limited attention to date (Burkhardt & Pariyar, 2016). It is tested here by an aerosol exclusion experiment with hydroponically grown poplars in two parallel greenhouses, one receiving unfiltered, ambient air (AA), the other one receiving filtered air (FA) almost without aerosols. Based on previous observations with synthetic aerosol application (Burkhardt & Pariyar, 2016), we hypothesized that in isohydric plants the additional water loss created by aerosols through the HAS mechanism would further lead to early stomatal closure and thus decrease Ψ. For anisohydric plants, we hypothesized that aerosol exposure would lead to higher E and greater decrease of Ψ. Therefore,

we hypothesized that stomatal regulation in anisohydric plants would be less sensitive to aerosol impact than isohydric plants.

For the current study, we identified two clones of hybrid poplar (isohydric clone: *Populus maximowiczii x nigra* and anisohydric clone: *Populus trichocarpa x maximowiczii*; Xu *et al.*, 2018) that appeared to differ in isohydricity. We used these clones to investigate the interaction of aerosol and isohydricity effects on a suite of physiological responses, including stomatal regulation, photosynthetic, and cuticular responses of the relatively isohydric and anisohydric clones to a gradient of VPD from 0.75 to 1.75 kPa, expanding upon methods and results of Chi *et al.* (2022). Water use efficiency (WUE) and the descriptive parameters of the Ball-Berry model (Ball *et al.*, 1987) were obtained and compared with direct measurements of related parameters (Medlyn *et al.*, 2017; Yi *et al.*, 2019; Yuan *et al.*, 2019; Pieters *et al.*, 2022). Scanning electron microscopy (SEM) images were obtained to evaluate leaf surface characteristics and stomatal structures. Aerosol impacts on poplar water relations were complex and expressed differentially in these divergent clones. Implications for the diversity of aerosol effects across the landscape are discussed.

3.2 Materials and methods

3.2.1 Plant material and growth conditions

Two hybrid poplar clones (*Populus maximowiczii x nigra* and *Populus trichocarpa x maximowiczii*) were grown in hydroponic solution containing all essential nutrients. Solutions were renewed weekly to avoid nutrient depletion in the root zone. The cloned differed in isohydricity with *P. maximowiczii x nigra* (clone ISO) exhibiting greater isohydric behavior and *P. trichocarpa x maximowiczii* (clone ANI) more anisohydric responses.

Poplar seedlings (n = 24) were assigned randomly to one of two greenhouses, one ventilated with ambient air (treatment AA, n = 12), and the other with filtered air (treatment FA, n = 12). Filtration in this greenhouse system removed about 99% of ambient aerosols (Grantz *et al.*, 2018). The relative humidity and temperature of the greenhouses were recorded as described previously (Pariyar *et al.*, 2013; Burkhardt & Pariyar, 2016). Temperature and leaf to air vapor pressure deficit (VPD) in the FA greenhouse were higher and relative humidity was lower than in the AA greenhouse, due to flow restrictions associated with filtration. Average temperature in AA was 24.49 ± 0.18°C, R.H. 60.23 ± 0.50%, and VPD 1.72 ± 0.04 kPa; and in FA 25.89 ± 0.16°C, 48.47 ± 0.36%, and 2.16 ± 0.04, respectively (*Figure 3.1*).

All measurements were obtained July to August 2021 and 2022, when plants had branched and attained a height of about 160 cm. All sampling was conducted on the youngest fully-expanded leaf of each branch.

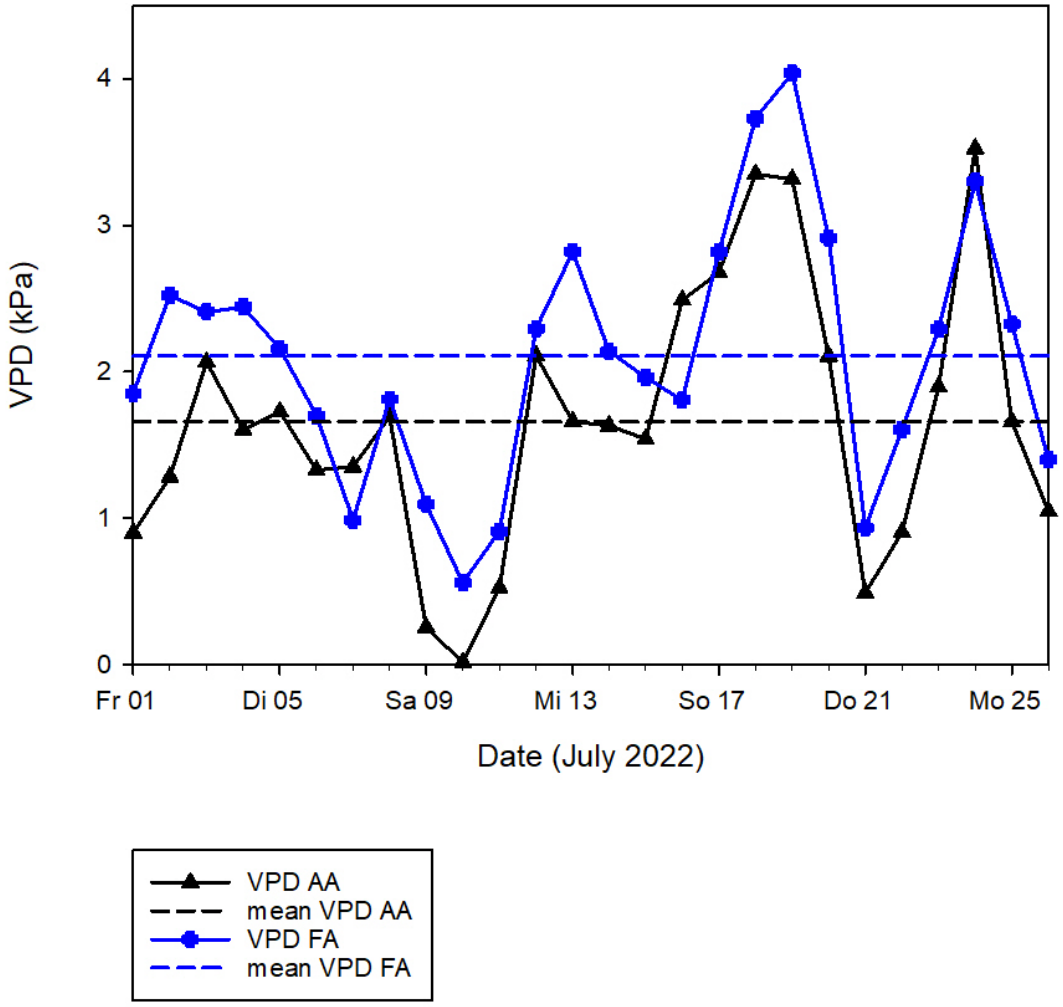

Figure 3.1. Daily values and means of VPD in the greenhouses throughout the 2022 measurements.

3.2.2 Gas exchange measurements

Photosynthetic light responses to light (A/PPFD curve) and to intercellular CO_2 concentration (A/Ci curve were measured using a Portable Photosynthesis System (LI-6800; LICOR Biosciences, Lincoln, NE, USA), using instrument settings as previously described (Chi *et al.*, 2022). Light saturated net photosynthetic rate (A_{sat}) (Herrick & Thomas, 1999; Oliveira & Penuelas, 2004), maximum carboxylation rate of Rubisco (V_{cmax}), maximum rate of electron transport for the given light intensity (J_{max}), and daytime respiration (R_d) were

extracted from these response curves, using the *plantecophys* package in R Studio (R; v. 4.0.3) (Sharkey *et al.*, 2007; Duursma, 2015).

The responses of stomatal conductance for water vapor (g_{sw}) to increasing vapor pressure deficit (VPD) at constant leaf temperature (25°C) were determined with the LI-6800. For these response curves, photosynthetic photon flux density (PPFD) was set to 1000 μmol m^{-2} s^{-1} to avoid photoinhibition, and sample cell CO_2 concentration was held constant at 400 μmol mol^{-1}. Gas exchange parameters were measured as a stepwise sequence of VPDs, as follows: 0.75 kPa (2 hr), 1.00 (1 hr), 1.25 (1 hr), 1.50 (1 hr), 1.75 (1 hr) kPa, respectively, allowing time for steady state conditions to be established.

The response curves to increasing VPD represented means of g_{sw}, E, and A at each VPD (n = 3). Additionally, g_{sw} was normalized to g_{sw} at the lowest VPD (0.75 kPa) and as the ratio of aerosol treatments at each VPD.

Intrinsic water use efficiency (WUE) (n = 3) was calculated as in Equation (3-1), at each VPD level: 0.75, 1.00, 1.25, 1.50, and 1.75 kPa, respectively (Medlyn *et al.*, 2017).

$$WUE = \frac{A_n}{g_{sw}} \tag{3-1}$$

The Ball-Berry model of gas exchange parameters (Equation (3-2)) was run using measured g_{sw} (n = 3) from the VPD curves.

$$g_{sw} = g_1 \times A_n \times \frac{H_s}{C_s} + g_0 \tag{3-2}$$

This model considers g_{sw} as a function of A_n, relative humidity at the leaf surface (H_s), and CO_2 concentration at the leaf surface (C_s, μmol mol^{-1}). The slope (g_1) and intercept (g_0) between measured g_{sw} and [$A_n \times \frac{H_s}{C_s}$] (the Ball-Berry Index) were calculated. The g_1 represents a compromise between the costs and benefits of increasing g_{sw} relative to the photosynthetic activity of the leaf. The intercept, g_0, represents an estimate of minimum leaf conductance (mol m^{-2} s^{-1})

(Ball *et al.*, 1987; Franks *et al.*, 2017; Medlyn *et al.*, 2017; Miner & Bauerle, 2017). These estimates were compared with directly measured leaf minimum conductance (g_{min}) and WUE.

To avoid artifact due to endogenous diurnal rhythms (McClung, 2006; Nozue & Maloof, 2006), all gas exchange measurements were conducted in similar hours of a day, and alternated between AA and FA.

3.2.3 Cuticular and stomatal characteristics

Leaf surfaces characteristics were visualized by scanning electron microscopy (SEM, Leo 1450VP, Zeiss, Jena, Germany). Fresh leaves were obtained from the two clones in both greenhouses, sealed in plastic zipper bags, and transferred immediately to the laboratory. Samples were sealed with laboratorial glue at the incisions to prevent water evaporation, and the surface was coated with palladium for high-vacuum SEM imaging. Images were processed using ImageJ (Schneider *et al.*, 2012).

The adaxial leaf surfaces contained few stomata. Abaxial leaf surfaces were analyzed for the length, width, and area of the stomatal complexes, and for stomatal density (n = 10).

Contact angles of 1-µl droplets of water on the cuticles were measured using a goniometer (DSA 30E; Kruess GmbH, Hamburg, Germany) (n = 18). The surface tension of the water and the contact angles were determined by the pendant drop method (Burkhardt *et al.*, 2012).

3.2.4 Indicators for stomatal responses to plant water use

3.2.4.1 Carbon isotope discrimination

The carbon isotope composition was measured with an isotope ratio mass spectrometer (IRMS, C-N-S Analyzer, and MS-2020; SerCon Ltd., Crewe, UK). The harvested fresh leaves were dried to constant weight and ground to fine powder (n = 8). 1 mg of ground sample was loaded into a tin capsule and subjected to oxidation. The purified gas stream was fractionated by gas

chromatography and the CO_2 was brought to the mass spectrometer. The ^{13}C value was calculated, and carbon isotope discrimination ($\delta^{13}C$) determined by comparison to a standard (Condon *et al.*, 2002; Burkhardt & Pariyar, 2016).

3.2.4.2 Leaf water potential at noon and at turgor loss point

Total leaf water potential was obtained at noon (ψ_{noon}, MPa). Fresh leaves were wrapped in aluminum foil then excised from both clones in both greenhouses. Samples were obtained in succession immediately prior to measurement. Scholander Pressure Chamber (Model 3005, Soil Moisture Equipment Corp., Santa Barbara, CA, USA) (n = 5) as previously described (Pariyar *et al.*, 2013; Chi *et al.*, 2022).

Leaf water potential at the turgor loss point (π_{tlp}, MPa) was determined using the method of (Bartlett *et al.*, 2012a). Leaf discs were prepared from excised fresh leaves with a 6 mm diameter cork borer Discs were quick-frozen in liquid nitrogen to fracture the cell walls (n = 8) and punctured to disrupt the cuticle, and then rapidly sealed in a vapor pressure osmometer (VAPRO 5600, Wescor, Inc, Logan, UT, USA). The osmolality (mmol kg^{-1}) was recorded at equilibrium, and converted to osmotic potential (π_o, MPa) using the Van't Hoff Equation (3-3). C_o is the molar solute concentration (mmol kg^{-1}), R is the universal gas constant (m^3 MPa K^{-1} mol^{-1}), and T is temperature (K) (Khare, 2015). Based on the strong correlation between π_o and π_{tlp} (R^2 = 0.91), π_{tlp} was calculated using Equation (3-4) (Bartlett *et al.*, 2012b; Sjoman *et al.*, 2015; Banks & Hirons, 2019).

$$\pi_o = -C_o \times R \times T \quad (3\text{-}3)$$

$$\pi_{tlp} = -0.2554 + 1.1243 \times \pi_o \quad (3\text{-}4)$$

3.2.4.3 Minimum leaf conductance

Fresh leaves were excised from both clones in both greenhouses (n = 6). The petioles were sealed with molten paraffin. Leaves were held in darkness and weighed every 90 minutes using a digital balance (EX125M, EXPLORER TSEMIMICRO, Ohaus Corporation, Parsippany, NJ, USA; 120 g x 0.01 mg). Temperature and humidity were continuously recorded to determine VPD and leaf area was analyzed with ImageJ. Minimum leaf conductance (g_{min}, mmol m^{-2} s^{-1}) was calculated as described (Sack & Scoffoni, 2011; Duursma *et al.*, 2019).

3.2.5 Data processing and statistical analysis

Based on preliminary research (Chi *et al.*, 2022), the minimum sample size to achieve an alpha of 0.05 and power of 80% of each measurement was estimated by using the *pwr* package in R Studio (R version 4.0.3). The sample size then resulted in the range from n = 3 to 8. The Shapiro–Wilk test was used to test data for normality. The F-test or Fligner–Killeen test was performed to compare the homogeneity of variances. For normally distributed data, mean separation was evaluated by two-tailed Student's t-test. For non-normally distributed data, the difference between medians was evaluated nonparametrically using the Wilcoxon–Mann–Whitney U-test (Sokal, 1982). Statistical analysis and visualization were performed utilizing R Studio. Significant differences are shown as asterisks ($p < 0.001$ ***; < 0.01 **; < 0.05 *), otherwise as p values.

3.3 Results

3.3.1 Effects of aerosol exposure on isohydric poplar in 2021

The results of exploratory measurements indicated that growth of poplar clone, ISO, in the presence of ambient aerosol (AA treatment) included several parameters associated with increased water deficit (*Table 3.1*), relative to plants grown in aerosol-free filtered air (FA treatment). Osmotic adjustment, reflected in the turgor loss point, π_{tlp}, and stomatal density, a developmentally determined morphological parameter, were lower in AA, while minimum leaf conductance, g_{min}, was higher (*Table 3.1*). The $\delta^{13}C$ values, reflecting long-term restriction of stomatal conductance, g_{sw}, and often a sign of water deficit, did not differ between the two growth environments.

Table 3.1. Effect of aerosol exposure on long-term indicators of water deficit in clone ISO in 2021.

Indicator (unit)		With aerosols	n	Without aerosols	n	Significance
$\delta^{13}C$		-32.7 ± 0.14	29	-32.8 ± 0.13	20	p = 0.60
π_{tlp}	(MPa)	-2.92 ± 0.04	24	-2.58 ± 0.05	24	***
g_{min}	(mmol m^{-2} s^{-1})	2.53 ± 0.09	28	2.12 ± 0.12	19	**
St. Density	(amount mm^{-2})	225.00 ± 14.91	10	265.00 ± 11.30	10	*

Values are means ± s.e., with significant differences (t-test) at p < 0.001 ***; < 0.01 **; < 0.05 *.

These preliminary observations, indicating that long-term aerosol exposure might degrade plant water relations, suggested that further in-depth studies would be informative.

3.3.2 Effects of aerosol exposure on isohydric poplar in 2022

Table 3.2. Effect of aerosols on indicators of long term water deficit in ISO in 2022.

Indicator (unit)		With aerosols	n	Without aerosols	n	Significance
$\delta^{13}C$		-28.27 ± 0.25	8	-28.77 ± 0.40	8	p = 0.29
π_{tlp}		-3.22 ± 0.06	8	-2.85 ± 0.14	8	*
ψ_{noon}	(MPa)	-1.17 ± 0.05	5	-1.07 ± 0.05	5	p = 0.21
g_{min}	(mmol m^{-2} s^{-1})	1.39 ± 0.14	6	1.19 ± 0.11	6	p = 0.28
St. Density	(amount mm^{-2})	215.91 ± 13.60	10	290.00 ± 12.47	10	***
St. Length	(µm)	21.33 ± 0.56	10	20.47 ± 0.44	10	p = 0.25
St. Width	(µm)	13.86 ± 0.46	10	12.33 ± 0.30	10	*
St. Area	(μm^2)	239.53 ± 8.57	10	236.02 ± 11.79	10	p = 0.81
St. Coverage	(%)	5.19 ± 0.40	10	6.84 ± 0.46	10	*
Contact angle	Adaxial (°)	97.33 ± 3.33	19	97.03 ± 2.17	18	p = 0.73
	Abaxial (°)	107.98 ± 1.81	18	106.94 ± 1.46	19	p = 0.66
A_{sat}	(µmol m^{-2} s^{-1})	25.28 ± 2.08	3	23.22 ± 2.30	3	p = 0.54
V_{cmax}	(µmol m^{-2} s^{-1})	112.75 ± 9.19	3	97.46 ± 6.16	3	p = 0.24
J_{max}	(µmol m^{-2} s^{-1})	157.19 ± 10.42	3	130.11 ± 5.21	3	p = 0.08
R_d	(µmol m^{-2} s^{-1})	0.88 ± 0.17	3	1.11 ± 0.22	3	p = 0.45

Values are means ± s.e., (except the adaxial contact angle is presented as median ± s.e. of medians) with significant differences (t-test except U-test for the adaxial contact angle) at p < 0.001 ***; < 0.01 **; < 0.05 *.

A more extensive set of potential indicators of long-term plant water deficit was evaluated in the same clone, ISO, in 2022 (*Table 3.2*). Confirming the preliminary studies in the previous year, values of π_{tlp} and stomatal density were lower in the AA plants. The g_{min} values were generally lower in 2022, the increase of the mean value with aerosol effect was to a similar percentage (17%); with fewer repetitions than in 2021, the increase was not significant (p = 0.28). Mean values of $\delta^{13}C$ were less negative, and ψ_{noon} more negative, in AA than FA (p = 0.29 and 0.21, respectively; *Table 3.2*).

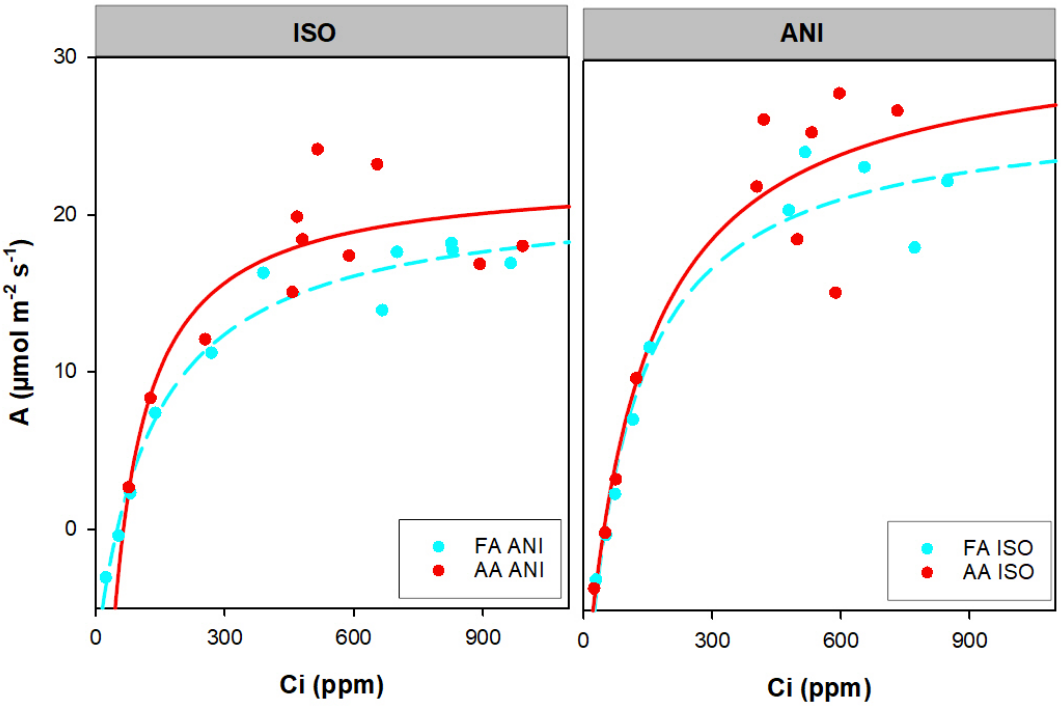

Figure 3.2. Response of carbon assimilation (A) to intercellular CO_2 concentration (C_i).

AC_i curves of two poplar clones grown with and without aerosols. Lines are rectangular hyperbolae fitted to averages (n = 3) of A and C_i at each of 9 target C_i levels.

Responses of assimilation rate (A) to intercellular CO_2 (A/C_i response curves; *Figure 3.2*) allowed calculation of the photosynthetic parameters, A_{sat}, V_{cmax}, J_{max}, and R_d in clone ISO. A was somewhat greater in AA than FA (*Table 3.2*). A_{sat} and R_d were unaffected by aerosol, while J_{max} was about 20% greater in AA ($p = 0.08$) and V_{cmax} was 16% greater ($p = 0.24$). These markers of dark and light photosynthetic competence may also reflect differences in long term plant water status.

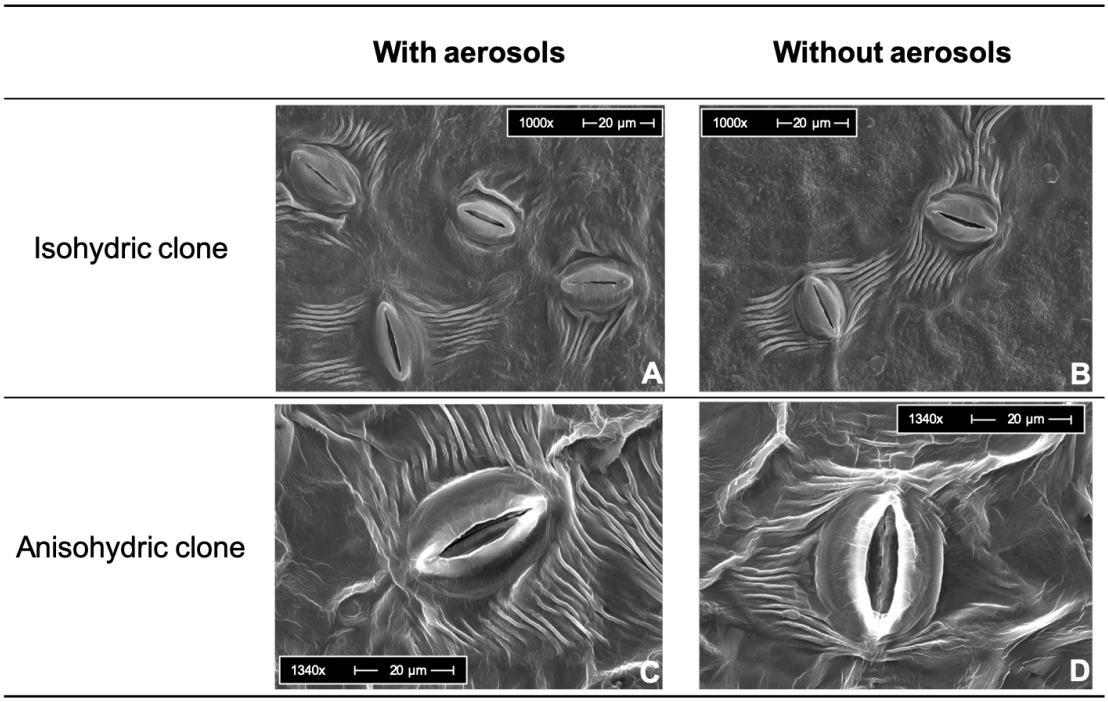

Figure 3.3. Scanning electron microscopy images on abaxial surfaces.

SEM images of two poplar clones grown in greenhouses with and without aerosols, the magnification and the scale are defined in each figure.

Scanning electron micrographs were obtained (*Figure 3.3*A, B) on abaxial surfaces of ISO to investigate effects of aerosol exposure on epidermal morphology (*Table 3.1*, *Table 3.2*). In AA ISO plants the surface morphology is only slightly striated, though local ridges are observed near the stomatal pore (*Figure 3.3*A). In FA ISO plants, the striations are clearly visible (*Figure 3.3*B). In

AA ANI plants, the stomatal pore is observed to be smaller than FA ANI plants. In both clones, the mean stomatal density, width and percent covered area were greater in the AA plants.

Robust stomatal closure with increasing VPD is a defining characteristic of isohydric behavior. This pronounced closure in ISO may have masked small aerosol effects on g_{sw} and other parameters. Therefore, responses to AA of a closely related, anisohydric poplar clone, ANI, were investigated.

3.3.3 Effects of aerosol exposure on anisohydric poplar in 2022

A similar extensive set of potential indicators of long term water deficit were obtained in the anisohydric clone, ANI (*Table 3.3*). The $\delta^{13}C$ was higher (i.e., less negative), while ψ_{noon} was lower (i.e., more negative), in AA than FA. π_{tlp} of ANI was lower (more negative) in AA, though not significantly. The mean value of g_{min} was substantially, though not significantly, greater in AA ($p = 0.09$) and $\delta^{13}C$ was higher (i.e., less negative), while ψ_{noon} was lower (i.e., more negative), in AA than FA (*Table 3.3*).

The photosynthetic parameters obtained from A/C_i response curves (*Figure 3.2*B), A_{sat}, J_{max}, and R_d, were not affected by aerosol in ANI (*Table 3.3*), but V_{cmax} was a third higher in AA than FA ($p = 0.11$).

Scanning electron micrographs of the abaxial surfaces of ANI (*Figure 3.3*C, D) showed similar striations in AA and FA. The ANI stomata were generally larger than ISO stomata and had lower density. Again, stomatal density and stomatal coverage were lower in AA ($p = 0.07$ and 0.09, respectively). Stomatal length and width did not vary with aerosol in ANI.

Table 3.3. Effect of aerosols on indicators of long term water deficit in ANI in 2022.

Indicator (unit)		With aerosols	n	Without aerosols	n	Significance
$\delta^{13}C$		-28.99 ± 0.29	8	-30.37 ± 0.38	8	**
π_{tlp}		-2.89 ± 0.10	8	-2.78 ± 0.06	8	p = 0.37
ψ_{noon}	(MPa)	-1.09 ± 0.06	5	-0.79 ± 0.08	5	*
g_{min}	(mmol m^{-2} s^{-1})	0.52 ± 0.15	6	0.22 ± 0.02	6	p = 0.09
St. Density	(amount mm^{-2})	120.45 ± 11.09	10	152.50 ± 12.61	10	p = 0.07
St. Length	(µm)	36.51 ± 0.77	10	36.41 ± 0.53	10	p = 0.91
St. Width	(µm)	25.26 ± 1.15	10	26.47 ± 0.51	10	p = 0.37
St. Area	(µm ^{2})	762.08 ± 40.88	10	795.44 ± 20.75	10	p = 0.49
St. Coverage	(%)	9.31 ± 1.11	10	12.22 ± 1.12	10	p = 0.09
Contact angle	Adaxial (°)	102.85 ± 0.99	17	100.66 ± 1.26	19	p = 0.19
	Abaxial (°)	109.30 ± 1.32	16	110.13 ± 1.13	16	p = 0.64
A_{sat}	(µmol m^{-2} s^{-1})	18.91 ± 3.11	3	19.39 ± 0.78	3	p = 0.89
V_{cmax}	(µmol m^{-2} s^{-1})	89.39 ± 5.21	3	67.35 ± 9.58	3	p = 0.11
J_{max}	(µmol m^{-2} s^{-1})	103.96 ± 5.72	3	96.56 ± 15.58	3	p = 0.68
R_d	(µmol m^{-2} s^{-1})	1.02 ± 0.32	3	0.94 ± 0.05	3	p = 0.83

Values are means ± s.e., (except $\delta^{13}C$ is presented as median ± s.e. of medians) with significant differences (t-test except U-test for $\delta^{13}C$) at p < 0.001 ***; < 0.01 **; < 0.05 *.

3.3.4 Relative magnitude of aerosol effects on different clones

In these data it became clear that ISO was generally less affected by aerosol than ANI. To visualize these differences, the values of selected parameters for each clone in AA were normalized by the mean value of the same parameter in FA (*Figure 3.4*A-F).

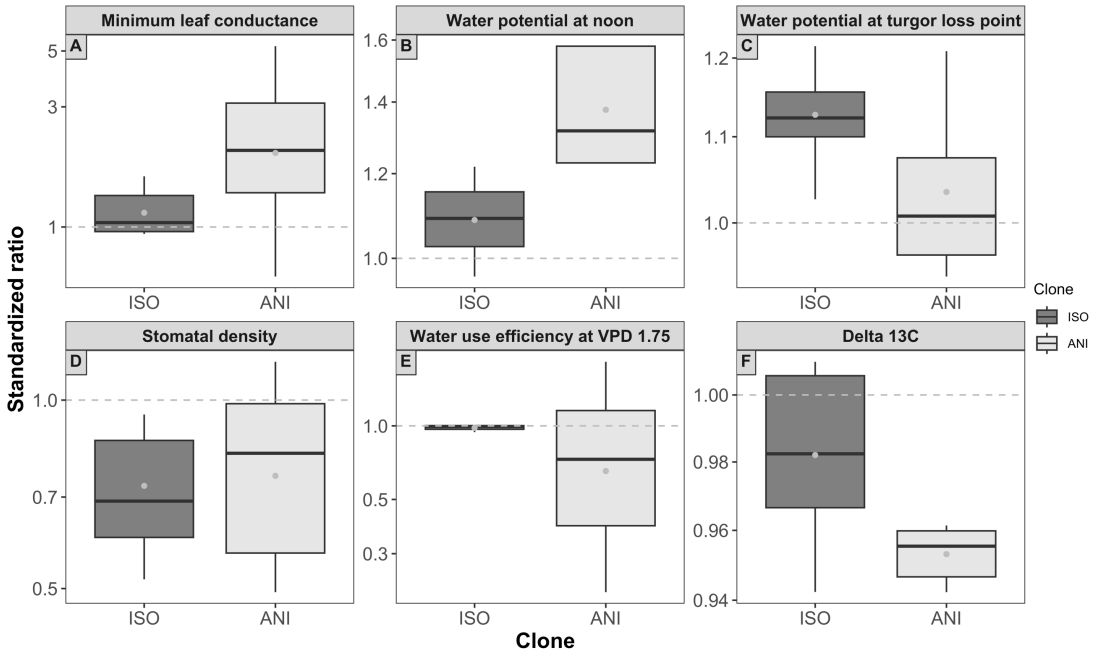

Figure 3.4. Relative magnitude of aerosol effects in two poplar clones.

Ratios were obtained by normalizing individual values obtained in AA by the within-clone mean of the respective parameter in FA . The box represented the 50% of the central data, starting from the first quartile and ending in the third, with the inner line of median and the dot of mean value. The outer line on each side of the box showed the furthest data without counting outliers.

Aerosol effects on g_{min}, ψ_{noon}, WUE (observed at VPD = 1.75 kPa), and $\delta^{13}C$ (*Figure 3.4*A, B, E, F) were all more pronounced (i.e. farther from the horizontal line at “ratio = 1”) in ANI than in ISO. In contrast, π_{tlp} and stomatal density exhibited greater response to aerosol in ISO than in ANI (*Figure 3.4*C, D).

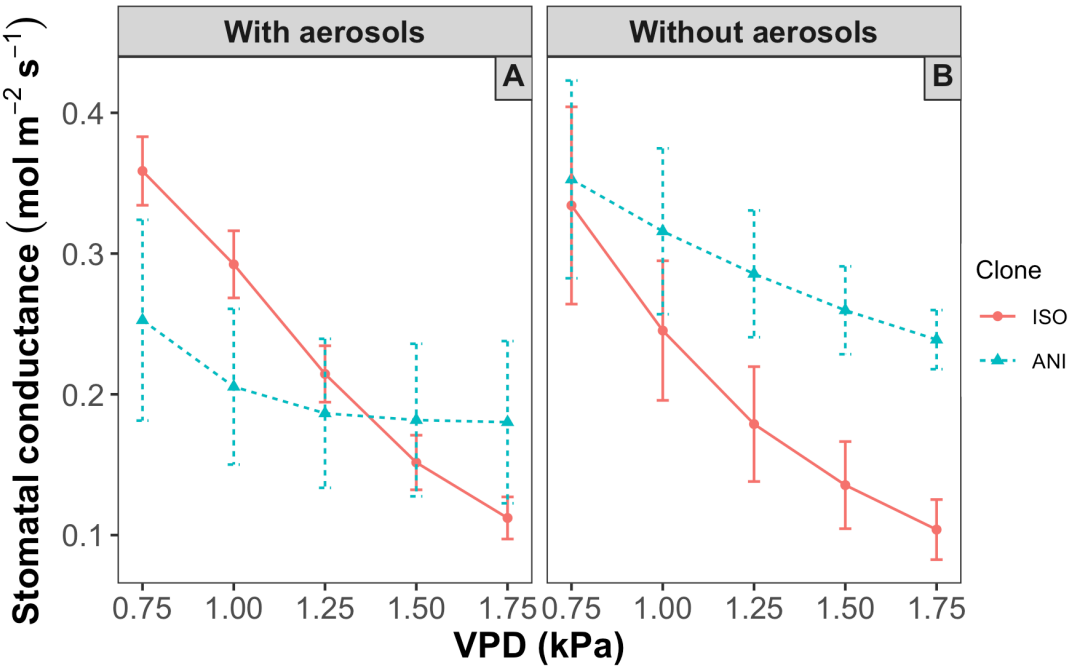

Figure 3.5. Response of stomatal conductance (g_{sw}) to VPD.

g_{sw} to VPD response curves of two poplar clones grown with and without aerosols. Data are means ± s.e. (n = 3).

Effect of aerosol exposure on the stomatal responses to increasing VPD differed in the two clones (*Figure 3.5*A, B). The ISO clone exhibited a monotonic decline of g_{sw} of 69% in both AA and FA (*Figure 3.5*). The ANI clone exhibited a much smaller response to aerosol, although g_{sw} at all VPD levels was reduced by AA. The decline in g_{sw} with increasing VPD resulted in a similar decrease of 29% and 32%, respectively, in g_{sw} of AA and FA. Thus in both aerosol treatments, the relative response of ANI was substantially less than of ISO.

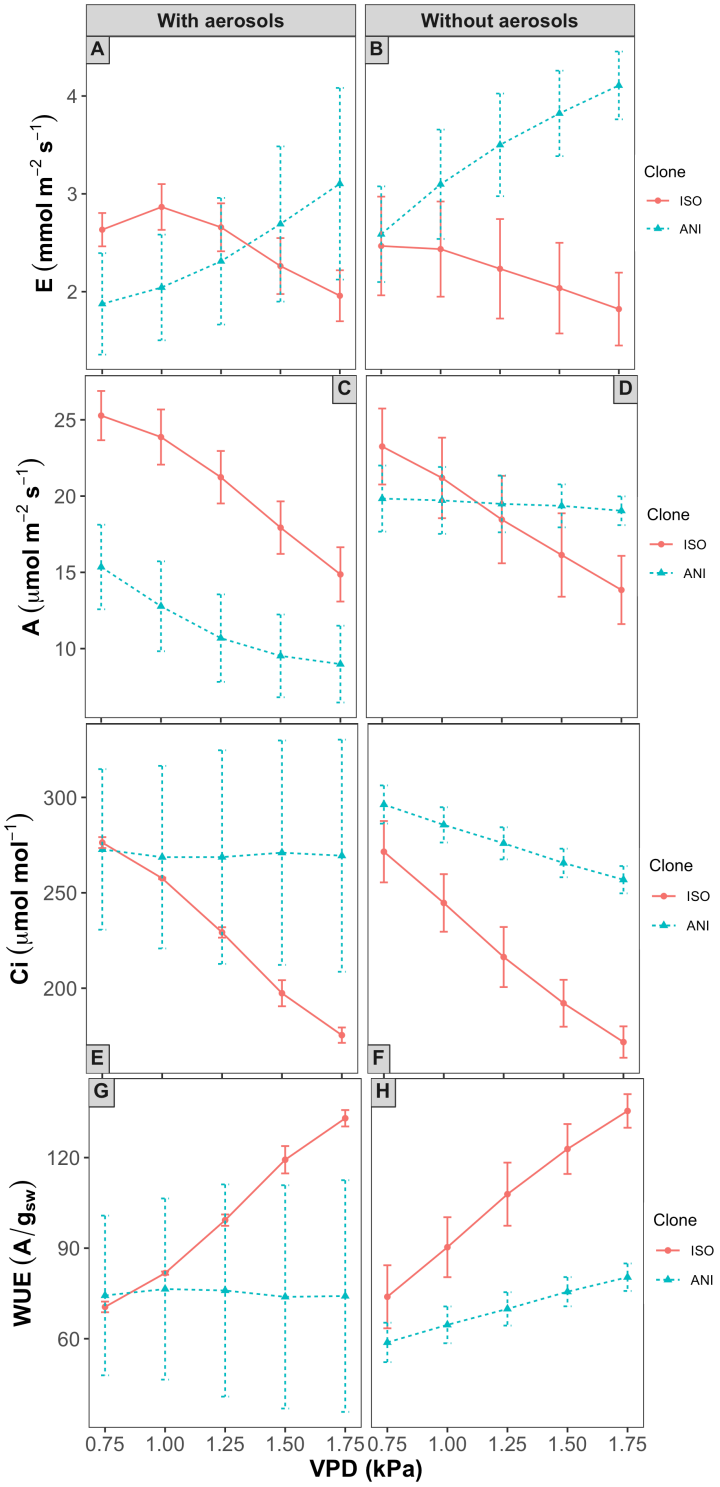

Figure 3.6. Effect of aerosol exposure on the response of E, A, Ci, and intrinsic water use efficiency, WUE, to increasing VPD of two poplar clones.

Transpiration rate (A, B); Assimilation rate (C, D); Intercellular CO_2 concentration (E, F); Intrinsic water use efficiency (G, H). Data are means ± s.e. (n = 3).

Increasing evaporative demand (increasing VPD at constant T) caused the transpiration rate (E, mmol m^{-2} s^{-1}; *Figure 3.6*A, B) to increase sharply and monotonically in the anisohydric clone, ANI. In contrast, E of ISO exhibited a biphasic response with little change at moderate VPD but declining below the level of E at low VPD as VPD increased above 1.25 kPa (*Figure 3.6*A, B).

Assimilation rate (A) of ANI was reduced in AA at all VPD levels relative to FA (*Figure 3.6*C, D). In ISO, aerosol had little effect on the magnitude nor on the substantial decline of A with increasing VPD. Aerosol had a profound effect on the response of ANI to VPD (cf. *Figure 3.6*C, D). A declined by a third with increasing VPD in AA but was stable across this range of VPD in FA.

Intercellular CO_2 concentration (C_i) of ISO was strongly reduced by VPD but did not change by aerosol. Aerosol influence on C_i of ANI was not distinguishable due to large variability between repetitions in AA. C_i of FA showed a moderate decrease with increasing VPD (*Figure 3.6*E, F).

Intrinsic water use efficiency (WUE, A/g_{sw}) of ISO increased substantially with rising VPD, in both FA and AA (*Figure 3.6*G, H). In ANI, WUE response to VPD was not distinguishable in AA (*Figure 3.6*G) and a modest increase in FA.

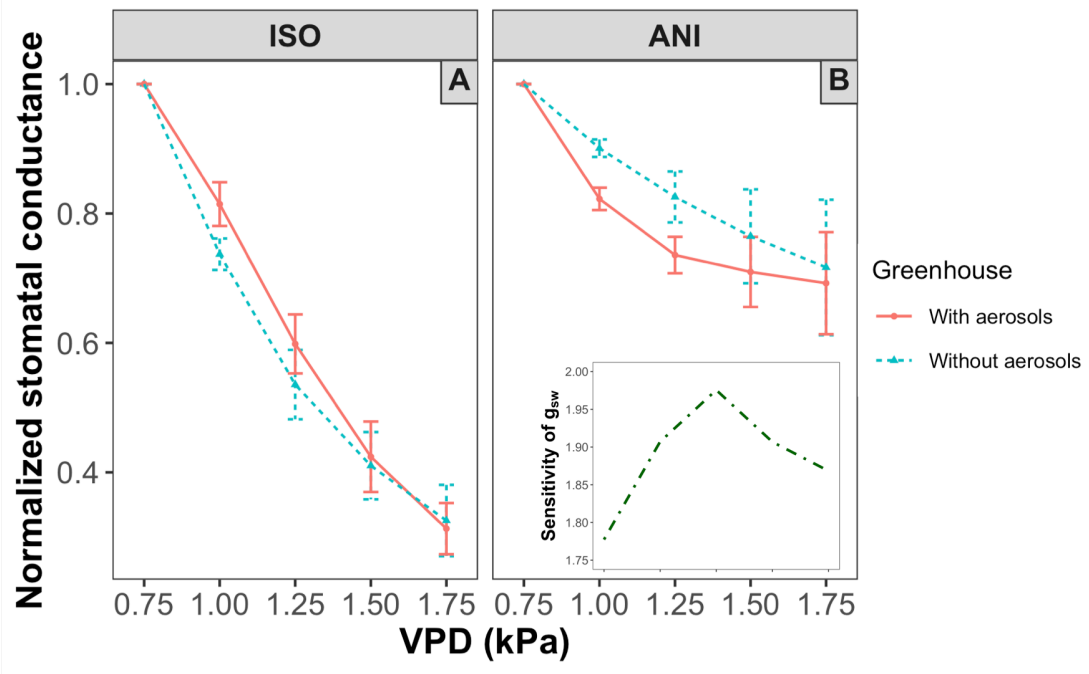

Figure 3.7. Response of g_{sw} to VPD (normalized).

g_{sw} to VPD response curves of two poplar clones grown with and without aerosols, normalized within each curve to the value at VPD = 0.75 kPa. Data are means ± s.e. (n = 3). Sensitivity of g_{sw} in ANI, estimated from g_{sw} (FA/AA, data from *Figure 3.5*) is additionally demonstrated in the side figure in B. Data are means ± s.e. (n = 3).

When normalized to their values at low VPD (*Figure 3.7*A, B; data from *Figure 3.5*A, B), the aerosol effect on g_{sw} of ISO was negligible, with a similar reduction at each VPD in both aerosol treatments. The final reduction was about 70%. In ANI, in contrast, the relative decline was greater at moderate VPD in the presence of aerosol, with recovery to a similar relative decline of about 30% at high VPD in both AA and FA (*Figure 3.7*B).

A biphasic nature of the sensitivity of the response of g_{sw} to aerosol with increasing VPD was emphasized in ANI (side figure in *Figure 3.7*B). In both clones, the greatest sensitivity was observed at moderate VPD.

3.3.5 The Ball-Berry model

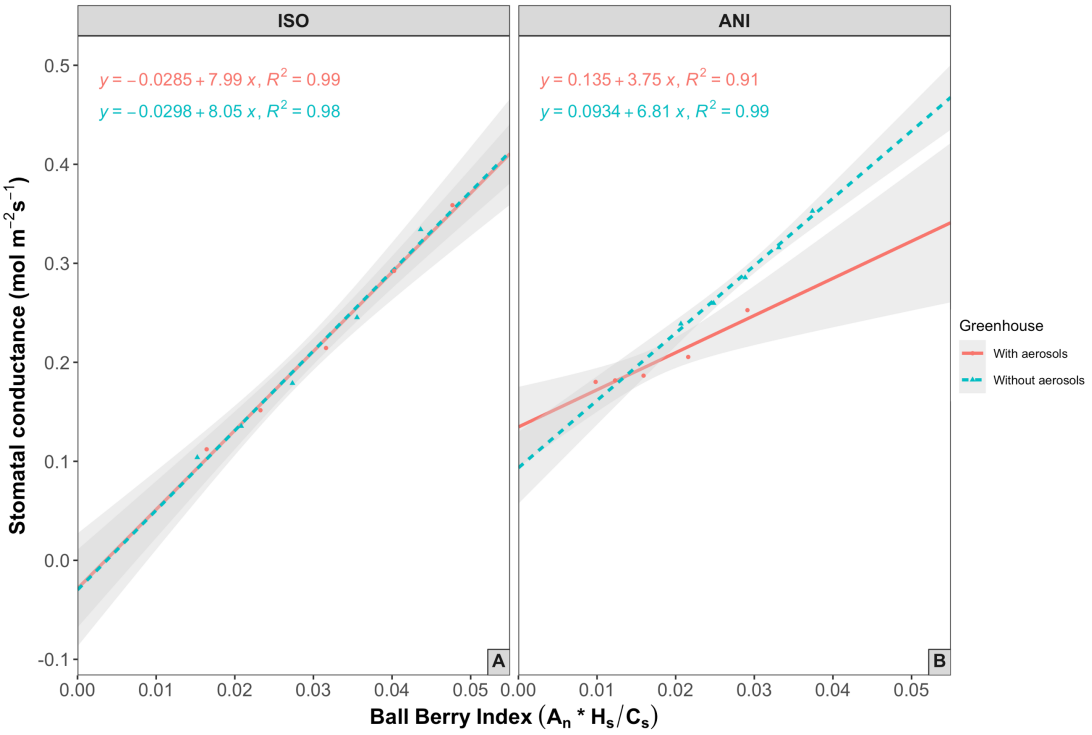

Figure 3.8. Ball-Berry Model of two poplar clones.

Relationship between measured stomatal conductance and the Ball-Berry Index for leaves from two poplar clones, grown with and without aerosols. The lines represent linear functions fitted to means (n = 3) of g_{sw} and the B-B Index calculated at each level of VPD. Shaded areas indicate 95% confidence intervals.

The broadly applicable Ball-Berry model of g_{sw} yields a central parameter, the B-B Index (A_n*H_s/C_s), that is related to measured g_{sw} through a linear slope, g_1, and intercept, g_0. In ISO there were significant linear relationships between g_{sw} and the B-B Index, but these relationships were not significantly affected by aerosol exposure. In ANI, however, the significant linear relationships between g_{sw} and the B-B Index ($R^2 > 0.90$), exhibited different slopes (g_1) that was reduced by about half with aerosol exposure ($p < 0.005$). The intercept of g_{sw} at B-B Index = 0 was somewhat greater in AA than in FA.

The sensitivity of g_0 to aerosol was greater in ANI than in ISO. This pattern in g_0 (*Figure 3.9*B), a measure of minimal g_{sw} when A = 0, was similar to that observed in the directly measured g_{min} (cf. *Figure 3.4*A, *Figure 3.9*B). Similarly, the sensitivity of g_1 was greater in ANI, similar to the directly measured WUE (cf. *Figure 3.4*E, *Figure 3.9*A).

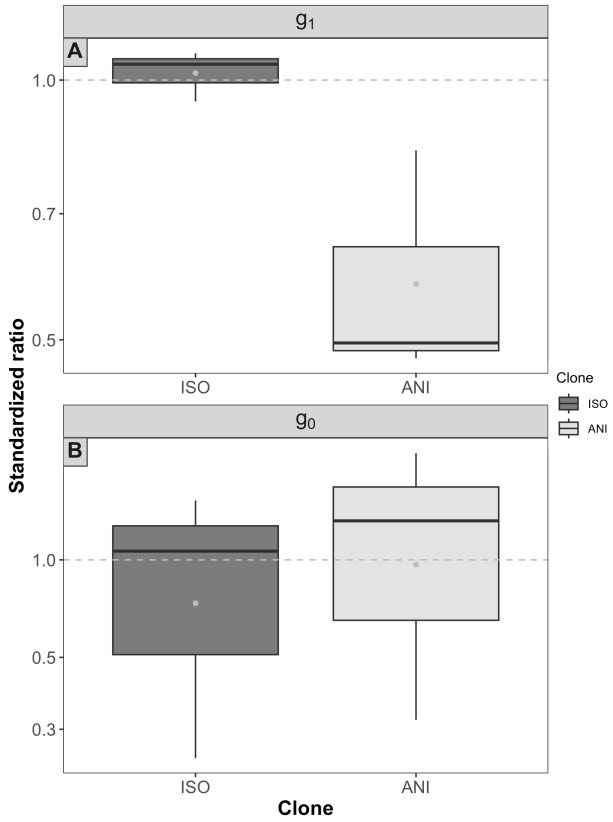

Figure 3.9. Relative magnitude of aerosol effects on parameters (A: g_1; B: g_0) of the Ball-Berry Model of g_{sw} in two poplar clones.

Ratios were obtained by normalizing individual values in AA by the within-clone mean of the respective parameter in FA. Each box represents the first and third quartile. The line is the median and the dot is the mean. The whiskers represent all data after removal of outliers.

3.4 Discussion

3.4.1 Plant water status

Exposure to ambient aerosol (AA treatment) enhanced symptoms of long term water deficit in both clones. These were consistent with other experiments, in which hygroscopic material was deposited either naturally or experimentally as a spray, and transpiration was recorded by sap flow (Burkhardt & Pariyar, 2016) or by leaf gas exchange (Burkhardt *et al.*, 2001; Grantz *et al.*, 2018).

Morphological changes, including reduced stomatal density and reduced percent coverage of the foliar surface by stomatal complexes, were observed in both clones in AA. Stomatal density has been negatively correlated with VPD and long-term water status in poplar (Miyazawa *et al.*, 2006; Monclus *et al.*, 2006) and other species (Silva *et al.*, 2009; Caine *et al.*, 2019). In the current study, stomatal density was reduced in both clones by >20%. These changes were significant in the more isohydric clone, ISO, and nearly so in the closely related anisohydric clone, ANI.

The mean of osmotic potential at turgor loss (π_{tlp}; a measure of osmotic adjustment to long term water deficit) was more negative in both clones in AA. The response was larger in ISO, significant in both years. Adjustment of π_{tlp} has been related to plant drought tolerance (Marechaux *et al.*, 2015) and to anisohydric water use strategies under soil drought conditions (Eller *et al.*, 2016; Nolan *et al.*, 2017), but here was more evident for ISO than ANI.

The greater osmotic adjustment in ISO suggests greater metabolic sensitivity to water deficit in the isohydric clone than in ANI, rather than more sustained water deficit. For example, the reduced π_{tlp} in ISO was associated with greater stomatal closure with increasing VPD (McDowell, 2011; Martinez-Vilalta & Garcia-Forner, 2017). Furthermore, and in contrast to π_{tlp}, water potential at midday (ψ_{noon}) was lower (more stressed) in both clones in the presence of aerosol, with greater and significant response in ANI, consistent with its anisohydric strategy (Klein, 2014; Meinzer *et al.*, 2016). The lower leaf water status reflected, at least in part, the additional liquid phase transpiration

associated with aerosol deposition. The less responsive stomata of ANI still responded to the additional flux, as noticeable from δ^{13}C values, but did not avoid further depression of ψ_{noon}.

A direct effect of aerosol deposition was observed in the increased magnitude of g_{min}, in AA in both clones, significantly in ISO and nearly so in ANI which exhibited a greater but more variable response (*Figure 3.4*). This is a measure of epidermal water loss under conditions of full stomatal closure and zero photosynthesis. This unregulated water loss may be a contributing factor to the long term reduction of plant water potential by aerosol exposure (Räsch *et al.*, 2018; Duursma *et al.*, 2019). An analytical approach to this minimal conductance, the mean value of intercept (g_0) of g_{sw} in the Ball-Berry relationship, was also greater in AA than in FA with ANI, consistent with the directly measured g_{min} ($p = 0.09$).

The increase of g_{min} by aerosol is consistent with previous results (Burkhardt & Pariyar, 2014; Grantz *et al.*, 2018) and reflects the presence of a parallel liquid transpiration pathway suggested by the HAS hypothesis. Alternative mechanisms of increased g_{min}, such as increased cuticular conductance in the AA greenhouse due to the slightly lower temperature and resulting higher relative humidity may be contributory (Tredenick *et al.*, 2018). However, the g_{min} measurements from both treatments were obtained under the same laboratory conditions over a period of several hours, equalizing cuticular conductance, and previous studies with multiple species in this same ambient exposure system demonstrated that E was increased by aerosol (Burkhardt *et al.*, 2001; Grantz *et al.*, 2018).

3.4.2 Stomatal regulation

Aerosol deposition and varying VPD are ubiquitous in the plant environment, and must be integrated by plant responses. The clones differed widely in stomatal regulation as evaporative demand (VPD) was varied, but both responded with pronounced stomatal closure. The ISO clone exhibited a large and continuous decline (70%) in g_{sw} with VPD in both AA and FA and the magnitude of g_{sw} was unaffected by aerosol. The incremental water loss due to the HAS pathway had little effect on these large stomatal movements. However, due to greater

sensitivity to water deficit in the isohydric clone, long term markers of water deficit responded vigorously to the additional drying influence of aerosol deposition.

The ANI clone exhibited reduced g_{sw} in AA at all VPD and a smaller absolute response to VPD (25% in both aerosol environments). The significantly lower water potential at midday in ANI in AA occurred despite this greater stomatal adjustment to aerosol exposure. The plants were grown hydroponically, with unlimited access to water in the root environment. The greater water deficit at midday in AA suggests a role for hydraulic conductance, presumably in the leaf which appears to be limiting (Kleaf; Brodribb & Holbrook, 2003; Sack *et al.*, 2003; Nolan *et al.*, 2017). This was not evaluated here.

Robust stomatal closure with increasing VPD is a defining characteristic of isohydric behavior (Tardieu & Simonneau, 1998; Schultz, 2003; Meinzer *et al.*, 2014; Skelton *et al.*, 2015; Martinez-Vilalta & Garcia-Forner, 2017). The sensitive stomatal behavior in ISO was associated with a higher density of smaller stomata. These characteristics have been linked to rapid stomatal dynamics in poplar (Durand *et al.*, 2019), an adaption that may reduce risk of hydraulic failure in episodically dry environments (Hetherington & Woodward, 2003; Drake *et al.*, 2013; Rosso *et al.*, 2023). However, these sensitive stomata did not respond to aerosol exposure. We speculate that the highly reactive but poorly tuned response to VPD in ISO was insensitive to the small additional demand for water due to the aerosol-mediated liquid transpiration pathway. In contrast, the less responsive stomata of ANI (25% decline with VPD) exhibited an aerosol-induced reduction in g_{sw} at all levels of VPD. The stomatal strategy of ANI may be less reactive but more sensitive to this incremental flux.

WUE is driven by relative changes in A and E. WUE of clone ANI was generally lower than of ISO, and the difference was significant at VPD above 1.25 kPa in FA aerosol environments. Intrinsic water use efficiency (WUE, A/g_{sw}) of ISO increased substantially with rising VPD, in both FA and AA, and was not affected by aerosol. In ANI, however, WUE increased modestly with VPD in FA, was unaffected by VPD in AA, yet was increased by aerosol, as indicated by the lower g_1. This reflected the contrasting extents of stomatal closure and resulting

responses of E and A (Hetherington & Woodward, 2003). Transpiration, E, increased with VPD in ANI, but was relatively stable in ISO, exhibiting a "feedforward" response of g_{sw} to evaporative demand (Buckley, 2005) above 1.25 kPa. Aerosol exposure reduced A_n of ANI at all VPD, but had little effect in ISO. These responses of A were associated with parallel changes in g_{sw} and C_i.

In ISO, the slope (g_1) between measured g_{sw} and the Ball-Berry Index (*Figure 3.8*) was unaffected by aerosol, but g_1 was reduced in ANI. Thus the sensitivity of g_1 reflected that of the directly measured WUE, supporting use of this parameter as a predictor of WUE (Knauer *et al.*, 2017; Miner & Bauerle, 2017).

Photosynthetic carbon isotope discrimination, integrating the g_{sw} under which carbon fixation occurred (Farquhar & Richards, 1984), was reduced (i.e., $\delta^{13}C$ was less negative) in AA than FA in both clones, significantly so in ANI. Less negative $\delta^{13}C$ indicates reduced stomatal opening, typically associated with water deficit, reduced g_{sw}, and increased WUE (Marron *et al.*, 2005; Monclus *et al.*, 2006; Broeckx *et al.*, 2014).

Reduction of plant water status associated with foliar deposition of hygroscopic aerosols appears to account for these $\delta^{13}C$ signals, despite slightly elevated temperature and VPD in FA (2.8 kPa when ψ_{noon} measured) than AA (2.1 kPa) due to aerosol filtration (Grantz *et al.*, 2018; Chi *et al.*, 2022). Stomatal opening driven by the slightly warmer FA environment is not consistent with reduced leaf water status in AA relative to FA (Esperon-Rodriguez *et al.*, 2021).

3.4.3 Role of aerosol and isohydricity

The increased markers of water deficit following aerosol exposure, observed to varying degrees in both clones, indicate that aerosol mediated an additional component of transpiration. This was enabled by a thin liquid film (estimated 100 nm thickness; Burkhardt, 2010) that lines the throat of the stomata, providing a liquid water pathway from mesophyll to leaf boundary layer. This effectively extends the liquid hydraulic system from soil to atmosphere. This parallel liquid transpiration stream may be efficient (Burkhardt, 2010; Grantz *et*

al., 2020), but lies wholly outside the control of the stomatal regulatory system, which functions effectively for diffusive flows of water vapor.

This transport pathway is derived from the thin aqueous film that coats all surfaces in the presence of atmospheric water vapor (Wylie, 1955; Ewing, 2005). In the presence of deliquescent salts, here derived from ambient aerosol deposited to foliar surfaces (Burkhardt & Grantz, 2017), additional solution is added to this film allowing a process of salt creep, reduction of surface tension, and penetration of the stomatal pore. This has been referred to as Hydraulic Activation of Stomata (HAS; for a review see Burkhardt, 2010; Burkhardt *et al.*, 2012; Burkhardt *et al.*, 2018). Increasing minimum leaf conductance by hygroscopic leaf surface material has repeatedly been documented (Burkhardt & Pariyar, 2014; Burkhardt *et al.*, 2018; Grantz *et al.*, 2018; Chi *et al.*, 2022) and the intrusion of deliquescent leaf surface material into stomatal structures has been directly observed by environmental scanning electron microscopy (see videos in Burkhardt & Pariyar, 2014).

The aerosol influence on E and g_{sw} has been largely omitted from models of water loss, in part because this incremental flux along thin aqueous films cannot be isolated by gas exchange measurements, appearing in the total water flux. These fluxes have been demonstrated indirectly by simultaneous measurement of gas exchange and stomatal pore aperture (Burkhardt *et al.*, 2001; Grantz *et al.*, 2018). In *Vicia faba*, aerosol decreased stomatal apertures at each level of VPD, as in the current study, suggesting an additional element of evaporative demand to which stomata responded, and increased stomatal conductance at each level of aperture (Grantz *et al.*, 2018). Aerosol deposition also reduced the heterogeneity of stomatal pore area (“patchiness”) in *V. faba*. Both observations are consistent with deposition of hygroscopic aerosol and creation of a thin aqueous film across the leaf surface and penetrating the pores that hydraulically connects neighboring stomata to each other and to the leaf interior (Grantz *et al.*, 2020).

In the current study, there was an apparent biphasic aspect of the sensitivity of the response of g_{sw} to aerosol with increasing VPD (*Figure 3.7*). In both clones,

the greatest sensitivity was observed at moderate VPD (i.e., 1 to 1.5 kPa). This biphasic response profile has not previously been described. We speculate that it reflects the dual nature of changing humidity in the context of the HAS hypothesis. Increasing VPD at constant temperature would both increase evaporative demand and reduce the adsorption of water vapor by hygroscopic aerosol, reducing the effectiveness of the HAS pathway. The consequences for water loss would thus become situation specific.

3.5 Conclusion

Both initial hypotheses were not supported. First, the isohydric poplar clone was expected to respond to aerosols by stomatal closure, which was not supported: ISO responded very sensitive to VPD and stabilized leaf water potential, but did not show additional effects by aerosols. Second, stomatal regulation of anisohydric plants was expected to be less sensitive than the regulation of isohydric plants, which was also not supported: Aerosols reduced both stomatal aperture and leaf water potential of ANI, but not ISO.

The reduction of stomatal densities showed that aerosols increased atmospheric drought for both clones, but their impact on the ANI clone was more obvious and their impact on the ISO clone was subtle. The aerosol effect on the turgor loss point of ISO probably came from invisible liquid water loss by leaky stomata, so it surpassed the defense line of ISO against atmospheric drought and decreased drought tolerance.

Chapter 4

The content of this chapter was presented in:

1. The 9th International Conference on Fog, Fog Collection, and Dew, 23-28 July, 2023, Fort Collins, Colorado, USA (Oral presentation).

Chi, C. J. E., Vega, C., Fernández, V., & Burkhardt, J. (2023) Invisible Dew Formation by Atmospheric Aerosols and Its Role for Nocturnal Transpiration of Poplars. In: *9th International Conference on Fog, Fog Collection, and Dew*.

2. Annual Conference of the German Society of Plant Nutrition (DGP), 25-27 September, 2023, Hohenheim, Germany (Poster presentation).

Chi, C. J. E., Vega, C., Fernández, V., & Burkhardt, J. (2023) Atmospheric Aerosols and Nocturnal Transpiration in Nutrient Deficient Poplars. In: *Annual Conference of the German Society of Plant Nutrition*.

4 Influence of Hygroscopic Leaf Surface Compounds on Nocturnal Transpiration for Nutrient Deficient Poplars

Abstract

Hygroscopic action of foliar nutrient applications and atmospheric aerosols depositing on foliage is considered as a hydraulic connection between leaf surface and interior. This connection is formed by highly concentrated filmy solutions after deliquescence and leads to additional liquid water loss as well as potential ionic movements at stomata. This study combines the hygroscopic action of foliar compounds with the recently-observed phenomena of stomata unusually opening during the night, which contributes sorely to water loss without carbon gain and thus leaves an unclear functional relevance in non-CAM plants. The aim of this study is to investigate whether hygroscopic compounds on foliage result in changes on nocturnal stomatal conductance for nutrient-deficient poplars. In order to eliminate the influence from indefinite atmospheric aerosols and the possible drought effect, the entire experiment was conducted in the greenhouse ventilated with aerosol-free air. Poplar seedlings (*Populus maxim. x nigra*) were grown in hydroponic solutions and arranged to different nutrient deficiency groups. After applying external nutrient solutions on leaf surfaces, the stomatal conductance was measured overnight. In addition, element analysis of leaf tissue, chemical characteristics and microstructure of different foliar applications on leaf surfaces were obtained for support. The results show that nocturnal stomatal response of nutrient-deficient poplars depends on the accessibility of a specific limiting nutrient on the leaf surface, suggesting that nocturnal stomatal conductance may be regulated not only by the nutrient deficiency at root zone, but also by the corresponding nutrient availability on the leaf surfaces. We provided possible explanations to the mechanisms and pathways of this trigger. Our findings contribute to reveal the possible connection between nocturnal stomatal regulations and plant nutrient regimes from the perspective of hygroscopic compounds on foliage, benefiting to establishing strategies for foliar applications and to calibrating current models on ecosystem respiratory CO_2 flux and plant water use.

4.1 Introduction

In recent years, due to the increasing level of air pollution, more and more studies have investigated the impact of air pollution on plants and ecosystems. These aerosol particles indirectly affect plant productivity via reducing incoming solar radiation, and directly have physical effects or further alter physiological responses after depositing on leaf surfaces (Mahowald *et al.*, 2017; Yamaguchi & Izuta, 2017). Centering on the hygroscopic action of deposited aerosols on foliage, it is indicated that the aerosols become mobile by deliquescence at stomata pore and form highly concentrated filmy solutions. The saturated thin film may enter the stomata and connect with the liquid water at the terminus of hydraulic system, regardless of the larger stomatal aperture and compensating CO_2 influx. This nature of stomatal regulation (i.e., hydraulic activation of stomata, HAS) modifies the microenvironments through vapor pressure deficit (VPD), subsequently leads to additional liquid water loss and potential ionic movements at stomata (Burkhardt, 2010; Song *et al.*, 2015; Burkhardt & Grantz, 2017).

On the other hand, recent research has observed an extraordinary phenomena of increased plant transpiration rate and stomatal conductance (g_{sw}) during the night. Similarly, it contributes sorely to water loss without carbon gain due to the absence of photosynthesis in the dark; the functional relevance of nocturnal transpiration thus has been widely discussed (Daley & Phillips, 2006; Kavanagh *et al.*, 2007; de Dios *et al.*, 2019; Kangur *et al.*, 2021). Until latest, studies of nocturnal g_{sw} have been centered with different plant species under various growth environments, different methods and scales, as well as the causes inducing such behavior and the possible consequences to plants (Barbour *et al.*, 2005; Caird *et al.*, 2007; Even *et al.*, 2018; Fricke, 2020).

Several hypotheses on the functions and benefits of nocturnal transpiration have been assessed to facilitate carbon fixation (de Dios *et al.*, 2016), to enhance the transport of dissolved oxygen and remediate oxygen scarcity in parenchyma cells (Daley & Phillips, 2006), to adapt to stresses such as drought and salinity (Even *et al.*, 2018; Sadok & Tamang, 2019; Schoppach *et al.*, 2020), or to simply caused by the uncontrollable stomatal leakiness (de Dios *et al.*, 2019). In addition,

nocturnal stomatal regulation may also intervene in nutrient supply and transport (Ludwig *et al.*, 2006), mediate nutrient uptake or nutrient distribution to distal parts of the plant (Scholz *et al.*, 2007; Rohula *et al.*, 2014), and respond positively to nutrient limitations to increase nutrient delivery under limited fertility (de Dios *et al.*, 2019). However, there are very few research focusing on the direct impact of foliar hygroscopic materials on nocturnal g_{sw}, neither on the possible explanation of the mechanisms and pathways involved (Fernandez & Eichert, 2009; Peirce *et al.*, 2014; Fernandez *et al.*, 2021). A comprehensive picture of the connection between these stomatal regulations causing unbeneficial water loss remain incomplete.

Hence, this study aims to reveal the correlation between leaf surface hygroscopic materials and nocturnal transpiration. Given that atmospheric aerosols may contribute to nourished depositions on leaf surface, serving as one of the sources of foliar nutrients (Anderson *et al.*, 2010; Burkhardt, 2010; Mahowald *et al.*, 2017), the research includes the concept of nutrient transport as the potential underlying purpose of nocturnal transpiration. This study investigates whether foliar nutrient availability derived from hygroscopic aerosols leads to changes in nocturnal g_{sw}, especially in the presence of root nutrient deficiency.

The entire experiment was conducted in the greenhouse ventilated with filtered air to eliminate the influences from atmospheric aerosols that are beyond the scope. The plants were grown in hydroponic solutions with commonly seen nutrient regimes: no nutrient deficiency, phosphorus (P) deficiency, nitrogen (N) deficiency, and sulfur (S) deficiency; later on, the leaves were treated with corresponding foliar sprays, representing hygroscopic leaf surface materials from common aerosol compounds' deposition. Based on the high correlation between transpiration and g_{sw}, g_{sw} was measured overnight and standardized with a certain time point of the measuring date, and the measurements of replications were alternated in between groups of treatments. Moreover, due to the fast-growing capacity (Xi *et al.*, 2021), the representative as an bioindicator of tree species (Yalaltdinova *et al.*, 2018; Gorka *et al.*, 2020), and the frequent occurrence of high nocturnal g_{sw} (Ceulemans *et al.*, 1988; Musselman & Minnick,

2000), a hybrid poplar clone (*Populus maxim. x nigra*) was taken as the research material to avoid genetic variability (Christman *et al.*, 2008). For visualization, the microstructure of foliar sprays deposition and the stomata characteristics in this study were as well obtained by scanning electron microscopy images. Ultimately, element analysis of leaf tissue was examined to cross-confirm the growth conditions of nutrient deficiency.

4.2 Materials and methods

4.2.1 Plant material and growth conditions

Fifty-six seedlings of the hybrid poplar clone (*Populus maxim. x nigra*) were grown in a hydroponic solution (containing all essential nutrients) in a greenhouse ventilated with filtered air, to provide an aerosol-free growth environment to eliminate the effects of water availability and foliar deposition from the ambient atmosphere (Musselman & Minnick, 2000; Ludwig *et al.*, 2006; Caird *et al.*, 2007; Grantz *et al.*, 2018). Once the seedlings had grown to around 150 cm tall, they were grouped into the following four nutrient deficiency treatments: no nutrient deficiency, phosphorus (P) deficiency, nitrogen (N) deficiency, and sulfur (S) deficiency (*Figure 4.1*). The deficient hydroponic solutions were renewed once a week to avoid nutrient depletion in the root zone. Sampling and measurements began two weeks after withdrawing an essential nutrient from the hydroponic culture. Samples consisted of the last fully expanded leaves. The entire experiment was carried out between September and October to ensure consistent environmental conditions.

4.2.2 Foliar sprays

The leaves of seedlings in each nutrient deficiency group were sprayed with different nutrient solutions using a calibrated hand-held spray bottle. Leaves were sprayed uniformly on both adaxial and abaxial sides until runoff (Peirce *et al.*, 2014) (*Figure 4.1*). The solutions used for spraying were 1 g l^{-1} diammonium hydrogen phosphate ($(NH_4)_2HPO_4$, hereafter called P Spray), 1 g l^{-1} sodium nitrate ($NaNO_3$, hereafter called N Spray), 1 g l^{-1} ammonium sulfate ($(NH_4)_2SO_4$,

hereafter called S Spray), and plain deionized water (hereafter called Water Spray).

The solutes were chosen based on the deliquescence humidity of the chemical compounds (McBeath *et al.*, 2020; Gorlach & Muhling, 2021). The deliquescence relative humidity (DRH) and efflorescence relative humidity (ERH) of the salts were also assessed with a climatic chamber (MKF 56, Binder, Germany) at 20°C under controlled relative humidity (R.H.). Two grams of each solid salt were placed in a Petri dish, which was kept open in the climatic chamber. The R.H. was gradually raised from 20% to 98% at a rate of 5% every half hour, while observing qualitatively the process of hydration with an optical microscope (DM300, Leica Microsystems, Germany). As the R.H. approached the DRH of the salts, the crystals began to lose their shape and became round. At this point, the R.H. was maintained for a longer period to clearly visualize the salts becoming liquid. After having identified the DRH, the salts were kept at 98% R.H. overnight to evaluate the process of water desorption. The following day, the ERH was determined by gradually reducing the R.H. (Fernandez *et al.*, 2020). In addition, the DRH and ERH of the salts were estimated from the water sorption and desorption dynamics of the salts at 20°C, as observed in dynamic vapor sorption isotherms (TGA Q5000, TA instruments, USA; Thermal Analysis and Calorimetry Service IQAC-CSIC, Barcelona Spain) (Fernandez *et al.*, 2020).

The water holding capacity of the poplar leaves was determined by weighing (n = 20) fresh leaves that had been sprayed with water uniformly on both adaxial and abaxial sides until runoff. Then, the water drops on the leaf surfaces were absorbed immediately by a preweighed laboratory tissue paper. The wet paper was weighed and the weight of the water was divided by the defined leaf area of both leaf sides. The water holding ability was expressed in thickness (mm). This value was used to calculate the amount of salt remaining on the leaf surfaces after spraying (Burkhardt & Pariyar, 2016). The water holding capacity of the poplar leaves was 0.157 ± 0.007 mm homogenous coverage. Thus, we estimated that 15.7 µg cm^{-2} deposits of the respective salts remained on the leaf surfaces.

4.2.3 Measurements of nocturnal g_{sw} and leaf R.H.

In order to estimate the possible reacting time for poplar seedings to regulate nocturnal g_{sw}, a time series trial was first carried out with the group of nitrate deficiency and N spray (n = 4). Nocturnal g_{sw} was measured 1 day, 2 days, 5 days, 9 days, and 15 days after foliar spraying. With this preliminary result and the reference of other previous research, the interval time between foliar spraying and measurements of nocturnal g_{sw} was then defined as 14 days (Gorlach & Muhling, 2021). Therefore, we measured nocturnal g_{sw} using an LI-6800 Portable Photosynthesis System (LI-COR Biosciences, Lincoln, NE, USA) at 14 days after applying the foliar sprays. Measurements were recorded every minute, and to ensure the stability of overnight measurements, the chamber environmental settings were tested prior to the experiment on various species and attended the optimized condition (Howard & Donovan, 2010; Chi *et al.*, 2022). The chamber settings were set to a flow rate of 300 mol s^{-1}, fan speed of 8000 rpm, ambient CO_2 (around 400 μmol mol^{-1}), and no light. Temperature and R.H. followed the ambient environment in the greenhouse. Data were extracted from 11:00 p.m. to 6:00 a.m. the following day to ensure a stable CO_2 concentration and a dark environment (Caird *et al.*, 2007; Eller *et al.*, 2017). To minimize the impacts of day length changes and growth stage of the plant on physiological regulations (Schwabe, 1952; Grulke *et al.*, 2004), the measurements on biological repetitions were always alternated between experimental groups (n = 4).

Additionally, leaf surface R.H. (%) was calculated from the vapor pressure in the chamber (kPa) and the saturation vapor pressure at leaf temperature (kPa) (n = 4). The results of the nocturnal g_{sw} and leaf surface R.H. of individual samples for each treatment are shown in the Supplementary information.

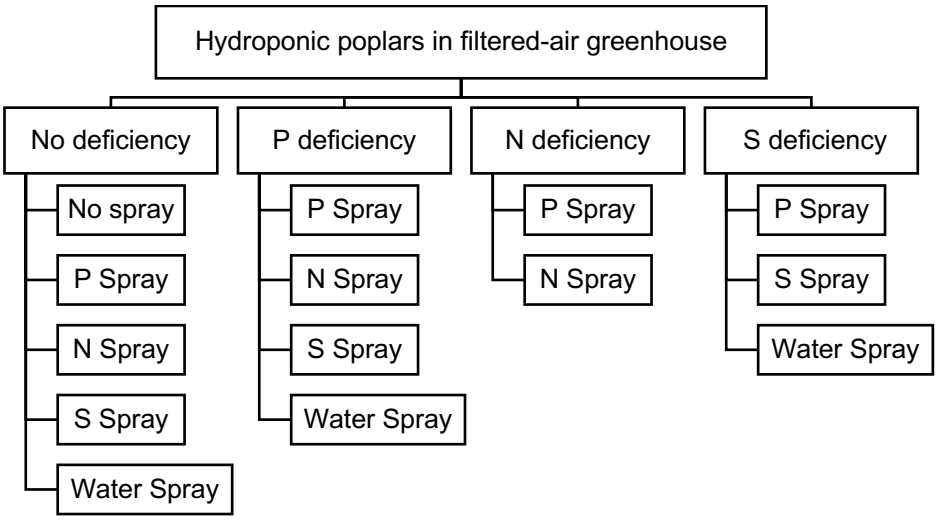

Figure 4.1. Experimental treatments based on nutrient deficiency conditions and foliar sprays.

Poplar seedlings were grown in hydroponic solutions with no nutrient deficiency and the following nutrient deficiencies: hydroponic solutions with phosphorus (P) deficiency, nitrogen (N) deficiency, and sulfur (S) deficiency. Corresponding foliar sprays were: 1 g l^{-1} diammonium hydrogen phosphate solution (P Spray), 1 g l^{-1} sodium nitrate solution (N Spray) , 1 g l^{-1} ammonium sulfate solution (S Spray), deionized water (Water Spray), and without additional foliar spray (No spray). Each foliar treatment replicate consisted of one poplar seedling. Each group of different nutrient regimes and foliar treatments contained 4 biologically independent replications.

4.2.4 Element analysis of leaf tissue

The element content of deficient leaf tissue was determined on poplar seedlings grown under different nutrient deficiencies. Leaf samples were harvested from each deficiency condition (n = 12) and dried in a laboratory oven at 60°C for one week until reaching the absolute dry weight. The dried leaves were ground into fine powder and analyzed by either inductively coupled plasma optical emission spectroscopy (ICP-OES, Thermo Fisher Scientific Inc., Waltham, MA, USA) or isotope ratio mass spectrometry (IRMS, C-N-S Analyzer, and MS-2020; SerCon Ltd., Crewe, UK).

4.2.5 Microstructure of foliar sprays on leaf surfaces

The feature and distribution of foliar application deposited on leaf surfaces were visualized by scanning electron microscopy (SEM, Leo 1450 VP, Zeiss, Jena, Germany). Fresh leaf samples of poplar seedlings from each deficiency condition were taken 14 days after foliar spraying. Both adaxial and abaxial sides were mounted on sample discs until air dried. The samples were coated with palladium prior to high-vacuum SEM imaging (Achneck *et al.*, 2010). Images were obtained as single point as well as area mapping. During image interpretation, the edges were avoided to eliminate the possible instabilities caused by the microscopy.

4.2.6 Data processing and statistical analysis

Sample size (n = 4) was defined by using Basic Functions for Power Analysis in R Studio (R version 4.0.3). The hypothesis of this study is to investigate on two deficient groups with a dichotomous outcome (g_{sw} increases or not). Based on the preliminary research, we suggested there is around 70% difference between the outcomes of two groups. The estimated output of sample size was 3.994761, under desired significance level 0.05, and with power 80%. In the end, a power test was conducted for confirmation. Samples were allocated into experimental groups randomly. The investigators were blinded to group allocation during data collection and analysis.

To account for different starting points, the values of nocturnal g_{sw} were normalized by dividing each data point by the 11:00 p.m. value at each measuring day (Eller *et al.*, 2017). Statistical analysis was performed using R Studio. Data are shown as means (n = 4). Both error bar and error envelop represent standard error. The Shapiro–Wilk test was used as a normality test for checking data distribution; either the F-test or Fligner–Killeen test was performed to compare the homogeneity of variances, depending on the data distribution. For normally distributed data, the difference of the means between groups was evaluated either by two-tailed Student's t-test (comparison between two groups) or ANOVA (comparison among multiple groups). Tukey's HSD (Honestly Significant Difference) test was applied after ANOVA for post-hoc analysis. For non-normally distributed data, differences between medians were evaluated nonparametrically by the Wilcoxon–Mann–Whitney U-test (Chi *et al.*, 2022). Statistical results were visualized by LOESS (Locally Estimated Scatterplot Smoothing) regression, with 95% confidence intervals. In all statistical analyses, differences were considered significant if $p < 0.05$.

4.3 Results

4.3.1 Characteristics of foliar sprays and their deposition

The compounds $(NH_4)_2HPO_4$, $NaNO_3$, $(NH_4)_2SO_4$ were chosen to simulate hygroscopic foliar depositions, primarily based on their closely matching DRH values, which were found to be 81.5%, 84.0%, and 84.6%, respectively. It should be noted that the ERH range spanning from 30% to 67% was considered; however, ERH did not serve as the primary selection criterion in this study. Each of the prepared solutions had a consistent mass concentration of 1 g/L. In accordance with the desired ionic contribution of each solution, the P Spray contributed approximately 7.5 mM of $[PO_4^{-3}]$, the N Spray with 12 mM of $[NO_3^{-1}]$, and the S Spray with 7.5 mM of $[SO_4^{-2}]$ (*Table 4.1*).

Figure 4.2 shows the microstructure of foliar sprays depositing on leaf surfaces, as grown under different nutrient deficiency. The deposited nutrient compounds formed either euhedral crystals such as cubic crystallization (N

Spray), or non-geometrical crystals such as clustered crystallization (P Spray and S Spray). Due to the characteristics of air-dried leaf samples, the aperture of stomata might not be significantly reliable in the images. However, it is shown that each foliar application (P, S, N Spray) had a certain level of compound deposition and retainment near the stomata on leaf surfaces under all the conditions of nutrient deficiency. From the last row of images, it is indicated that with foliar water spray, there seemed to be no specific crystals formed on the leaf surfaces.

Table 4.1. Hygroscopic characteristics of the spraying compounds.

Measurement	**DRH (%)**	**ERH (%)**	**Mass concentration**	**Target ionic contribution**
$(NH_4)_2HPO_4$	81.5	31.0	1 g/L	PO_4^{-3}, 7.5 mM
$NaNO_3$	84.0	67.0	1 g/L	NO_3^{-1}, 12 mM
$(NH_4)_2SO_4$	84.6	30.0	1 g/L	SO_4^{-2}, 7.5 mM

Deliquescence relative humidity (DRH) and efflorescence relative humidity (ERH) of the spraying compounds at 20ºC, determined from dynamic vapor sorption (DVS) isotherms.

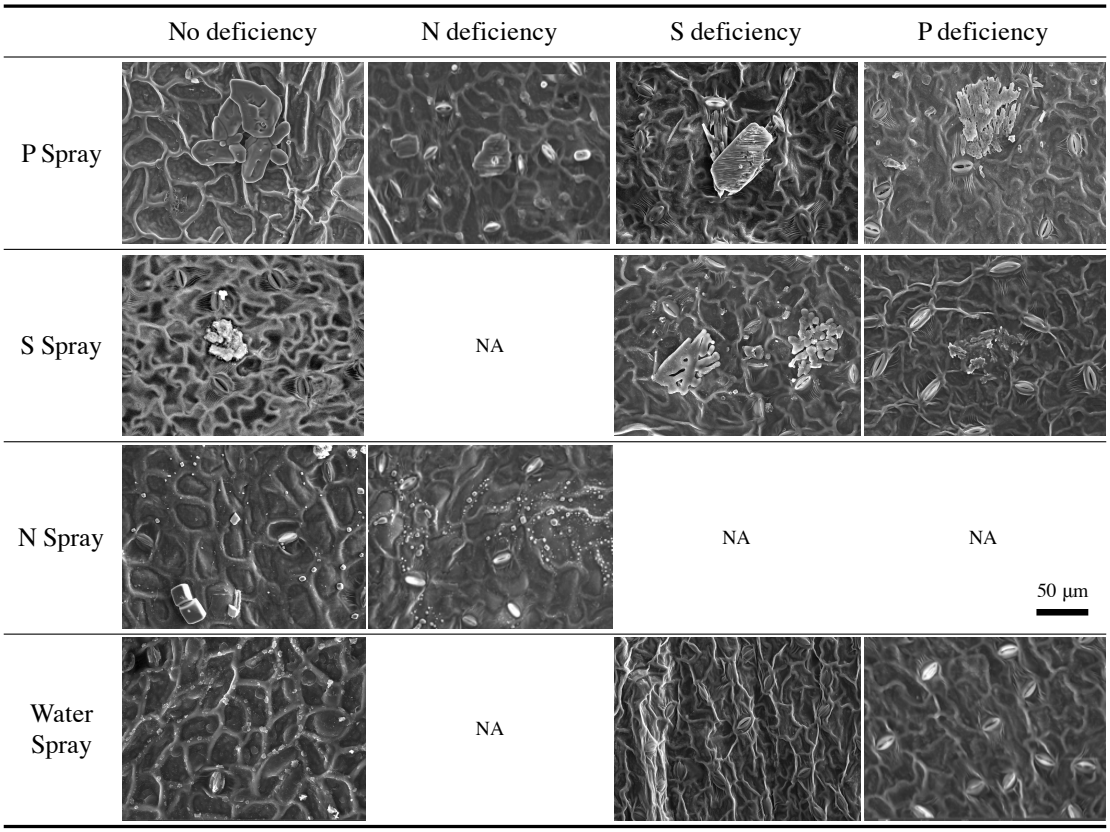

Figure 4.2. Microstructure of different foliar sprays on leaf surfaces.

Rows represent the conditions of nutrient deficiency from root zone: no nutrient deficiency, phosphorus (P) deficiency, sulfur (S) deficiency, and nitrogen (N) deficiency. Columns are the different foliar applications: P Spray, S Spray, N Spray, and deionized water spray. NAs are the unavailable treatments. The length of the black bar is 50 µm. All images to same scale.

4.3.2 Element analysis of leaf tissue

Table 4.2 reconfirms the consequence of nutrient deficiency in poplar leaves from the prescriptions of hydroponic growth control. Two weeks after withdrawing an essential nutrient from the hydroponic culture, the percentages of leaf P, N, and S concentrations relative to plants grown in complete nutrient solutions were 76.0 ± 5.1, 90.5 ± 6.8, and 70.1 ± 3.5%, respectively.

Table 4.2. Level of nutrient deficiency compared to fully-nourished poplars (%).

Nutrient status	P	N	S
No deficiency	100	100	100
P deficiency	75.97 ± 5.14	-	-
N deficiency	-	90.49 ± 6.77	-
S deficiency	-	-	70.11 ± 3.52

Data are means ± s.e. (P, S: n = 12, N: n = 8). Letters indicate significant differences between groups with different nutrient deficiency at root zone (ANOVA, $p < 0.05$).

4.3.3 Time series

Figure 4.3 shows the fluctuation of standardized stomatal conductance (g_{sw}) throughout the night from 11:00 p.m. until 6:00 a.m. the next day. Within the first few days such as 1 day, 2 days, 5 days, 9 days after foliar spraying, g_{sw} did not show a remarkable increase or decrease through the nighttime (*Figure 4.3*a-d). In addition, there were higher variations in g_{sw} during the measuring time especially after around 2:00 to 3:00 a.m., and the variations had been increasing since then until 6:00 a.m. However, the high variations in g_{sw} were not found in the measurements of 9 days, 14 days, and 15 days after foliar spraying (*Figure 4.3*d-f). On the 14th and 15th day after foliar spraying, g_{sw} increased continuously, leading to over 50% and 30% growth at 6:00 a.m. comparing to the g_{sw} value at 11:00 p.m., respectively.

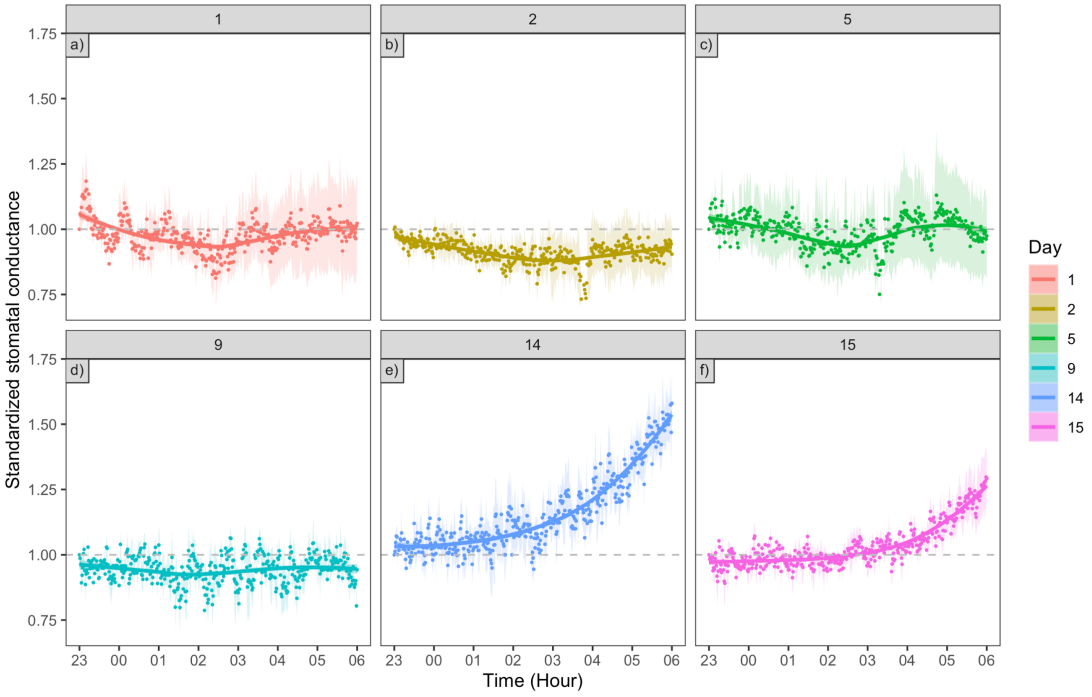

Figure 4.3. Normalized stomatal conductance after different days of foliar N spraying.

Measurements were taken 1 day, 2 days, 5 days, 9 days, and 15 days after foliar spray. Data are normalized by the respective initial (11:00 p.m.) values; error envelopes are standard errors; n = 4. Lines are smoothed with LOESS (Locally Estimated Scatterplot Smoothing) regression for clear visualization.

4.3.4 Nocturnal stomatal regulations

Figure 4.4 displays the standardized g_{sw} throughout the night for the different plant nutrient regimes evaluated. In the control group with no nutrient deficiency and no foliar spray application (purple line in *Figure 4.4*a-d), the standardized g_{sw} remained below the initial value throughout most of the night with little variation between replications; a slight increase in conductance occurred after 3:00 a.m., with a high degree of variation among replicates. However, the g_{sw} values did not significantly exceed the initial value.

*Figure 4.4*a shows the response of poplar plants that grew without any nutrient deficiency. None of the foliar sprays (P, N, S, and water) increased the standardized nocturnal g_{sw}, although overall g_{sw} increased in variation after around 2:00 a.m.

*Figure 4.4*b, c, d show the nocturnal g_{sw} readings from plant leaves grown under P, N, and S deficiency, respectively, with each deficiency treatment later sprayed with the corresponding solution of the limiting nutrient. *Figure 4.4*b shows the g_{sw} of leaves grown under P deficiency after P spray increasing constantly throughout the entire measuring time, becoming significant at 1:40 a.m. (*Figure 4.5*), and reaching twice the initial value by the end of the night (6:00 a.m.). g_{sw} also increased significantly after 3:00 a.m. for N-deficient poplar leaves after N spray (*Figure 4.4*c, *Figure 4.5*), whereas neither P spray (also containing ammonium) to N-deficient plants (*Figure 4.5*) nor any other foliar application treatments caused a comparable response (Supplementary information). While the g_{sw} of S-deficient leaves after S spray appeared to increase constantly throughout the night (*Figure 4.4*d), the trend was not statistically significant (*Figure 4.5*).

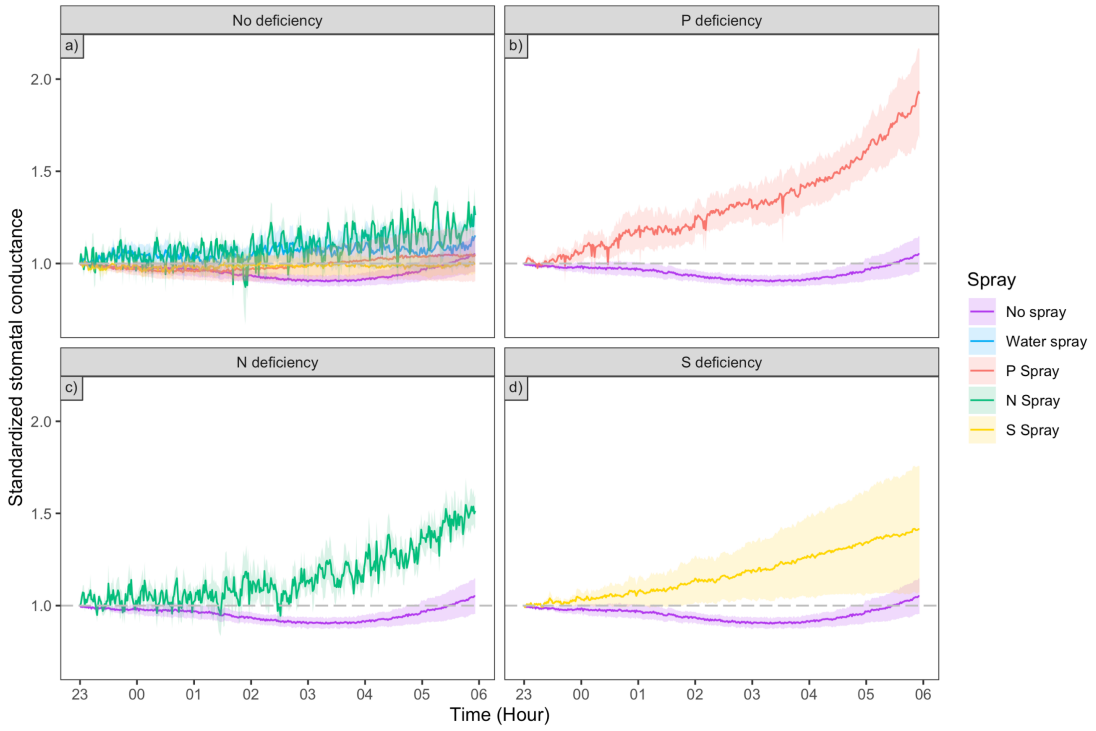

Figure 4.4. Normalized nocturnal stomatal conductance of poplar leaves under different nutrient regimes and with/without foliar treatments.

The purple line, present in a–d, is the nocturnal g_{sw} of plant leaves grown without nutrient deficiency and without spray. a) effect of foliar P, N, S, and water sprays applied to leaves of plants having no nutrient deficiency, b) effect of foliar P spray to P-deficient poplar plants, c) effect of foliar N spray to N-deficient poplar plants, d) effect of foliar S spray to S-deficient poplar plants. Data are normalized by the respective initial (11:00 p.m.) values; error envelopes are standard errors; n = 4.

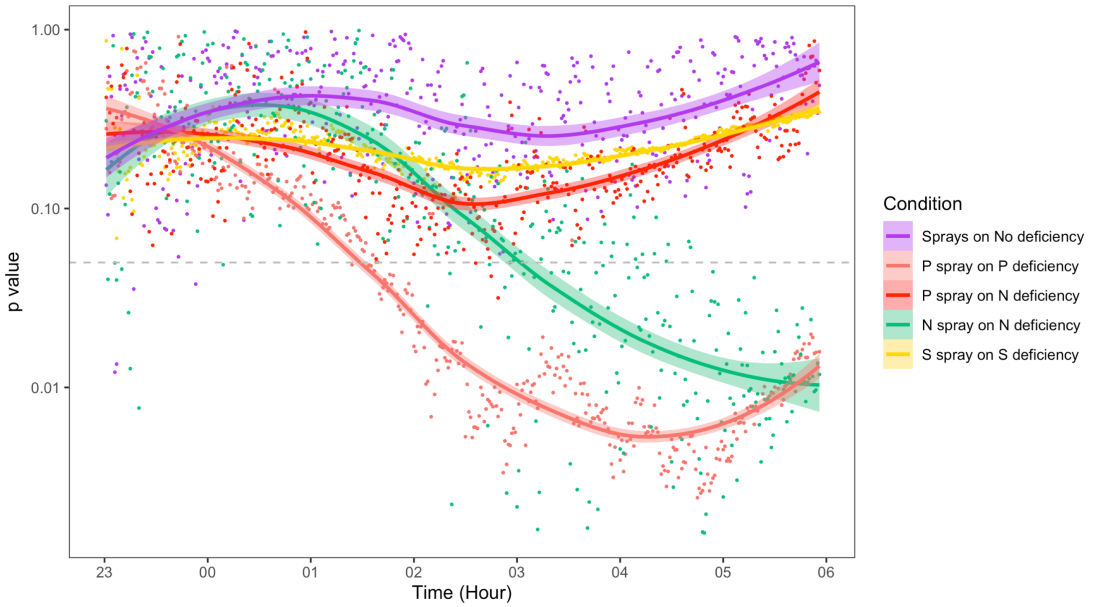

Figure 4.5. Nocturnal course of statistical significance values.

Significances were calculated by ANOVA (no deficiency) and Student's t-test (P, N, S deficiency). The y-axis is logarithmic, the dashed line is at 0.05. The purple line (sprays on no deficiency) corresponds to Fig.1a, the lower red line (P spray on P deficiency) to Fig.1b, green line (N spray on N deficiency) to Fig.1c, yellow line (S spray on S deficiency) to Fig.1d. The upper red line shows the significance level for P spray (containing ammonium) on N-deficient plants. Data represent LOESS (Locally Estimated Scatterplot Smoothing) regression of p values between different nutrient deficiencies and sprays, with 95% confidence interval; n = 4.

4.4 Discussion

4.4.1 Nocturnal transpiration and nocturnal stomatal conductance

The recently observed nocturnal transpiration may undertake a significant 5 to 10% of daily transpiration rate in a diverse range of plant species, resulting in substantial water loss but without beneficial carbon gain (Caird *et al.*, 2007). This transpirational process is considered being strongly correlated with leaf conductance which includes both cuticular conductance and stomatal conductance (g_{sw}); however, the cuticular conductance is often two orders of magnitude lower than the g_{sw} (< 10 mmol m^{-2} s^{-1}) and may be neglectable (Cirelli *et al.*, 2016; Duursma *et al.*, 2019). Similar to previous research, it is thus assumed that g_{sw} dominates the nocturnal conductance in this study (de Dios *et al.*, 2019). On the other hand, nocturnal transpiration and nocturnal g_{sw} are different processes. They are not always linearly correlated because of the inconsistent environmental effects, e.g., increasing vapor pressure deficit increases transpiration, but it may lead to either higher or lower g_{sw} (Caird *et al.*, 2007; Claverie *et al.*, 2018; de Dios *et al.*, 2019). Therefore, instead of nocturnal transpiration, the focused parameter for measurements in this study is nocturnal g_{sw}.

4.4.2 Potential drivers of nocturnal stomatal regulation

The most common explanation for the occurrence of nocturnal g_{sw} is that stomata do not completely close and are leaky at night (Barbour *et al.*, 2005), however, different drivers affecting nocturnal g_{sw} were found and thus imply that it is actively regulated, rather than a simple consequence of stomata leakiness (Zeppel *et al.*, 2014; Cirelli *et al.*, 2016; de Dios *et al.*, 2019). Several research investigated on the comparison between daytime and nocturnal g_{sw}, suggesting that the drivers for nocturnal g_{sw} may be different from those for daytime regulations (Cirelli *et al.*, 2016). Comparable with daytime g_{sw}, nocturnal g_{sw} is found negatively correlated with predawn water potential, air temperature, environmental stress such as salinity; and positively correlated with soil water content, anatomical features such as leaf specific area and stomatal density

(Caird *et al.*, 2007; Chowdhury *et al.*, 2022). However, nocturnal g_{sw} may decrease with increasing vapor pressure deficit species-specifically, which is in contrast with daytime g_{sw} (Bucci *et al.*, 2004; Howard & Donovan, 2010). Moreover, daytime g_{sw} of plants usually declines under elevated CO_2 concentration, but nocturnal g_{sw} is often higher than which under ambient CO_2 concentration (Ainsworth & Rogers, 2007; Easlon & Richards, 2009; Zeppel *et al.*, 2014). Furthermore, previous research has indicated that only nocturnal g_{sw} may have habitat preference, especially within *Populus* species (Cirelli *et al.*, 2016).

Eller *et al.* (2017) showed that nocturnal g_{sw} may be prominent starting from 11:00 p.m. species-specifically, the g_{sw} in this study was thus standardized respectively with the original value at 11:00 p.m. each measuring day. Similarly, the nocturnal g_{sw} of *Populus maxim. x nigra* in this study was not stable throughout the night, showing a constantly increasing trend until the end of the night (Schwabe, 1952; Dodd *et al.*, 2005; Howard & Donovan, 2010). This phenomena has been interpreted as the stomatal regulation resulting from plants circadian rhythms, and one of the potential effects of predawn stomatal opening is to prime photosynthesis (the anticipation hypothesis, de Dios *et al.*, 2016); in other words, such circadian-driven stomatal priming could reduce the time to attain operating steady-state g_{sw} in the morning for carbon assimilation (Dodd *et al.*, 2005; Drake *et al.*, 2013; de Dios *et al.*, 2019). However, it is important to notice that the increasing nocturnal g_{sw} only has an indirect effect on carbon assimilation by altering the response time to illumination, but not essentially alters predawn g_{sw} (Drake *et al.*, 2013; de Dios *et al.*, 2019). According to the statements above, this study suggests that there are other consequences caused by such circadian-driven stomatal opening, and attempting foliar uptake might be one of the potentials.

Nevertheless, the impacts of nutrient status on nocturnal g_{sw} have not reached consensuses among previous studies. It is generally supposed that nocturnal g_{sw} increases with nutrient deficit from soil (i.e. root zone), for the purpose of raising the nutrient transport rate (Ludwig *et al.*, 2006; Scholz *et al.*, 2007; Kupper *et al.*, 2012), but the occurrence is likely depending on the mobility

of ionic nutrient compounds (Chowdhury *et al.*, 2022). Howard & Donovan (2010) concluded that g_{sw} of *Populus angustifolia* and *Populusbalsamifera L. spp. trichocarpa* are not regulated at night in response to soil nitrogen availability. Eller *et al.* (2017) indicated that nocturnal g_{sw} of *Fraxinus excelsior* increases under soil N deficiency but decreases under soil P deficiency, while de Dios *et al.* (2013) claimed that nocturnal g_{sw} of *Eucalyptus tereticornis* increases under soil P deficiency. Further research is needed for integration.

4.4.3 Possible mechanisms and pathways involved in selective stomatal regulation

In the present study, the nocturnal g_{sw} of poplar leaves increased only when a deficient nutrient compound was available on the leaf surface. Neither the deficiency of a nutrient in the root zone alone nor the availability of a non-deficient nutrient on the leaf surface caused increasing nocturnal g_{sw} (*Figure 4.4*). It is indicated that the plants likely regulate g_{sw} at nighttime in order to uptake specific nutrients from foliage. The selective response of the stomatal aperture also suggests a sensing mechanism that enables the leaves to recognize the availability of the missing nutrients on leaf surfaces.

Previous research has examined the penetration and possible pathways of foliar application with different nutrient compounds on various species; conventionally, the absorption of foliar-applied compounds is considered strongly related to the surface characteristics of plant leaves, physicochemical properties of the applied chemicals, supplement type and concentration, and environmental conditions (Schlegel *et al.*, 2005; Will *et al.*, 2012; Fernandez & Brown, 2013; Xie *et al.*, 2020). Under the effect of water sorption to polysaccharides (i.e., swelling and shrinking of cuticle volume), high percentage of chemical compounds on foliage would be bound to cell walls and then enter into the leaves (Riederer, 2006; Fernandez *et al.*, 2016; Xie *et al.*, 2020).

On the other hand, while it is addressed with the nanoscale of foliar deposition and additional nutrient application, the contribution of atmospheric aerosols should not be neglected (Musselman & Minnick, 2000; Sparks, 2009). Burkhardt (2010) specified that hygroscopic aerosols deposited close to

transpiring stomata are often deliquescent, forming a nourished concentrated solution which may be taken up by stomata. This establishment of a continuous liquid water connection along stomatal walls affects individual stomata (i.e., hydraulic activation of stomata), and enables the efficient bidirectional transport of water and solutes between the leaf interior and leaf surface (Eichert & Goldbach, 2008; Eichert *et al.*, 2008). The uptake of solutes from hygroscopic leaf surface compounds, such as foliar applications or nourished aerosols, is therefore able to be illustrated as a direct and effective diffusion process, which is driven by concentration gradients (Burkhardt & Eiden, 1994; Eichert & Goldbach, 2008; Burkhardt, 2010; Fernandez *et al.*, 2021). The entire experiment of this study was conducted in the greenhouse ventilated with filtered air, which excludes the effects of diverse atmospheric aerosols which are out of scope, and only focus on the specific foliar compounds, thus validly displays their correlation with stomata responses. Taking this aerosols deposition into consideration, the inconsistency of previous research on nocturnal g_{sw} under nutrient deficiency might be as well explained.

As the foliar nutrient is absorbed over both leaf sides (Gorlach & Muhling, 2021), and nutrient deficiency might alter the composition of plant epidermal structures such as stomata and trichomes, it is strongly dependent on the plant species (Fernandez *et al.*, 2014; Henningsen *et al.*, 2022). Associated with the theory of hydraulic activation of stomata, the potential foliar uptake might happen to each stomatal pore individually (Burkhardt, 2010); this is assisted by the time series results (*Figure 4.3*), showing a reacting time of circa 10 to 13 days is required for plants to develop the increased stomatal conductance during nighttime.

4.4.4 Chemical characteristics of leaf surface compounds

As mentioned above, the establishment of salt solution films on the hydrophobic layers covering the leaf surface and the internal part of the guard cells requires a duration (Nonami *et al.*, 1991; Burkhardt, 2010; Vega *et al.*, 2023), but has been shown to occur from the exterior through salts deliquescing and efflorescing due to humidity fluctuations (Qazi *et al.*, 2019). The process mainly

depends on the deliquescence humidity (DRH) of the salt (Burkhardt & Eiden, 1994) and the position of the ions in the Hofmeister series; the latter affects the surface tension of deliquescent salts (Burkhardt *et al.*, 2012).

In this study, the DRH values of all three compound forms used for spraying were between 80 and 85% at 20°C (*Table 4.1*), and the recorded leaf surface humidity within the ventilated chamber did not exceed 75% (Supplementary information). However, given the calm greenhouse conditions and the resulting thick leaf boundary layers, the DRH values of the sprayed compounds were plausibly exceeded on leaf surfaces with transpiring stomata during the 14 days between spraying and measurements. Once the DRH is exceeded, liquid water can remain in a metastable state (i.e., as a concentrated solution) (Fernandez *et al.*, 2020) between DRH and efflorescence relative humidity (ERH), particularly for the ammonium salts (P spray and S spray) with ERH values of about 30 to 40%. Either ERH differences or contrasting Hofmeister series positioning of nitrate and ammonium as a chaotrope and kosmotrope, respectively, may have resulted in a more efficient response to nitrate than to ammonium in N-deficient plants. Moreover, a recent study showed that P-deficient plants acidified the leaf surface to mobilize P from desert dust through foliage (Gross et al., 2021).

In reference to the present case, the increased nocturnal g_{sw} and the consequent nocturnal transpiration potentially fulfilled the function to enhance the mobility of the hygroscopic salts and was not merely a side effect of stomatal opening for nutrient uptake.

4.5 Conclusion

This study explains the possible connection between nocturnal stomatal regulations and plant nutrient regimes, from the perspective of hygroscopic leaf surface compounds. Future investigations need to better characterize sensing/signaling mechanisms, nocturnal nutrient uptake from leaf surfaces, correlation with stomata characteristics and level of plant nutrient deficiency, and nocturnal stomatal responses to foliar nutrient applications. These processes are potentially pivotal in interpreting and optimizing foliar fertilization treatments, as well as calibrating current models on ecosystem respiratory CO_2 flux and plant water relations.

Chapter 5

This chapter presents the general discussion and concluding remarks referring to the initially stated research objectives in each study, as well as provides the outlook for future research.

5 General Discussion and Conclusion

5.1 Deposition and deliquescence of hygroscopic leaf surface material

As observed in the current research and previous studies, deliquescent hygroscopic material (e.g., atmospheric aerosols and agricultural foliar applications) depositing on leaf surfaces forms amorphous crusts on the cuticle, and results in an accumulated thin layer that covers the tubular wax fibrils (Burkhardt, 2010; Burkhardt *et al.*, 2018). Consequently, this hygroscopic surface material causes notable morphological changes, leading to reduced heterogeneity of stomata, and indirectly to lower stomatal density and lower stomatal coverage (Study 1 and Study 2).

5.2 Functions of hydraulic activation of stomata

Centering on the hygroscopic action of leaf surface material, it is indicated that these compounds depositing close to transpiring stomata exhibit mobility by deliquescence under high relative humidity in the leaf boundary layer (Burkhardt & Hunsche, 2013) and form saturated film-like solutions (blue line in *Figure 5.1*). These saturated thin films enter into the stomata and connect with the liquid water coming from the roots (green line in *Figure 5.1*), thus forming a continuous liquid water layer that can transport water and dissolved substances in accordance with the concentration gradient. Independently of the stomatal aperture and the concurrent CO_2 influx, the hygroscopic compounds and the concentrated solutions reduce saturation vapor pressure and alter vapor pressure deficit (VPD). This “hydraulic activation of stomata” (HAS) may result in additional liquid water loss and potential ionic movements into and out of stomata (Burkhardt, 2010; Song *et al.*, 2015; Burkhardt & Grantz, 2017).

The original HAS theory regards the highly concentrated thin film as a parallel liquid transpiration pathway (blue and green pathways in *Figure 5.1*; illustrations are adjusted from Forseth, 2010). When the turbulence caused by wind on the leaf surface triggers the temporary removal of leaf boundary layer,

the moisture gradient between the highly concentrated film and the atmosphere increases and results in water evaporation. Thus, the water potential of the leaf surface material decreases and this information is instantly transmitted along the hydraulic film to the interior of the leaf, from where new liquid water is drawn to the surface. That is to say, the HAS effect enhances transpirational processes (blue dotted arrows in *Figure 5.1*), becoming a significant contributor to non-beneficial water loss in plants. After the formation of this thin film, it remains in place, functioning in accordance with the water potential gradient and the water-use strategy specific to different plant species. This concept is thoroughly examined and discussed in Study 1 and Study 2.

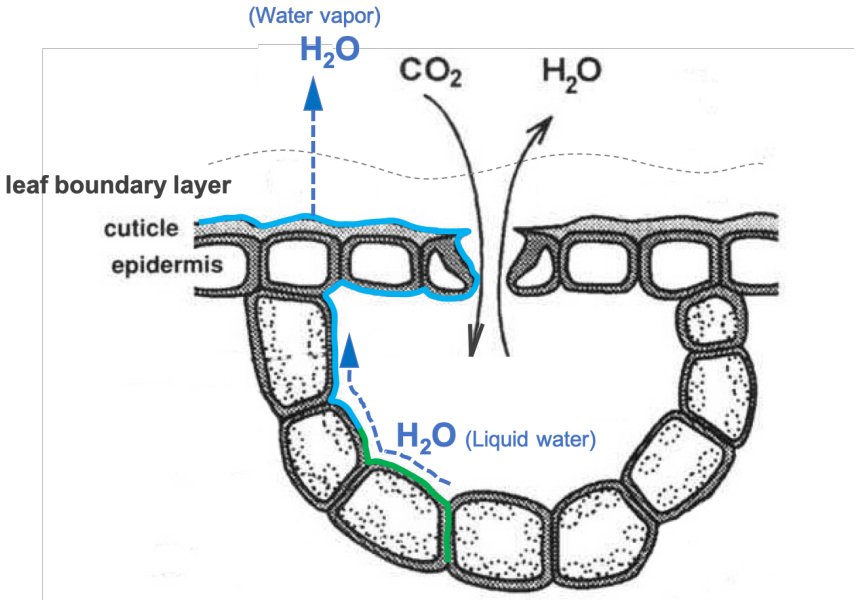

Figure 5.1. The diffusion pathway for CO_2 and H_2O from the surrounding air through the stomata (with HAS effect, daytime).

Black solid arrows indicate the direction of CO_2 and H_2O fluxes during natural plant photosynthesis process in daytime. Blue and green solid lines are the pathway of highly concentrated solutions from leaf surface material and liquid water coming from the roots, respectively. Blue dotted arrows show the direction of additional water loss cause by HAS effect.

During nighttime with high atmospheric relative humidity, this HAS pathway exhibits distinct bidirectionality (blue dotted arrows in *Figure 5.2*). In such stable nighttime environment, when the atmospheric relative humidity exceeds the deliquescence point of the hygroscopic compound (i.e., deliquescence relative humidity, DRH), these compounds absorb and dissolve into the water at the leaf surface. This process is recognized as foliar water uptake and aligned with the concept of "invisible dew condensation", disregarding the conventional prerequisite for dew formation associated with reaching 100% relative humidity. Conversely, if the nocturnal relative humidity remains below the DRH, the hygroscopic leaf surface material may continue to serve as the transpirational pathway, resulting in additional water loss as in the original HAS theory mentioned above. Therefore, the direction of liquid water and water vapor movements is determined by the overall water potential gradient of hygroscopic material at the leaf surface.

On the other hand, as foliar water uptake occurs in response to the high relative humidity in the nighttime, there is also facilitated movement of ions at the leaf surface (red dotted arrows in *Figure 5.2*). The humidified leaf surface allows the expansion of the highly concentrated thin film, likely converting the mobility of ionic compounds into foliar nutrient uptake through the HAS pathway. The finding that poplars opened stomata exclusively when the deficient nutrient was present on the leaf surface strongly implies that plants have the capability to detect and respond to nutrient deficiency. This underscores the existence of a trade-off between foliar nutrient uptake and water fluxes, operating through the same HAS pathway (Study 3). Further (molecular) research is needed to identify and describe the underlying mechanism of foliar nutrient uptake.

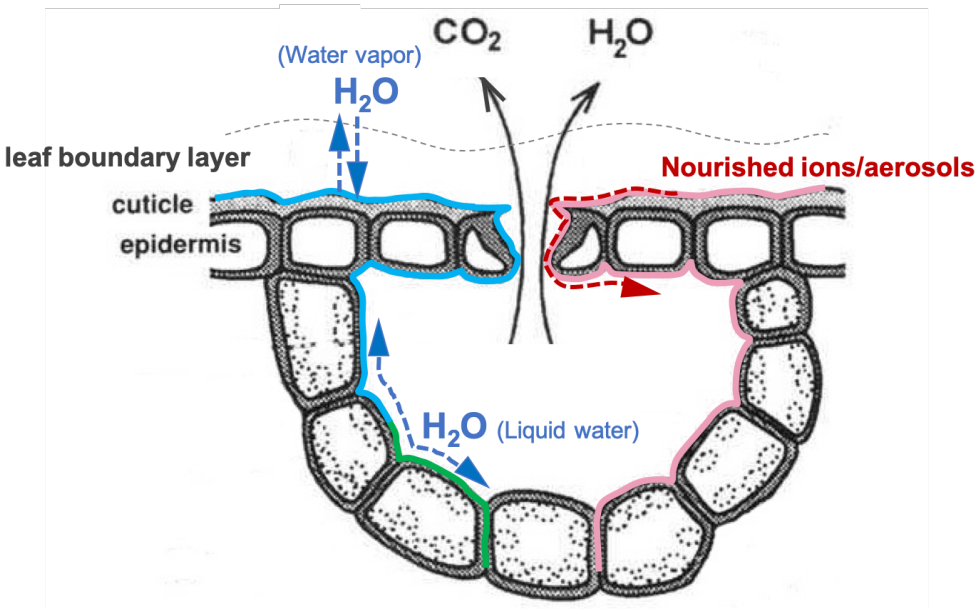

Figure 5.2. The diffusion pathway for CO_2, H_2O, and ions from the surrounding air through the stomata (with HAS effect, nighttime).

Black solid arrows are the direction of CO_2 and H_2O fluxes during natural plant respiration in nighttime. Blue dotted arrows show the bidirectional possibilities of H_2O fluxes through the HAS pathway. Additionally, red dotted arrow indicates the direction of ionic movements as the potential foliar uptake function of the HAS pathway (illustrated as pink solid line).

5.3 Impacts of hygroscopic actions on stomatal responses related to plant water use

Given that VPD reflects the gradient of atmospheric moisture at a specific temperature and is the driving force for plant transpiration, traditional theories regarding stomatal regulation have been predominantly focused on this factor alone. However, the inclusion of hygroscopic leaf surface material (e.g., atmospheric aerosols) suggests a more complex interplay of factors. The deliquescence of these compounds induces changes in saturation vapor pressure, consequently affecting VPD within the leaf boundary layer and the substomatal cavity. These altered evaporative demands influence transpiration and g_{sw}, leading to dynamic fluctuations backwards to VPD as plants strive to achieve physiological balance (Wang *et al.*, 2018; Wang, B *et al.*, 2021).

In addition to the perspective of changes in relative humidity and VPD which happening in the leaf boundary layer, the HAS theory introduced an additional dimension of water loss based on the thin film structure, independent of stomatal aperture and gaseous flux (Burkhardt, 2010; Burkhardt & Grantz, 2017). That is to say, in the presence of hygroscopic material on leaf surfaces, three main factors regulate stomatal control over plant water use at the leaf-level scale:

(i) variations in VPD from the environment to the inner leaf;
(ii) VPD alterations induced by hygroscopic material;
(iii) the HAS pathway (parallel liquid transpiration pathway).

However, these factors are interdependent, making it challenging to isolate the impact of each individual factor from the overall effect.

On a related note, research on hygroscopic leaf surface material has revealed three distinct effects on stomatal responses (Grantz *et al.*, 2018):

(i) reduced stomatal apertures of *Vicia faba (L.)* at each examined VPD level;
(ii) increased stomatal conductance at similar stomatal aperture;
(iii) lower heterogeneity between apertures of single pores, i.e., reduced patchiness.

Due to the varying magnitude of changes in stomatal apertures to VPD (effect i) and stomatal conductance to stomatal aperture (effect ii), as well as the impacts of hygroscopic material on different plant species, the overall effect on stomatal responses can sometimes complicate investigations (Study 1).

In general, hygroscopic leaf surface material enhances symptoms of long-term plant water deficit, which was observed even for hydroponic plants. The influences are observed with varying degrees in higher g_{min}, lower leaf water potential at turgor loss, lower leaf water potential at noon, and alter water use efficiency. It is concluded that the effects of hygroscopic material on stomatal responses vary among plants with different levels of isohydricity. With a specific focus on the examined poplar clones, anisohydric poplars demonstrate larger changes of stomatal aperture and water potential caused by hygroscopic material, with higher variations between individuals. In contrast, isohydric poplars significantly regulate stomatal responses in response to atmospheric VPD changes and seemed to be less influenced by hygroscopic leaf surface material (Study 1 and Study 2). However, the hygroscopic compounds such as aerosols compromise the natural protection plants usually have from stomatal closure and lead to increased g_{min}, which could be critical during drought conditions. The differences found in isohydric and anisohydric plants contribute to explain the inconsistencies in experimental indicators from previous studies. It also highlights the species-specific and environment-specific nature of the HAS effect.

Despite these findings, the practical application of hygroscopic aerosols impacts in the field remains challenging. Varying environmental conditions and inconsistent monitoring standards can affect data accuracy. In addition, the influence of different ionic compounds and their individual effects on plant physiology may lead to various degrees of influence, necessitating further clarification (Study 1 and Study 3).

5.4 Outlooks

This study reinforces the HAS theory, highlighting the significance of the desiccant impact of hygroscopic aerosols on plants. It provides a thorough examination of leaf-level gas exchange and stomatal responses to plant water utilization under hygroscopic actions, confirming different reactions based on the isohydricity of plants. Additionally, it supports the idea of the HAS pathway being multifunctional, contributing to a comprehensive explanation of potential foliar uptake and nocturnal transpiration.

Based on these findings, future research should consider adjustments to water use efficiency (WUE) calculations based on gas exchange models (e.g., g_1 in Ball-Berry model) and $\delta^{13}C$ values. In addition, it is needed to simulate a new model and quantify the changes in water flux induced by the HAS effect. These efforts aim to evaluate the magnitude of HAS contribution to overall water loss and its interaction with VPD, enriching our understanding of the mechanisms governing plant water relations.

Future research should also focus on expanding to larger scales, integrating with whole-plant and ecosystem-level interactions, or delving into the sensing and signaling mechanisms of stomatal regulations. Exploring these directions will contribute to a more holistic understanding of plant-environment interactions and the implications for ecosystem dynamics.

Reference

Achneck HE, Serpe MJ, Jamiolkowski RM, Eibest LM, Craig SL, Lawson JH. 2010. Regenerating titanium ventricular assist device surfaces after gold/palladium coating for scanning electron microscopy. *Microsc Res Tech* **73**(1): 71-76.

Acosta-Motos JR, Ortuno MF, Bernal-Vicente A, Diaz-Vivancos P, Sanchez-Blanco MJ, Hernandez JA. 2017. Plant Responses to Salt Stress: Adaptive Mechanisms. *Agronomy-Basel* **7**(1).

Ainsworth EA, Rogers A. 2007. The response of photosynthesis and stomatal conductance to rising [CO2]: mechanisms and environmental interactions. *Plant Cell and Environment* **30**(3): 258-270.

Anderson LD, Faul KL, Paytan A. 2010. Phosphorus associations in aerosols: What can they tell us about P bioavailability? *Marine Chemistry* **120**(1-4): 44-56.

Andreae MO. 2007. Aerosols before pollution. *Science* **315**(5808): 50-51.

Aphalo PJ, Jarvis PG. 1993. An Analysis of Balls Empirical-Model of Stomatal Conductance. *Annals of Botany* **72**(4): 321-327.

Ball JT, Woodrow IE, Berry JA 1987. A model predicting stomatal conductance and its contribution to the control of photosynthesis under different environmental conditions. *Progress in photosynthesis research: volume 4 proceedings of the VIIth international congress on photosynthesis providence, Rhode Island, USA, august 10–15, 1986*: Springer. 221-224.

Banks JM, Hirons AD. 2019. Alternative methods of estimating the water potential at turgor loss point in Acer genotypes. *Plant Methods* **15**.

Barbour MM, Cernusak LA, Whitehead D, Griffin KL, Turnbull MH, Tissue DT, Farquhar GD. 2005. Nocturnal stomatal conductance and implications for modelling delta O-18 of leaf-respired CO2 in temperate tree species. *Functional Plant Biology* **32**(12): 1107-1121.

Bartlett MK, Scoffoni C, Ardy R, Zhang Y, Sun SW, Cao KF, Sack L. 2012a. Rapid determination of comparative drought tolerance traits: using an osmometer to predict turgor loss point. *Methods in Ecology and Evolution* **3**(5): 880-888.

Bartlett MK, Scoffoni C, Sack L. 2012b. The determinants of leaf turgor loss point and prediction of drought tolerance of species and biomes: a global meta-analysis. *Ecology Letters* **15**(5): 393-405.

Basi S, Burkhardt J, Noga G, Hunsche M. 2014. Hygroscopic salts support the stomatal penetration of glyphosate and influence its biological efficacy. *Weed Biology and Management* **14**(3): 186-197.

Bates LS, Waldren RP, Teare ID. 1973. Rapid Determination of Free Proline for Water-Stress Studies. *Plant and Soil* **39**(1): 205-207.

Bauerle WL, Bowden JD. 2011. Separating foliar physiology from morphology reveals the relative roles of vertically structured transpiration factors within red maple crowns and limitations of larger scale models. *Journal of Experimental Botany* **62**(12): 4295-4307.

Bengtson C, Larsson S, Liljenberg C. 1978. Effects of Water Stress on Cuticular Transpiration Rate and Amount and Composition of Epicuticular Wax in Seedlings of 6 Oat Varieties. *Physiologia Plantarum* **44**(4): 319-324.

Berriel V, Perdomo C, Monza J. 2020. Carbon Isotope Discrimination and Water-Use Efficiency in Crotalaria Cover Crops under Moderate Water Deficit. *Journal of Soil Science and Plant Nutrition* **20**(2): 537-545.

Berry JA, Beerling DJ, Franks PJ. 2010. Stomata: key players in the earth system, past and present. *Current Opinion in Plant Biology* **13**(3): 232-239.

Bi HH, Kovalchuk N, Langridge P, Tricker PJ, Lopato S, Borisjuk N. 2017. The impact of drought on wheat leaf cuticle properties. *Bmc Plant Biology* **17**.

Bressi M, Cavalli F, Putaud JP, Fröhlich R, Petit JE, Aas W, Äijälä M, Alastuey A, Allan JD, Aurela M, et al. 2021. A European aerosol phenomenology - 7: High-time resolution chemical characteristics of submicron particulate matter across Europe. *Atmospheric Environment-X* **10**.

Brodribb TJ, Holbrook NM. 2003. Stomatal closure during leaf dehydration, correlation with other leaf physiological traits. *Plant physiology* **132**(4): 2166-2173.

Brodribb TJ, McAdam SAM, Jordan GJ, Martins SCV. 2014. Conifer species adapt to low-rainfall climates by following one of two divergent pathways. *Proceedings of the National Academy of Sciences of the United States of America* **111**(40): 14489-14493.

Broeckx LS, Fichot R, Verlinden MS, Ceulemans R. 2014. Seasonal variations in photosynthesis, intrinsic water-use efficiency and stable isotope composition of poplar leaves in a short-rotation plantation. *Tree Physiology* **34**(7): 701-715.

Bucci SJ, Scholz FG, Goldstein G, Meinzer FC, Hinojosa JA, Hoffmann WA, Franco AC. 2004. Processes preventing nocturnal equilibration between leaf and soil water potential in tropical savanna woody species. *Tree Physiology* **24**(10): 1119-1127.

Buck AL. 1981. New Equations for Computing Vapor-Pressure and Enhancement Factor. *Journal of Applied Meteorology* **20**(12): 1527-1532.

Buckley TN. 2005. The control of stomata by water balance. *New Phytologist* **168**(2): 275-291.

Buckley TN, Mott KA. 2013. Modelling stomatal conductance in response to environmental factors. *Plant Cell and Environment* **36**(9): 1691-1699.

Burkhardt J. 2010. Hygroscopic particles on leaves: nutrients or desiccants? *Ecological Monographs* **80**(3): 369-399.

Burkhardt J, Basi S, Pariyar S, Hunsche M. 2012. Stomatal penetration by aqueous solutions - an update involving leaf surface particles. *New Phytologist* **196**(3): 774-787.

Burkhardt J, Eiden R. 1990. The ion concentration of dew condensed on Norway spruce (Picea abies (L.) Karst.) and Scots pine (Pinus sylvestris L.) needles. *Trees-Structure and Function* **4**(1): 22-26.

Burkhardt J, Eiden R. 1994. Thin Water Films on Coniferous Needles. *Atmospheric Environment* **28**(12): 2001-2011.

Burkhardt J, Grantz DA 2017. Plants and Atmospheric Aerosols. In: Cánovas FM, Lüttge U, Matyssek R eds. *Progress in Botany Vol. 78*. Cham: Springer International Publishing, 369-406.

Burkhardt J, Hunsche M. 2013. "Breath figures" on leaf surfaces-formation and effects of microscopic leaf wetness. *Frontiers in Plant Science* **4**.

Burkhardt J, Kaiser H, Kappen L, Goldbach HE. 2001. The possible role of aerosols on stomatal conductivity for water vapour. *Basic and Applied Ecology* **2**(4): 351-364.

Burkhardt J, Pariyar S. 2014. Particulate pollutants are capable to 'degrade' epicuticular waxes and to decrease the drought tolerance of Scots pine (Pinus sylvestris L.). *Environ Pollut* **184**: 659-667.

Burkhardt J, Pariyar S. 2016. How does the VPD response of isohydric and anisohydric plants depend on leaf surface particles? *Plant Biology* **18**: 91-100.

Burkhardt J, Zinsmeister D, Grantz DA, Vidic S, Sutton MA, Hunsche M, Shyam P. 2018. Camouflaged as degraded wax: hygroscopic aerosols contribute to leaf desiccation, tree mortality, and forest decline. *Environmental Research Letters* **13**(8).

Bussotti F, Grossoni P, Pantani F. 1995. The Role of Marine Salt and Surfactants in the Decline of Tyrrhenian Coastal Vegetation in Italy. *Annales Des Sciences Forestieres* **52**(3): 251-261.

Cabrera-Bosquet L, Molero G, Bort J, Nogues S, Araus JL. 2007. The combined effect of constant water deficit and nitrogen supply on WUE,

NUE and Delta C-13 in durum wheat potted plants. *Annals of Applied Biology* **151**(3): 277-289.

Caine RS, Yin XJ, Sloan J, Harrison EL, Mohammed U, Fulton T, Biswal AK, Dionora J, Chater CC, Coe RA, et al. 2019. Rice with reduced stomatal density conserves water and has improved drought tolerance under future climate conditions. *New Phytologist* **221**(1): 371-384.

Caird MA, Richards JH, Donovan LA. 2007. Nighttime stomatal conductance and transpiration in C-3 and C-4 plants. *Plant Physiology* **143**(1): 4-10.

Cavender-Bares J, Sack L, Savage J. 2007. Atmospheric and soil drought reduce nocturnal conductance in live oaks. *Tree Physiology* **27**(4): 611-620.

Ceulemans R, Impens I, Imler R. 1988. Stomatal Conductance and Stomatal Behavior in Populus Clones and Hybrids. *Canadian Journal of Botany-Revue Canadienne De Botanique* **66**(7): 1404-1414.

Chadwick OA, Derry LA, Vitousek PM, Huebert BJ, Hedin LO. 1999. Changing sources of nutrients during four million years of ecosystem development. *Nature* **397**(6719): 491-497.

Chameides WL, Yu H, Liu SC, Bergin M, Zhou X, Mearns L, Wang G, Kiang CS, Saylor RD, Luo C, et al. 1999. Case study of the effects of atmospheric aerosols and regional haze on agriculture: An opportunity to enhance crop yields in China through emission controls? *Proceedings of the National Academy of Sciences of the United States of America* **96**(24): 13626-13633.

Chappelka AH, Neufeld HS. 2018. A link between physical and chemical climate change: the enhancement of vegetative water loss by atmospheric aerosols. *New Phytologist* **219**(1): 9-11.

Chen H, Xia DS, Wang B, Liu H, Ma XY. 2022. Pollution monitoring using the leaf-deposited particulates and magnetism of the leaves of 23 plant species in a semi-arid city, Northwest China. *Environmental Science and Pollution Research* **29**(23): 34898-34911.

Chen HL, Li CP, Tang CS, Lung SCC, Chuang HC, Chou DW, Chang LT. 2020. Risk Assessment for People Exposed to PM2.5 and Constituents at Different Vertical Heights in an Urban Area of Taiwan. *Atmosphere* **11**(11).

Chen LX, Liu CM, Zhang L, Zou R, Zhang ZQ. 2017. Variation in Tree Species Ability to Capture and Retain Airborne Fine Particulate Matter (PM2.5). *Scientific Reports* **7**.

Chen MJ, Yang PH, Hsieh MT, Yeh CH, Huang CH, Yang CM, Lin GM. 2018. Machine learning to relate PM2.5 and PM10 concentrations to outpatient visits for upper respiratory tract infections in Taiwan: A nationwide analysis. *World Journal of Clinical Cases* **6**(8): 200-206.

Chi CE, Zinsmeister D, Lai IL, Chang SC, Kuo YL, Burkhardt J. 2022. Aerosol impacts on water relations of camphor (Cinnamomum camphora). *Front Plant Sci* **13**: 892096.

Chou CCK, Lee CT, Cheng MT, Yuan CS, Chen SJ, Wu YL, Hsu WC, Lung SC, Hsu SC, Lin CY, et al. 2010. Seasonal variation and spatial distribution of carbonaceous aerosols in Taiwan. *Atmospheric Chemistry and Physics* **10**(19): 9563-9578.

Chowdhury FI, Arteaga C, Alam MS, Alam I, de Dios VR. 2022. Drivers of nocturnal stomatal conductance in C-3 and C-4 plants. *Science of the Total Environment* **814**.

Christman MA, Richards JH, Mckay JK, Stahl EA, Juenger TE, Donovan LA. 2008. Genetic variation in Arabidopsis thaliana for night-time leaf conductance. *Plant Cell and Environment* **31**(8): 1170-1178.

Cirelli D, Equiza MA, Lieffers VJ, Tyree MT. 2016. Populus species from diverse habitats maintain high night-time conductance under drought. *Tree Physiology* **36**(2): 229-242.

Claverie E, Meunier F, Javaux M, Sadok W. 2018. Increased contribution of wheat nocturnal transpiration to daily water use under drought. *Physiologia Plantarum* **162**(3): 290-300.

Collatz GJ, Ball JT, Grivet C, Berry JA. 1991. Physiological and Environmental-Regulation of Stomatal Conductance, Photosynthesis and Transpiration - a Model That Includes a Laminar Boundary-Layer. *Agricultural and Forest Meteorology* **54**(2-4): 107-136.

Condon AG, Richards RA, Farquhar GD. 1992. The Effect of Variation in Soil-Water Availability, Vapor-Pressure Deficit and Nitrogen Nutrition on Carbon Isotope Discrimination in Wheat. *Australian Journal of Agricultural Research* **43**(5): 935-947.

Condon AG, Richards RA, Rebetzke GJ, Farquhar GD. 2002. Improving intrinsic water-use efficiency and crop yield. *Crop Science* **42**(1): 122-131.

Conte MH, Weber JC, Carlson PJ, Flanagan LB. 2003. Molecular and carbon isotopic composition of leaf wax in vegetation and aerosols in a northern prairie ecosystem. *Oecologia* **135**(1): 67-77.

Coopman RE, Nguyen HT, Mencuccini M, Oliveira RS, Sack L, Lovelock CE, Ball MC. 2021. Harvesting water from unsaturated atmospheres: deliquescence of salt secreted onto leaf surfaces drives reverse sap flow in a dominant arid climate mangrove, Avicennia marina. *New Phytologist* **231**(4): 1401-1414.

Daley MJ, Phillips NG. 2006. Interspecific variation in nighttime transpiration and stomatal conductance in a mixed New England deciduous forest. *Tree Physiology* **26**(4): 411-419.

de Dios VR, Chowdhury FI, Granda E, Yao YA, Tissue DT. 2019. Assessing the potential functions of nocturnal stomatal conductance in C-3 and C-4 plants. *New Phytologist* **223**(4): 1696-1706.

de Dios VR, Loik ME, Smith R, Aspinwall MJ, Tissue DT. 2016. Genetic variation in circadian regulation of nocturnal stomatal conductance enhances carbon assimilation and growth. *Plant Cell and Environment* **39**(1): 3-11.

de Dios VR, Turnbull MH, Barbour MM, Ontedhu J, Ghannoum O, Tissue DT. 2013. Soil phosphorous and endogenous rhythms exert a larger impact than CO2 or temperature on nocturnal stomatal conductance in Eucalyptus tereticornis. *Tree Physiology* **33**(11): 1206-1215.

Dodd AN, Salathia N, Hall A, Kevei E, Toth R, Nagy F, Hibberd JM, Millar AJ, Webb AAR. 2005. Plant circadian clocks increase photosynthesis, growth, survival, and competitive advantage. *Science* **309**(5734): 630-633.

Dolatabadian A, Sanavy SAMM, Chashmi NA. 2008. The effects of foliar application of ascorbic acid (Vitamin C) on antioxidant enzymes activities, lipid peroxidation and proline accumulation of canola (Brassica napus L.) under conditions of salt stress. *Journal of Agronomy and Crop Science* **194**(3): 206-213.

Drake PL, Froend RH, Franks PJ. 2013. Smaller, faster stomata: scaling of stomatal size, rate of response, and stomatal conductance. *Journal of Experimental Botany* **64**(2): 495-505.

Durand M, Brendel O, Buré C, Le Thiec D. 2019. Altered stomatal dynamics induced by changes in irradiance and vapour-pressure deficit under drought: impacts on the whole-plant transpiration efficiency of poplar genotypes. *New Phytologist* **222**(4): 1789-1802.

Dutcher CS, Wexler AS, Clegg SL. 2010. Surface Tensions of Inorganic Multicomponent Aqueous Electrolyte Solutions and Melts. *Journal of Physical Chemistry A* **114**(46): 12216-12230.

Duursma RA. 2015. Plantecophys - An R Package for Analysing and Modelling Leaf Gas Exchange Data. *Plos One* **10**(11).

Duursma RA, Blackman CJ, Lopez R, Martin-StPaul NK, Cochard H, Medlyn BE. 2019. On the minimum leaf conductance: its role in models of plant water use, and ecological and environmental controls. *New Phytologist* **221**(2): 693-705.

Dzierzanowski K, Popek R, Gawronska H, Saebo A, Gawronski SW. 2011. Deposition of Particulate Matter of Different Size Fractions on Leaf Surfaces and in Waxes of Urban Forest Species. *International Journal of Phytoremediation* **13**(10): 1037-1046.

Easlon HM, Richards JH. 2009. Photosynthesis affects following night leaf conductance in Vicia faba. *Plant Cell and Environment* **32**(1): 58-63.

Eichert T, Goldbach HE. 2008. Equivalent pore radii of hydrophilic foliar uptake routes in stomatous and astomatous leaf surfaces - further evidence for a stomatal pathway. *Physiologia Plantarum* **132**(4): 491-502.

Eichert T, Goldbach HE, Burkhardt J. 1998. Evidence for the uptake of large anions through stomatal pores. *Botanica Acta* **111**(6): 461-466.

Eichert T, Kurtz A, Steiner U, Goldbach HE. 2008. Size exclusion limits and lateral heterogeneity of the stomatal foliar uptake pathway for aqueous solutes and water-suspended nanoparticles. *Physiologia Plantarum* **134**(1): 151-160.

Eller CB, Lima AL, Oliveira RS. 2016. Cloud forest trees with higher foliar water uptake capacity and anisohydric behavior are more vulnerable to drought and climate change. *New Phytologist* **211**(2): 489-501.

Eller F, Jensen K, Reisdorff C. 2017. Nighttime stomatal conductance differs with nutrient availability in two temperate floodplain tree species. *Tree Physiology* **37**(4): 428-440.

Esperon-Rodriguez M, Power SA, Tjoelker MG, Marchin RM, Rymer PD. 2021. Contrasting heat tolerance of urban trees to extreme temperatures during heatwaves. *Urban Forestry & Urban Greening* **66**: 127387.

Even M, Sabo M, Meng DL, Kreszies T, Schreiber L, Fricke W. 2018. Night-time transpiration in barley (Hordeum vulgare) facilitates respiratory carbon dioxide release and is regulated during salt stress. *Annals of Botany* **122**(4): 569-582.

Ewing GE. 2005. What is thin film water, and does it matter? *Abstracts of Papers of the American Chemical Society* **229**: U731-U731.

Fang GC, Chang SC. 2010. Atmospheric particulate (PM10 and PM2 (5)) mass concentration and seasonal variation study in the Taiwan area during 2000-2008. *Atmospheric Research* **98**(2-4): 368-377.

Farquhar GD, Caemmerer SV, Berry JA. 1980. A Biochemical-Model of Photosynthetic Co2 Assimilation in Leaves of C-3 Species. *Planta* **149**(1): 78-90.

Farquhar GD, Ehleringer JR, Hubick KT. 1989. Carbon Isotope Discrimination and Photosynthesis. *Annual Review of Plant Physiology and Plant Molecular Biology* **40**: 503-537.

Farquhar GD, Richards RA. 1984. Isotopic Composition of Plant Carbon Correlates with Water-Use Efficiency of Wheat Genotypes. *Australian Journal of Plant Physiology* **11**(6): 539-552.

Feng XH, Dietze M. 2013. Scale dependence in the effects of leaf ecophysiological traits on photosynthesis: Bayesian parameterization of photosynthesis models. *New Phytologist* **200**(4): 1132-1144.

Fernandez V, Brown PH. 2013. From plant surface to plant metabolism: the uncertain fate of foliar-applied nutrients. *Frontiers in Plant Science* **4**.

Fernandez V, Eichert T. 2009. Uptake of Hydrophilic Solutes Through Plant Leaves: Current State of Knowledge and Perspectives of Foliar Fertilization. *Critical Reviews in Plant Sciences* **28**(1-2): 36-68.

Fernandez V, Gil-Pelegrin E, Eichert T. 2021. Foliar water and solute absorption: an update. *Plant Journal* **105**(4): 870-883.

Fernandez V, Guzman P, Peirce CAE, McBeath TM, Khayet M, McLaughlin MJ. 2014. Effect of wheat phosphorus status on leaf surface properties and permeability to foliar-applied phosphorus. *Plant and Soil* **384**(1-2): 7-20.

Fernandez V, Guzman-Delgado P, Graca J, Santos S, Gil L. 2016. Cuticle Structure in Relation to Chemical Composition: Re-assessing the Prevailing Model. *Frontiers in Plant Science* **7**.

Fernandez V, Pimentel C, Bahamonde HA. 2020. Salt hydration and drop drying of two model calcium salts: Implications for foliar nutrient absorption and deposition. *Journal of Plant Nutrition and Soil Science* **183**(5): 592-601.

Forseth IN. 2010. The Ecology of Photosynthetic Pathways. *Nature Education Knowledge* **3**(10): 4.

Franks PJ, Berry JA, Lombardozzi DL, Bonan GB. 2017. Stomatal Function across Temporal and Spatial Scales: Deep-Time Trends, Land-Atmosphere Coupling and Global Models. *Plant Physiology* **174**(2): 583-602.

Franks PJ, Doheny-Adams TW, Britton-Harper ZJ, Gray JE. 2015. Increasing water-use efficiency directly through genetic manipulation of stomatal density. *New Phytologist* **207**(1): 188-195.

Fricke W. 2020. Energy costs of salinity tolerance in crop plants: night-time transpiration and growth. *New Phytologist* **225**(3): 1152-1165.

Gorka M, Bartz W, Skuridina A, Potysz A. 2020. Populus nigra Italica Leaves as a Valuable Tool for Mineralogical and Geochemical Interpretation of Inorganic Atmospheric Aerosols' Genesis. *Atmosphere* **11**(10).

Gorlach BM, Muhling KH. 2021. Phosphate foliar application increases biomass and P concentration in P deficient maize. *Journal of Plant Nutrition and Soil Science* **184**(3): 360-370.

Grantz DA, Karr M, Burkhardt J. 2020. Heterogeneity of Stomatal Pore Area Is Suppressed by Ambient Aerosol in the Homobaric Species,Vicia faba. *Frontiers in Plant Science* **11**.

Grantz DA, Zinsmeister D, Burkhardt J. 2018. Ambient aerosol increases minimum leaf conductance and alters the aperture-flux relationship as stomata respond to vapor pressure deficit (VPD). *New Phytologist* **219**(1): 275-286.

Griffin-Nolan RJ, Ocheltree TW, Mueller KE, Blumenthal DM, Kray JA, Knapp AK. 2019. Extending the osmometer method for assessing drought tolerance in herbaceous species. *Oecologia* **189**(2): 353-363.

Grulke NE, Alonso R, Nguyen T, Cascio C, Dobrowolski W. 2004. Stomata open at night in pole-sized and mature ponderosa pine: implications for O3 exposure metrics. *Tree Physiology* **24**(9): 1001–1010.

Guerrieri R, Belmecheri S, Ollinger SV, Asbjornsen H, Jennings K, Xiao JF, Stocker BD, Martin M, Hollinger DY, Bracho-Garrillo R, et al. 2019. Disentangling the role of photosynthesis and stomatal conductance on rising forest water-use efficiency. *Proceedings of the National Academy of Sciences of the United States of America* **116**(34): 16909-16914.

Hamilton DS. 2015. Natural aerosols and climate: Understanding the unpolluted atmosphere to better understand the impacts of pollution. *Weather* **70**(9): 264-268.

Heinsoo K, Koppel A. 1998. Minimum epidermal conductance of Norway spruce (Picea abies) needles: influence of age and shoot position in the crown. *Annales Botanici Fennici* **35**(4): 257-262.

Henningsen JN, Gorlach BM, Fernandez V, Dolger JL, Buhk A, Muhling KH. 2022. Foliar P application cannot fully restore photosynthetic capacity, P nutrient status, and growth of P deficient maize (Zea mays L.). *Plants-Basel* **11**(21).

Heroult A, Lin YS, Bourne A, Medlyn BE, Ellsworth DS. 2013. Optimal stomatal conductance in relation to photosynthesis in climatically contrasting Eucalyptus species under drought. *Plant Cell and Environment* **36**(2): 262-274.

Herrick JD, Thomas RB. 1999. Effects of CO2 enrichment on the photosynthetic light response of sun and shade leaves of canopy sweetgum trees (Liquidambar styraciflua) in a forest ecosystem. *Tree Physiology* **19**(12): 779-786.

Hetherington AM, Woodward FI. 2003. The role of stomata in sensing and driving environmental change. *Nature* **424**(6951): 901-908.

Ho CC, Chen LJ, Hwang JS. 2020. Estimating ground-level PM2.5 levels in Taiwan using data from air quality monitoring stations and high coverage of microsensors. *Environmental Pollution* **264**.

Hofmeister F. 1888. Zur lehre von der wirkung der salze: zweite mittheilung. *Archiv für experimentelle Pathologie und Pharmakologie* **24**: 247-260.

Howard AR, Donovan LA. 2010. Soil nitrogen limitation does not impact nighttime water loss in Populus. *Tree Physiology* **30**(1): 23-31.

Hsieh H-J. 1981. Survey of diseases of woody plants in Taiwan (4). *Quarterly Journal of Chinese Forestry* **14**(3): 77-85.

Hubick K, Farquhar G. 1989. Carbon Isotope Discrimination and the Ratio of Carbon Gained to Water Lost in Barley Cultivars. *Plant Cell and Environment* **12**(8): 795-804.

Jordan GJ, Brodribb TJ. 2007. Incontinence in aging leaves: deteriorating water relations with leaf age in Agastachys odorata (Proteaceae), a shrub with very long-lived leaves. *Functional Plant Biology* **34**(10): 918-924.

Kangur O, Steppe K, Schreel JDM, von der Crone JS, Sellin A. 2021. Variation in nocturnal stomatal conductance and development of predawn disequilibrium between soil and leaf water potentials in nine temperate deciduous tree species. *Funct Plant Biol* **48**(5): 483-492.

Kannenberg SA, Driscoll AW, Szejner P, Anderegg WRL, Ehleringer JR. 2021. Rapid increases in shrubland and forest intrinsic water-use efficiency during an ongoing megadrought. *Proceedings of the National Academy of Sciences of the United States of America* **118**(52).

Katata G, Held A. 2021. Combined measurements of microscopic leaf wetness and dry-deposited inorganic compounds in a spruce forest. *Atmospheric Pollution Research* **12**(2): 217-224.

Kavanagh KL, Pangle R, Schotzko AD. 2007. Nocturnal transpiration causing disequilibrium between soil and stem predawn water potential in mixed conifer forests of Idaho. *Tree Physiol* **27**(4): 621-629.

Keenan TF, Hollinger DY, Bohrer G, Dragoni D, Munger JW, Schmid HP, Richardson AD. 2013. Increase in forest water-use efficiency as atmospheric carbon dioxide concentrations rise. *Nature* **499**(7458): 324-+.

Kerstiens G. 1996. Cuticular water permeability and its physiological significance. *Journal of Experimental Botany* **47**(305): 1813-1832.

Khare R. 2015. A new approach to derivation of Van' t Hoff equation for osmotic pressure of a dilute solution. *Am Int J Res Sci, Technol, Eng & Math* **11**: 172-174.

Kishcha P, Wang SH, Lin NH, da Silva A, Lin TH, Lin PH, Liu GR, Starobinets B, Alpert P. 2018. Differentiating between Local and Remote Pollution over Taiwan. *Aerosol and Air Quality Research* **18**(7): 1788-1798.

Klein T. 2014. The variability of stomatal sensitivity to leaf water potential across tree species indicates a continuum between isohydric and anisohydric behaviours. *Functional Ecology* **28**(6): 1313-1320.

Knauer J, Zaehle S, Reichstein M, Medlyn BE, Forkel M, Hagemann S, Werner C. 2017. The response of ecosystem water-use efficiency to rising atmospheric CO2 concentrations: sensitivity and large-scale biogeochemical implications. *New Phytologist* **213**(4): 1654-1666.

Kosugi Y, Matsuo N. 2006. Seasonal fluctuations and temperature dependence of leaf gas exchange parameters of co-occurring evergreen and deciduous trees in a temperate broad-leaved forest. *Tree Physiology* **26**(9): 1173-1184.

Kuo Y-L, Yang Y-P, Peng S-H. 2017. Variations in the predawn leaf water potential and photosynthetic rate during the dry season and drought-tolerance mechanisms of coastal tree species. *Taiwan J. For. Sci* **32**: 131-144.

Kupper P, Rohula G, Saksing L, Sellin A, Lohmus K, Ostonen I, Helmisaari HS, Sober A. 2012. Does soil nutrient availability influence night-time water flux of aspen saplings? *Environmental and Experimental Botany* **82**: 37-42.

Lee M, Lin L, Chen C-Y, Tsao Y, Yao T-H, Fei M-H, Fang S-H. 2020. Forecasting air quality in Taiwan by using machine learning. *Scientific reports* **10**(1): 4153.

Leuning R. 1995. A Critical-Appraisal of a Combined Stomatal-Photosynthesis Model for C-3 Plants. *Plant Cell and Environment* **18**(4): 339-355.

Li Q, Zhang HM, Yan HG, Qi WY, Lin JG, Li JQ. 2020. Emission of Volatile Camphor Compounds from Cinnamomum Camphora Wood. *Wood Research* **65**(4): 663-673.

Li T-C, Yuan C-S, Huang H-C, Lee C-L, Wu S-P, Tong C. 2016. Inter-comparison of seasonal variation, chemical characteristics, and source identification of atmospheric fine particles on both sides of the Taiwan Strait. *Scientific reports* **6**(1): 22956.

Lin C-H, Wu Y-L, Lai C-H, Watson JG, Chow JC. 2008. Air quality measurements from the southern particulate matter supersite in Taiwan. *Aerosol and Air Quality Research* **8**(3): 233-264.

Lindberg SE, Lovett GM, Richter DD, Johnson DW. 1986. Atmospheric Deposition and Canopy Interactions of Major Ions in a Forest. *Science* **231**(4734): 141-145.

Liu X, Zhang X, Zhang X. 2016. A review of the research on crop responses to the increase in aerial aerosol. *Acta Ecol. Sin* **36**: 2084-2090.

Lu CQ, Tian HQ. 2017. Global nitrogen and phosphorus fertilizer use for agriculture production in the past half century: shifted hot spots and nutrient imbalance. *Earth System Science Data* **9**(1): 181-192.

Ludwig F, Jewitt RA, Donovan LA. 2006. Nutrient and water addition effects on day- and night-time conductance and transpiration in a C3 desert annual. *Oecologia* **148**(2): 219-225.

Mackova J, Vaskova M, Macek P, Hronkova M, Schreiber L, Santrucek J. 2013. Plant response to drought stress simulated by ABA application: Changes in chemical composition of cuticular waxes. *Environmental and Experimental Botany* **86**: 70-75.

Mahowald NM, Scanza R, Brahney J, Goodale CL, Hess PG, Moore JK, Neff J. 2017. Aerosol Deposition Impacts on Land and Ocean Carbon Cycles. *Current Climate Change Reports* **3**(1): 16-31.

Maneke-Fiegenbaum F, Klemm O, Lai YJ, Hung CY, Yu JC. 2018. Carbon Exchange between the Atmosphere and a Subtropical Evergreen Mountain Forest in Taiwan. *Advances in Meteorology* **2018**.

Marechaux I, Bartlett MK, Sack L, Baraloto C, Engel J, Joetzjer E, Chave J. 2015. Drought tolerance as predicted by leaf water potential at turgor loss point varies strongly across species within an Amazonian forest. *Functional Ecology* **29**(10): 1268-1277.

Marron N, Villar M, Dreyer E, Delay D, Boudouresque E, Petit J-M, Delmotte FM, Guehl J-M, Brignolas F. 2005. Diversity of leaf traits related to productivity in 31 Populus deltoides× Populus nigra clones. *Tree Physiology* **25**(4): 425-435.

Mart KB, Veneklaas EJ, Bramley H. 2016. Osmotic potential at full turgor: an easily measurable trait to help breeders select for drought tolerance in wheat. *Plant Breeding* **135**(3): 279-285.

Martinez-Vilalta J, Garcia-Forner N. 2017. Water potential regulation, stomatal behaviour and hydraulic transport under drought: deconstructing the iso/anisohydric concept. *Plant Cell and Environment* **40**(6): 962-976.

McBeath TM, Facelli E, Peirce CAE, Arachchige VK, McLaughlin MJ. 2020. Assessment of foliar-applied phosphorus fertiliser formulations to enhance phosphorus nutrition and grain production in wheat. *Crop & Pasture Science* **71**(9): 795-806.

McClung CR. 2006. Plant circadian rhythms. *Plant Cell* **18**(4): 792-803.

McDowell NG. 2011. Mechanisms Linking Drought, Hydraulics, Carbon Metabolism, and Vegetation Mortality. *Plant Physiology* **155**(3): 1051-1059.

Medlyn BE, De Kauwe MG, Lin YS, Knauer J, Duursma RA, Williams CA, Arneth A, Clement R, Isaac P, Limousin JM, et al. 2017. How do leaf and ecosystem measures of water-use efficiency compare? *New Phytologist* **216**(3): 758-770.

Meinzer FC, Smith DD, Woodruff DR, Marias DE, McCulloh KA, Howard AR, Magedman AL. 2017. Stomatal kinetics and photosynthetic gas exchange along a continuum of isohydric to anisohydric regulation of plant water status. *Plant Cell and Environment* **40**(8): 1618-1628.

Meinzer FC, Woodruff DR, Marias DE, McCulloh KA, Sevanto S. 2014. Dynamics of leaf water relations components in co-occurring iso- and anisohydric conifer species. *Plant Cell and Environment* **37**(11): 2577-2586.

Meinzer FC, Woodruff DR, Marias DE, Smith DD, McCulloh KA, Howard AR, Magedman AL. 2016. Mapping "hydroscapes' along the iso- to anisohydric continuum of stomatal regulation of plant water status. *Ecology Letters* **19**(11): 1343-1352.

Miner GL, Bauerle WL. 2017. Seasonal variability of the parameters of the Ball-Berry model of stomatal conductance in maize (Zea mays L.) and sunflower (Helianthus annuus L.) under well-watered and water-stressed conditions. *Plant Cell and Environment* **40**(9): 1874-1886.

Miner GL, Bauerle WL, Baldocchi DD. 2017. Estimating the sensitivity of stomatal conductance to photosynthesis: a review. *Plant Cell and Environment* **40**(7): 1214-1238.

Mitchell PJ, O'Grady AP, Tissue DT, White DA, Ottenschlaeger ML, Pinkard EA. 2013. Drought response strategies define the relative contributions of hydraulic dysfunction and carbohydrate depletion during tree mortality. *New Phytologist* **197**(3): 862-872.

Miyazawa SI, Livingston NJ, Turpin DH. 2006. Stomatal development in new leaves is related to the stomatal conductance of mature leaves in poplar (Populus trichocarpa × P. deltoides). *Journal of Experimental Botany* **57**(2): 373-380.

Mo L, Ma ZY, Xu YS, Sun FB, Lun XX, Liu XH, Chen JG, Yu XX. 2015. Assessing the Capacity of Plant Species to Accumulate Particulate Matter in Beijing, China. *Plos One* **10**(10).

Monclus R, Dreyer E, Villar M, Delmotte FM, Delay D, Petit JM, Barbaroux C, Thiec D, Bréchet C, Brignolas F. 2006. Impact of drought on productivity and water use efficiency in 29 genotypes of Populus deltoides x Populus nigra. *New Phytologist* **169**(4): 765-777.

Monteith JL. 1995. A Reinterpretation of Stomatal Responses to Humidity. *Plant Cell and Environment* **18**(4): 357-364.

Musselman RC, Minnick TJ. 2000. Nocturnal stomatal conductance and ambient air quality standards for ozone. *Atmospheric Environment* **34**(5): 719-733.

Navarro A, Banon S, Olmos E, Sanchez-Blanco MJ. 2007. Effects of sodium chloride on water potential components, hydraulic conductivity, gas exchange and leaf ultrastructure of Arbutus unedo plants. *Plant Science* **172**(3): 473-480.

News T. 2018. Taiwan's Scenic Hualien Area Considers Solution to Landfill Problem. Available online at: https://www.taiwannews.com.tw/en/news/3340588.

Nolan RH, Tarin T, Santini NS, McAdam SAM, Ruman R, Eamus D. 2017. Differences in osmotic adjustment, foliar abscisic acid dynamics, and stomatal regulation between an isohydric and anisohydric woody angiosperm during drought. *Plant Cell and Environment* **40**(12): 3122-3134.

Nonami H, Schulze ED, Ziegler H. 1991. Mechanisms of Stomatal Movement in Response to Air Humidity, Irradiance and Xylem Water Potential. *Planta* **183**(1): 57-64.

Novick KA, Ficklin DL, Stoy PC, Williams CA, Bohrer G, Oishi AC, Papuga SA, Blanken PD, Noormets A, Sulman BN. 2016. The increasing importance of atmospheric demand for ecosystem water and carbon fluxes. *Nature climate change* **6**(11): 1023-1027.

Nozue K, Maloof JN. 2006. Diurnal regulation of plant growth. *Plant Cell and Environment* **29**(3): 396-408.

Oliveira G, Penuelas J. 2004. Effects of winter cold stress on photosynthesis and photochemical efficiency of PSII of the Mediterranean Cistus albidus L. and Quercus ilex L. *Plant Ecology* **175**(2): 179-191.

Pariyar S, Eichert T, Goldbach HE, Hunsche M, Burkhardt J. 2013. The exclusion of ambient aerosols changes the water relations of sunflower (Helianthus annuus) and bean (Vicia faba) plants. *Environmental and Experimental Botany* **88**: 43-52.

Pariyar S, Noga G. 2018. Rainfall does not impair particulate matter accumulation on peri-urban field crops, but improves photosynthetic activity at UV exposure. *Environmental and Experimental Botany* **156**: 288-297.

Peirce CAE, McBeath TM, Fernandez V, McLaughlin MJ. 2014. Wheat leaf properties affecting the absorption and subsequent translocation of foliar-applied phosphoric acid fertiliser. *Plant and Soil* **384**(1-2): 37-51.

Pieters A, Giese M, Schmierer M, Johnson K, Asch F. 2022. Chamber-based system for measuring whole-plant transpiration dynamics. *Plant-Environment Interactions* **3**(6): 243-253.

Pourkhabbaz A, Rastin N, Olbrich A, Langenfeld-Heyser R, Polle A. 2010. Influence of Environmental Pollution on Leaf Properties of Urban Plane Trees, Platanus orientalis L. *Bulletin of Environmental Contamination and Toxicology* **85**(3): 251-255.

Premachandra GS, Saneoka H, Fujita K, Ogata S. 1992. Leaf Water Relations, Osmotic Adjustment, Cell-Membrane Stability, Epicuticular Wax Load and Growth as Affected by Increasing Water Deficits in Sorghum. *Journal of Experimental Botany* **43**(257): 1569-1576.

Putaud JP, Van Dingenen R, Alastuey A, Bauer H, Birmili W, Cyrys J, Flentje H, Fuzzi S, Gehrig R, Hansson HC, et al. 2010. A European aerosol phenomenology-3: Physical and chemical characteristics of particulate matter from 60 rural, urban, and kerbside sites across Europe. *Atmospheric Environment* **44**(10): 1308-1320.

Qazi MJ, Salim H, Doorman CAW, Jambon-Puillet E, Shahidzadeh N. 2019. Salt creeping as a self-amplifying crystallization process. *Science Advances* **5**(12).

Riederer M. 2006. Thermodynamics of the water permeability of plant cuticles: characterization of the polar pathway. *Journal of Experimental Botany* **57**(12): 2937-2942.

Rohula G, Kupper P, Raim O, Sellin A, Sober A. 2014. Patterns of night-time water use are interrelated with leaf nitrogen concentration in shoots of 16 deciduous woody species. *Environmental and Experimental Botany* **99**: 180-188.

Rosso L, Cantamessa S, Bergante S, Biselli C, Fricano A, Chiarabaglio PM, Gennaro M, Nervo G, Secchi F, Carra A. 2023. Responses to Drought Stress in Poplar: What Do We Know and What Can We Learn? *Life* **13**(2): 533.

Räsch A, Hunsche M, Mail M, Burkhardt J, Noga G, Pariyar S. 2018. Agricultural adjuvants may impair leaf transpiration and photosynthetic activity. *Plant Physiology and Biochemistry* **132**: 229-237.

Sack L, Cowan P, Jaikumar N, Holbrook N. 2003. The 'hydrology'of leaves: co-ordination of structure and function in temperate woody species. *Plant, Cell & Environment* **26**(8): 1343-1356.

Sack L, Scoffoni C. 2011. Minimum epidermal conductance (gmin, aka cuticular conductance). *PrometheusWiki* **35**: 257-262.

Sadok W, Tamang BG. 2019. Diversity in daytime and night-time transpiration dynamics in barley indicates adaptation to drought regimes across the Middle-East. *Journal of Agronomy and Crop Science* **205**(4): 372-384.

Santrucek J, Simanova E, Karbulkova J, Simkova M, Schreiber L. 2004. A new technique for measurement of water permeability of stomatous cuticular membranes isolated from Hedera helix leaves. *Journal of Experimental Botany* **55**(401): 1411-1422.

Sase H, Takamatsu T, Yoshida T, Inubushi K. 1998. Changes in properties of epicuticular wax and the related water loss in Japanese cedar (Cryptomeria japonica) affected by anthropogenic environmental factors. *Canadian Journal of Forest Research-Revue Canadienne De Recherche Forestiere* **28**(4): 546-556.

Sazeides CI, Fyllas NM, Christopoulou A 2021. Seasonal variation in foliar properties in Mediterranean Pine forests of different post-fire age. *EGU General Assembly Conference Abstracts*. EGU21-1064.

Schlegel TK, Schonherr J, Schreiber L. 2005. Size selectivity of aqueous pores in stomatous cuticles of Vicia faba leaves. *Planta* **221**(5): 648-655.

Schneider CA, Rasband WS, Eliceiri KW. 2012. NIH Image to ImageJ: 25 years of image analysis. *Nat Methods* **9**(7): 671-675.

Scholz FG, Bucci SJ, Goldstein G, Meinzer FC, Franco AC, Miralles-Wilhelm F. 2007. Removal of nutrient limitations by long-term fertilization decreases nocturnal water loss in savanna trees. *Tree Physiology* **27**(4): 551-559.

Schoppach R, Sinclair TR, Sadok W. 2020. Sleep tight and wake-up early: nocturnal transpiration traits to increase wheat drought tolerance in a Mediterranean environment. *Functional Plant Biology* **47**(12): 1117-1127.

Schultz HR. 2003. Differences in hydraulic architecture account for near-isohydric and anisohydric behaviour of two field-grown Vitis vinifera L. cultivars during drought. *Plant Cell and Environment* **26**(8): 1393-1405.

Schuster AC, Burghardt M, Riederer M. 2017. The ecophysiology of leaf cuticular transpiration: are cuticular water permeabilities adapted to ecological conditions? *Journal of Experimental Botany* **68**(19): 5271-5279.

Schwabe WW. 1952. Effects of photoperiodic treatment on stomatal movement. *Nature* **169**(4312): 1053-1054.

Shabnam N, Oh J, Park S, Kim H. 2021. Impact of particulate matter on primary leaves of Vigna radiata (L.) R. Wilczek. *Ecotoxicology and Environmental Safety* **212**.

Sharkey TD. 2016. What gas exchange data can tell us about photosynthesis. *Plant Cell and Environment* **39**(6): 1161-1163.

Sharkey TD, Bernacchi CJ, Farquhar GD, Singsaas EL. 2007. Fitting photosynthetic carbon dioxide response curves for C-3 leaves. *Plant Cell and Environment* **30**(9): 1035-1040.

Shen H, Yuan C-S, Lu C-C, Jiang Y, Jing G, Hu G, Yu R. 2019. Chemical composition and health risk of PM2. 5 from near-ground firecracker burning in micro region of eastern Taiwan. *Aerosol and Air Quality Research* **19**(10): 2252-2266.

Shen HZ, Yang TM, Lu CC, Yuan CS, Hung CH, Lin CT, Lee CW, Ling GH, Hu GR, Lo KC. 2020. Chemical fingerprint and source apportionment of PM2.5 in highly polluted events of southern Taiwan. *Environmental Science and Pollution Research* **27**(7): 6918-6935.

Silva EC, Nogueira RJ, Vale FH, Araújo FPd, Pimenta MA. 2009. Stomatal changes induced by intermittent drought in four umbu tree genotypes. *Brazilian Journal of Plant Physiology* **21**: 33-42.

Sjoman H, Hirons AD, Bassuk NL. 2015. Urban forest resilience through tree selection-Variation in drought tolerance in Acer. *Urban Forestry & Urban Greening* **14**(4): 858-865.

Skelton RP, West AG, Dawson TE. 2015. Predicting plant vulnerability to drought in biodiverse regions using functional traits. *Proceedings of the National Academy of Sciences of the United States of America* **112**(18): 5744-5749.

Sokal RR. 1982. Citation Classic - Biometry - the Principles and Practice of Statistics in Biological-Research. *Current Contents/Agriculture Biology & Environmental Sciences*(41): 22-22.

Song YS, Maher BA, Li F, Wang XK, Sun X, Zhang HX. 2015. Particulate matter deposited on leaf of five evergreen species in Beijing, China: Source identification and size distribution. *Atmospheric Environment* **105**: 53-60.

Sparks JP. 2009. Ecological ramifications of the direct foliar uptake of nitrogen. *Oecologia* **159**(1): 1-13.

Steiner AL, Chameides WL. 2005. Aerosol-induced thermal effects increase modelled terrestrial photosynthesis and transpiration. *Tellus Series B-Chemical and Physical Meteorology* **57**(5): 404-411.

Takanashi S, Kosugi Y, Matsuo N, Tani M, Ohte N. 2006. Patchy stomatal behavior in broad-leaved trees grown in different habitats. *Tree Physiology* **26**(12): 1565-1578.

Tardieu F, Simonneau T. 1998. Variability among species of stomatal control under fluctuating soil water status and evaporative demand: modelling isohydric and anisohydric behaviours. *Journal of Experimental Botany* **49**: 419-432.

Tarin T, Nolan RH, Medlyn BE, Cleverly J, Eamus D. 2020. Water-use efficiency in a semi-arid woodland with high rainfall variability. *Global Change Biology* **26**(2): 496-508.

Tredenick EC, Farrell TW, Forster WA. 2018. Mathematical modeling of diffusion of a hydrophilic ionic fertilizer in plant cuticles: surfactant and hygroscopic effects. *Frontiers in plant science* **9**: 1888.

Tsai YI, Chen CL. 2006. Atmospheric aerosol composition and source apportionments to aerosol in southern Taiwan. *Atmospheric Environment* **40**(25): 4751-4763.

Tsai YI, Kuo SC. 2005. PM2.5 aerosol water content and chemical composition in a metropolitan and a coastal area in southern Taiwan. *Atmospheric Environment* **39**(27): 4827-4839.

Vega C, Chi CE, Fernández V, Burkhardt J. 2023. Nocturnal Transpiration May Be Associated with Foliar Nutrient Uptake. *Plants* **12**(3): 531.

Victório CP, dos Santos MS, Simas NK. 2022. Phthalates: environmental pollutants detected in leaf epicuticular wax of Avicennia schaueriana and Rhizophora mangle from a mangrove ecosystem. *International Journal of Environmental Studies* **79**(1): 114-123.

Vogado NO, Winter K, Ubierna N, Farquhar GD, Cernusak LA. 2020. Directional change in leaf dry matter delta C-13 during leaf development is widespread in C-3 plants. *Annals of Botany* **126**(6): 981-990.

Wang B, Wang Z, Wang C, Wang X, Li J, Jia Z, Li P, Wu J, Chen M, Liu L. 2021. Field evidence reveals conservative water use of poplar saplings under high aerosol conditions. *Journal of Ecology* **109**(5): 2190-2202.

Wang H, Shi H, Wang Y. 2015. Effects of weather, time, and pollution level on the amount of particulate matter deposited on leaves of Ligustrum lucidum. *The Scientific World Journal* **2015**.

Wang X, Chengzhang; W, Jin; W, Guofang; M, Min; C, Shuli; C, Songhan; W, Zhengfei; G, Zhenhua; W, Bin; W, et al. 2021. Intermediate Aerosol Loading Enhances Photosynthetic Activity of Croplands. *Geophysical Research Letters* **48**(7): e2020GL091893.

Wang X, Wang CZ, Wu J, Miao GF, Chen M, Chen SL, Wang SH, Guo ZF, Wang ZH, Wang B, et al. 2021. Intermediate Aerosol Loading Enhances Photosynthetic Activity of Croplands. *Geophysical Research Letters* **48**(7).

Wang X, Wu J, Chen M, Xu XT, Wang ZH, Wang B, Wang CZ, Piao SL, Lin WL, Miao GF, et al. 2018. Field evidences for the positive effects of aerosols on tree growth. *Global Change Biology* **24**(10): 4983-4992.

Wang YS, Chang LC, Chang FJ. 2021. Explore Regional PM2.5 Features and Compositions Causing Health Effects in Taiwan. *Environmental Management* **67**(1): 176-191.

Will S, Eichert T, Fernandez V, Muller T, Romheld V. 2012. Boron foliar fertilization of soybean and lychee: Effects of side of application and formulation adjuvants. *Journal of Plant Nutrition and Soil Science* **175**(2): 180-188.

Wolz KJ, Wertin TM, Abordo M, Wang D, Leakey ADB. 2017. Diversity in stomatal function is integral to modelling plant carbon and water fluxes. *Nature Ecology & Evolution* **1**(9): 1292-1298.

Wu CH, Lo YH, Blanco JA, Chang SC. 2015. Resilience Assessment of Lowland Plantations Using an Ecosystem Modeling Approach. *Sustainability* **7**(4): 3801-3822.

Wylie R. 1955. A new absolute hygrometer of high accuracy. *Nature* **175**(4446): 118-119.

Xi BY, Clothier B, Coleman M, Duan J, Hu W, Li DD, Di N, Liu Y, Fu JY, Li JS, et al. 2021. Irrigation management in poplar (Populus spp.) plantations: A review. *Forest Ecology and Management* **494**.

Xie RH, Zhao JQ, Lu LL, Brown P, Guo JS, Tian SK. 2020. Penetration of foliar-applied Zn and its impact on apple plant nutrition status: in vivo evaluation by synchrotron-based X-ray fluorescence microscopy. *Horticulture Research* **7**(1).

Xu B, Long Y, Feng X, Zhu X, Sai N, Chirkova L, Betts A, Herrmann J, Edwards EJ, Okamoto M, et al. 2021. GABA signalling modulates stomatal opening to enhance plant water use efficiency and drought resilience. *Nature Communications* **12**(1).

Xu H, Zhang ZQ, Chen JQ, Xiao JF, Zhu MX, Kang MC, Cao WX. 2018. Regulations of cloudiness on energy partitioning and water use strategy in a riparian poplar plantation. *Agricultural and Forest Meteorology* **262**: 135-146.

Xu XW, Yu XX, Bao L, Desai AR. 2019. Size distribution of particulate matter in runoff from different leaf surfaces during controlled rainfall processes. *Environmental Pollution* **255**.

Xu XW, Zhang ZM, Bao L, Mo L, Yu XX, Fan DX, Lun XX. 2017. Influence of rainfall duration and intensity on particulate matter removal from plant leaves. *Science of the Total Environment* **609**: 11-16.

Yalaltdinova A, Kim J, Baranovskaya N, Rikhvanov L. 2018. Populus nigra L. as a bioindicator of atmospheric trace element pollution and potential toxic impacts on human and ecosystem. *Ecological Indicators* **95**: 974-983.

Yamaguchi M, Izuta T 2017. Effects of Aerosol Particles on Plants. In: Izuta T ed. *Air Pollution Impacts on Plants in East Asia*. Tokyo: Springer Japan, 283-293.

Yang HY, Tseng YL, Chuang HL, Li TC, Yuan CS, Lee JJ. 2017. Chemical Fingerprint and Source Identification of Atmospheric Fine Particles Sampled at Three Environments at the Tip of Southern Taiwan. *Aerosol and Air Quality Research* **17**(2): 529-542.

Yang YJ, Bi MH, Nie ZF, Jiang H, Liu XD, Fang XW, Brodribb TJ. 2021. Evolution of stomatal closure to optimize water-use efficiency in response to dehydration in ferns and seed plants. *New Phytologist* **230**(5): 2001-2010.

Yi K, Maxwell JT, Wenzel MK, Roman DT, Sauer PE, Phillips RP, Novick KA. 2019. Linking variation in intrinsic water-use efficiency to isohydricity: a comparison at multiple spatiotemporal scales. *New Phytologist* **221**(1): 195-208.

Yuan WP, Zheng Y, Piao SL, Ciais P, Lombardozzi D, Wang YP, Ryu Y, Chen GX, Dong WJ, Hu ZM, et al. 2019. Increased atmospheric vapor pressure deficit reduces global vegetation growth. *Science Advances* **5**(8).

Zeppel MJB, Lewis JD, Phillips NG, Tissue DT. 2014. Consequences of nocturnal water loss: a synthesis of regulating factors and implications for capacitance, embolism and use in models. *Tree Physiology* **34**(10): 1047-1055.

Zhang L, Zhang ZQ, Chen LX, McNulty S. 2019. An investigation on the leaf accumulation-removal efficiency of atmospheric particulate matter for five urban plant species under different rainfall regimes. *Atmospheric Environment* **208**: 123-132.

Zhou SJ, Cong L, Liu Y, Xie LM, Zhao SQ, Zhang ZM. 2021. Rainfall intensity plays an important role in the removal of PM from the leaf surfaces. *Ecological Indicators* **128**.

Zhou SJ, Yan GX, Wu YN, Zhai JX, Cong L, Zhang ZM. 2020. The PM removal process of wetland plant leaves with different rainfall intensities and duration. *Journal of Environmental Management* **275**.

Zhou SX, Duursma RA, Medlyn BE, Kelly JWG, Prentice IC. 2013. How should we model plant responses to drought? An analysis of stomatal and non-stomatal responses to water stress. *Agricultural and Forest Meteorology* **182**: 204-214.

Zhou Y, Yan WD. 2016. Conservation and applications of camphor tree (Cinnamomum camphora) in China: ethnobotany and genetic resources. *Genetic Resources and Crop Evolution* **63**(6): 1049-1061.

Appendix

The processed data from Study 3 are included in the chapter and the Supporting Information below. The raw data files are available in the bonndata repository (https://bonndata.uni-bonn.de/; Chi, Chia-Ju; Burkhardt, Juergen, 2023, "Nocturnal Stomatal Conductance Measurements_LI-6800 Raw Data Files", with the doi number of https://doi.org/10.60507/FK2/BBXVXR).

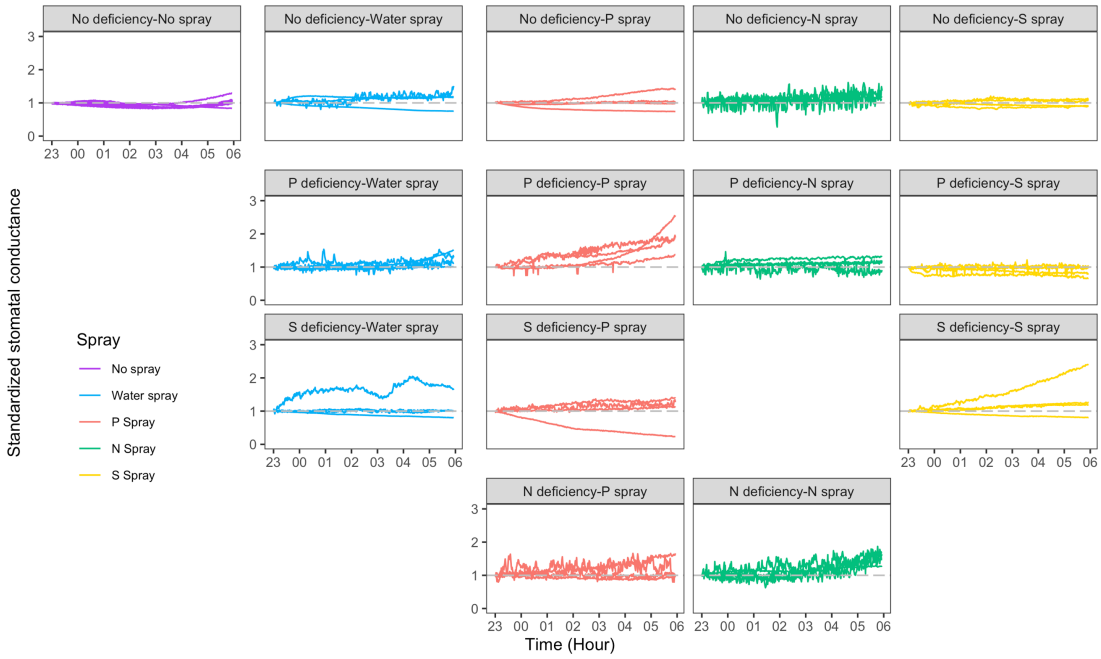

Figure S.1. Individual data of standardized nocturnal stomatal conductance in each group. Each group included four biologically independent replications.

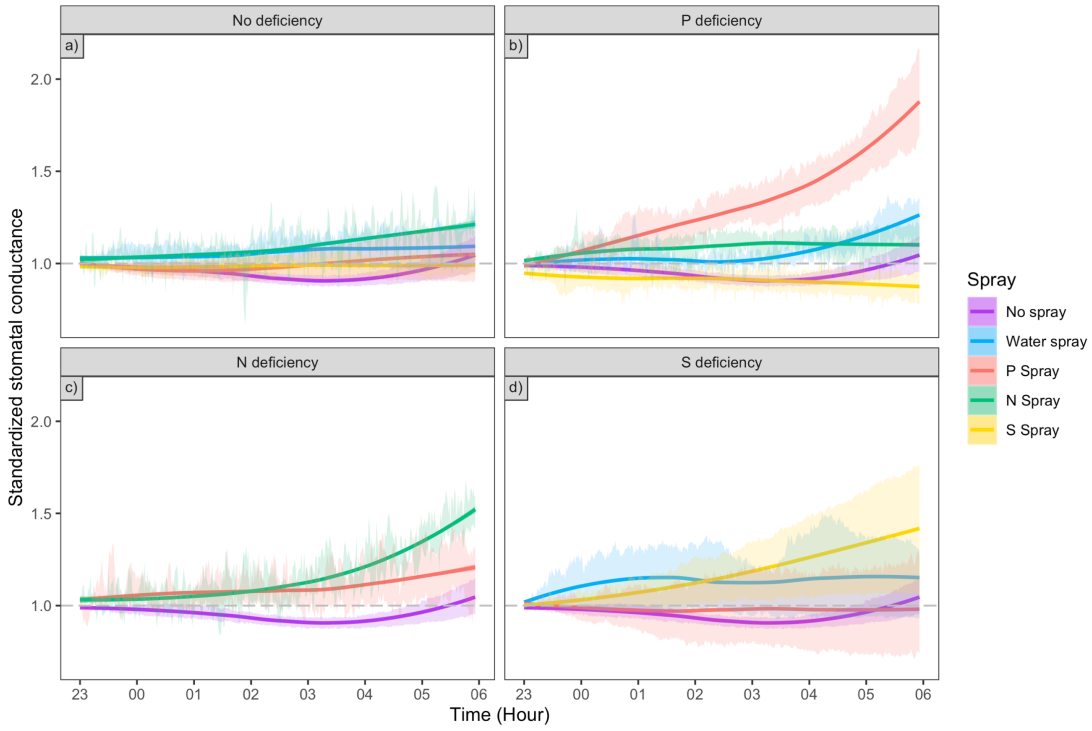

Figure S.2. Supplement data for *Figure 4.4*.

Range of $R.H._{leaf}$ for individual sample in each treatment (%)			
Treatment	Tree label	Minimum	Maximum
No deficiency-No spray	35xx	41.79	43.62
	1xx	44.57	45.31
	36xx	48.63	52.26
	4xx	70.55	74.20
	mean	**51.38**	**53.85**
No deficiency-Water spray	1fh	41.04	43.49
	2fh	50.85	74.78
	3fh	55.29	61.57
	4fh	68.88	72.58
	mean	**54.02**	**63.11**
P deficiency-Waterspray	5ph	48.63	50.44
	8ph	66.68	68.48
	11ph	44.28	47.49
	4ph	49.76	52.90
	mean	**52.34**	**54.83**
S deficiency-Water spray	17sh	40.97	51.87
	20sh	51.47	70.62
	23sh	57.53	60.31
	26sh	56.54	61.33
	mean	**51.63**	**61.03**
No deficiency-Pspray	1fp	55.94	56.61
	2fp	49.72	51.31
	3fp	57.96	67.26
	4fp	57.74	63.85
	mean	**55.34**	**59.76**
P deficiency-Pspray	9pp	52.73	57.77
	12pp	61.64	68.57
	6pp	62.13	68.77
	2pp	34.28	51.41
	mean	**52.70**	**61.63**
S deficiency-Pspray	18sp	62.93	71.99
	21sp	38.65	40.43
	24sp	58.37	68.01
	27sp	41.77	44.62
	mean	**50.43**	**56.26**
N deficiency-Pspray	6np	49.26	51.50
	8np	48.33	50.51
	10np	42.56	56.25
	12np	56.12	57.79
	mean	**49.07**	**54.01**
No deficiency-N spray	2fn	65.61	66.63
	1fn	49.78	54.18
	3fn	54.19	68.90
	4fn	65.07	67.12
	mean	**58.66**	**64.21**
P deficiency-N spray	4pn	57.93	62.19
	1pn	45.35	50.44
	2pn	40.16	44.62
	3pn	48.18	54.07
	mean	**47.91**	**52.83**
N deficiency-N spray	11nn	62.35	63.91
	7nn	43.55	47.09
	9nn	39.53	52.29
	8nn	62.74	66.43
	mean	**52.04**	**57.43**
No deficiency-Sspray	1fs	53.64	56.46
	2fs	64.89	72.85
	3fs	47.06	52.50
	4fs	69.56	73.98
	mean	**58.79**	**63.95**
P deficiency-Sspray	7ps	42.71	47.49
	13ps	50.73	53.22
	16ps	49.21	62.53
	4ps	59.15	62.27
	mean	**50.45**	**56.38**
S deficiency-Sspray	19ss	39.26	46.70
	22ss	63.82	70.91
	25ss	45.70	55.29
	28ss	54.96	58.09
	mean	**50.93**	**57.75**

Table S.1. Range of leaf surface relative humidity ($R.H._{leaf}$) during the night. Data shows the minimum and maximum leaf relative humidity of individual sample from 11 p.m. to 6 a.m. Each treatment included 4 biological replications.